FIRAT UNIVERSITY
GRADUATE SCHOOL OF NATURAL AND APPLIED SCIENCES
TÜRKİYE

THERMAL, ELECTRICAL AND DIELECTRIC PROPERTIES OF COPOLYSTYRENES BEARING POLAR SİDE GROUPS AND THEIR COMPOSITES

Abdullahi Musa ABUBAKAR

Doctoral Thesis

DEPARTMENT OF CHEMISTRY

Division of Physical Chemistry

JANUARY 2022

FIRAT UNIVERSITY
GRADUATE SCHOOL OF NATURAL AND APPLIED SCIENCES
TÜRKİYE

Department of Chemistry

Doctoral Thesis

THERMAL, ELECTRICAL AND DIELECTRIC PROPERTIES OF COPOLYSTYRENES BEARING POLAR SİDE GROUPS AND THEIR COMPOSITES

Author
Abdullahi Musa ABUBAKAR

Supervisor
Prof. Dr. Kadir DEMIRELLI

JANUARY 2022
ELAZIG

FIRAT UNIVERSITY
GRADUATE SCHOOL OF NATURAL AND APPLIED SCIENCES
TÜRKİYE

Department of Chemistry

Doctoral Thesis

Title:	Thermal, Electrıcal and Dıelectrıc Properties of Copolystyrenes Bearıng Polar Side Groups and Theır Composıtes
Author:	Abdullahi Musa ABUBAKAR
Submission Date:	20 December 2021
Defense Date:	20 January 2022

THESIS APPROVAL

This thesis, which was prepared according to the thesis writing rules of the Graduate School of Natural and Applied Sciences, Fırat University, was evaluated by the committee members who have signed the following signatures and was unanimously approved after the defense exam made open to the academic audience.

		Signature
Supervisor:	Prof. Dr. Kadir DEMIRELLI Firat University, Faculty of Science, Department of Chemistry	Approved
Chair:	Prof. Dr. Esin KAYA Muş Alparslan University, Education Fac., Dep. of Science Education	Approved
Member:	Prof. Dr. Hülya TUNCER Firat University, Faculty of Science, Department of Chemistry	Approved
Member:	Prof. Dr. Habibe ÖZMEN Firat University, Faculty of Science, Department of Chemistry	Approved
Member:	Prof. Dr. Aslışah AÇIKSES Munzur University, Faculty of Fine Arts, Design and Architecture	Approved

This thesis was approved by the Administrative Board of the Graduate School on

..... / ..... / 20 .....

Signature

Prof. Dr. Kürşat Esat ALYAMAÇ
Director of the Graduate School

DECLARATION

I hereby declare that I wrote this Doctoral Thesis titled "Thermal, Electrıcal and Dıelectrıc Properties of Copolystyrenes Bearıng Polar Side Groups and Theır Composıtes " in consistent with the thesis writing guide of the Graduate School of Natural and Applied Sciences, Firat University. I also declare that all information in it is correct, that I acted according to scientific ethics in producing and presenting the findings, cited all the references I used, express all institutions or organizations or persons who supported the thesis financially. I have never used the data and information I provide here in order to get a degree in any way.

20 January 2022

Abdullahi Musa ABUBAKAR

PREFACE

SCP-CoPcs are well-rounded conjugated macrocycles that have attracted a great deal of attention as useful organic material components, and are remarkable materials because of their electrical and optical properties. In this research, SCP-ball type CoPcs were synthesized via intermolecular formation of cobalt phthalocyanines from P(PNDEAMSt-co-St) as precursor. The SCP-ball type CoPcs were confirmed by FT-IR, ^{1}H-NMR, UV/Vis spectroscopy and MALDI-TOF-MS techniques. Activation energies of the thermal behavior, and electrical characterization of SCP-ball type CoPcs and their composites prepared with GO were carried out

Praise be to Allah by whose grace good things are accomplished. I would like to express my sincere gratitude to Prof. Dr. Kadir Demirelli, my research supervisor, for his continued support of my research and his patience, inspiration, enthusiasm and tremendous knowledge. I would like to express my sincere gratitude to Prof. Dr. Hülya Tuncer for her or their time, assistance and encouragement during my stay in Elazığ7TURKEY

I owe my deepest gratitude gratitude to my late Father Alhj Musa Abubakar, who died last year and for whose prayers I am eternally grateful and I pray for Almighty Allas's mercy on him and my Mother Hajiya Mairo Audi Dambatta, their prayers sustain me at all times.

Finally, I want to express my gratitude for my siblings' and friends for their love and encouragement.

Abdullahi Musa ABUBAKAR
ELAZIG, 2022

TABLE OF CONTENTS

ABSTRACT

Thermal, Electrıcal and Dıelectrıc Properties of Copolystyrenes Bearıng Polar Side Groups and Theır Composıtes

Abdullahi Musa ABUBAKAR

Doctoral Thesis

FIRAT UNIVERSITY
Graduate School of Natural and Applied Sciences

Department of Chemistry

January 2022, Page: xiv + 99

The greenish single-chain polymeric molecule-ball type cobalt phthallocyanines (SCPM-ball type CoPcs) were prepared via the macrocyclization reaction of cobalt phthalocyanine from poly(styrene-co-poly[4,4'-((((4-vinylbenzyl)azanediyl)bis(ethane-2,1diyl))bis(oxy))diphthalonitrile]) [P(PNDEAMSt-co-St)] (linear copolymer precursor) under diluted conditions at 140-150 ^{o}C in presence of cyclohexanol. The ball-type phthalocyanine moieties were incorporated into one side of the polymer chain. Both linear copolymer precursor and formation of ball-type cobalt phthalocyanine within a single-chain polymer were confirmed by FT-IR, ^{1}H-NMR, UV/Vis spectroscopy and MALDI-TOF-MS techniques. Particularly, the formation of SCP-ball type CoPc complexes were characterized by almost disappearance of –C≡N band at 2230 cm^{-1} in the FT-IR spectrum and appearance of Q band between 600 and 673 nm in the UV-Vis spectrum. Two degradation models including Flynn-Wall-Ozawa (FWO) and Kissinger-Akahira-Sunose (KAS) methods were used to determine the apparent activation energies for approximately 70-80% for the thermal decomposition of linear copolymer precursor and SCPM-ball type CoPc at the range of room temperature and 500 ^{o}C at various heating rates. The SCPM-ball type CoPc/graphite oxide (GO) composites were prepared by Ultrasonic Homogeniser Sonicator. Dielectric constant of SCPM-ball type CoPc/GO composites show a slight increase with the increasing content of GO due to poor distribution and dispersion of GO in the SCPM-ball type CoPc. The composites treated with concentration-treated had a significant performance in dielectric constant but with a relatively higher dielectric loss compared with those of SCPM-ball type CoPc. The dc conductivity increased exponentially over the studied range of temperatures. The dc electrical conductivity of linear copolymer precursor/GO and SCPM-ball type CoPc/GO composites increased with increasing amount of GO. The conductivity mechanism of polymer composites exhibited Correlated Barrier Hoping (CBH) mechanism.

Keywords: Single chain polymer, phthalocyanine, characterization, composite, kinetic

ÖZET

Polar yan gruplar taşıyan kopolistirenler ve kompozitlerinin termal, elektriksel ve dielektrik özellikleri

Abdullahi Musa ABUBAKAR

Doktora Tezi

FIRAT ÜNİVERSİTESİ
Fen Bilimleri Enstitüsü

Kimya Anabilim Dalı

Ocak 2022, Sayfa: xiv + 99

Yeşilimsi tek zincirli polimerik molekül-top tipi kobalt ftalosiyaninler (SCPM-top tipi CoPc), poli(stiren-ko-poli[4,4'-((((4-vinilbenzil)azanediil)bis(etan-2,1diil))bis(oksi))diftalonitril])'den kobalt ftalosiyanin'in makrosiklizasyon reaksiyonu yoluyla hazırlandı. [P(PNDEAMst-co-St)] (lineer kopolimer öncüsü) seyreltik koşullarda 140-150 ^{o}C'de sikloheksanol varlığında. top tipi ftalosiyanin birimleri, polimer zincirinin yan grupları olarak oluşturuldu. Tek zincirli bir polimer molekülü üzerinde hem lineer kopolimer öncüsü hem de top tipi kobalt ftalosiyanin oluşumu FT-IR, ^{1}H-NMR, UV/Vis spektroskopisi ve MALDI-TOF-MS teknikleri ile doğrulandı. Özellikle, SCP-top tipi CoPc komplekslerinin oluşumu, FT-IR'da 2230 cm^{-1} deki –C≡N bandının neredeyse kaybolması ve UV-vis ölçümlerinde 600 ile 673 nm arasında Q bandının ortaya çıkması ile karakterize edildi. Lineer kopolimer öncüsü ve SCPM-top tipi CoPc'nin termal ayrışmasına yönelik yaklaşık %70-80'i için görünen aktivasyon enerjilerini belirlemek için Flynn Wall Ozawa (FWO) ve Kissinger-Akahira-Sunose (KAS) yöntemlerini içeren iki bozunma modeli kullanıldı. Oda sıcaklığı ve 500 ^{o}C aralığında çeşitli ısıtma hızlarında. SCPM-top tipi CoPc/grafit oksit (GO) kompozitleri, Ultrasonik Homojenleştirici Sonikator ile hazırlandı. SCPM-top tipi CoPc/GO kompozitlerinin dielektrik sabiti, SCPM-top tipi CoPc'de zayıf grafit oksit dağılımındand dolayı artan GO içeriğine bağlı hafif bir artış gösterir. Konsantrasyon işlemine tabi tutulmuş kompozitler, dielektrik sabitinde önemli bir artış gösterdi. Ancak SCPM- top tipi CoPc ile karşılaştırıldığında nispeten daha yüksek bir dielektrik kaybı vardı. DC iletkenliği, uygulanan sıcaklık aralığında katlanarak artış gösterdi. Lineer kopolimer öncüsü/GO ve SCPM-top tipi CoPc/GO kompozitlerinin dc elektriksel iletkenliği, artan GO miktarı ile artış gösterdi. Polimer komplekslerinin iletkenlik mekanizması Korelasyonlu Bariyer Sıçraması (CBH)'nı gösterdi.

Anahtar Kelimeler: Tek zincirli polimer, ftalosiyanin, karakterizasyon, kompozit, kinetik.

LIST OF FIGURES

Page

LIST OF TABLES

Page

SYMBOLS AND ABBREVIATIONS

Symbols

T_g	: Glass transition temperature
T_i	: Initial decomposition temperature
T_f	: Final decomposition Temperature
Ω	: Angular frequency
ε′	: Dielectric constant
ε″	: Dielectric loss
σ_{ac}	: Alternating electrical conductivity
σ_{dc}	: Direct electrical conductivity
E_a	: Activation Energy

Abbreviations

AIBN	: 2,2'-Azobisisobutyronitrile
DSC	: Differential Scanning Calorimetry
TGA	: Thermogravimetric analysis
SCP	: Single-Chain Polymer
PNDEAMSt	: Phthalonitrile diethanolamine styrene
St	: Styrene
Pc	: Phthalocyanine
CoPc	: Cobaltphthalocyanine

1. INTRODUCTION

Throughout the twentieth century, due to its large properties, polymers had replaced other materials in most applications. Today, most of the materials we use in our daily activities are made of polymers such as clothes, carrying bags, containers, packaging products, snacks, drink bottles, furniture, syringes and adhesives [1]. Polymers were also discovered in engineering aspect like gears and structural parts by chance or unexpected use. Their characteristics can be easily altered by selecting appropriate synthetic methods or environmental conditions, as well as adding additives in large-scale drug production using machinery [2]. Compared to other material classes most polymers can be handled very quickly. It allows the producer to generate a larger number of products that consume less energy [1]. Polymers are generally synthesized through a process called a polymerization process, in which a single unit or monomer reacts with each or to form a longer chain of polymeric molecules. A monomer unit is a molecule that has two or more reactive sites, forming a cross-linked network or long chain [3, 4]. The number of active sites that are reactive possessed in the monomer is called a functionality. These are important parameters which guide the structures of polymers [4].

1.1. Polymerization Reaction

Polymerization is the technique whereby short molecules named monomers join to connect to form chains of polymer or networks of three-dimensional in a chemical reaction. There are many types of polymerization, and various classification mechanisms exist. Below shows polymerization of monomer of styrene to polystyrene chain indicated in the Figure 1.1 shows the scheme showing polymerization of styrene undergoing polymerization reaction to polystyrene chain [5]. Figure 1.1 shows polymerization of monomer of styrene under going polymerization reaction to polystyrene chain.

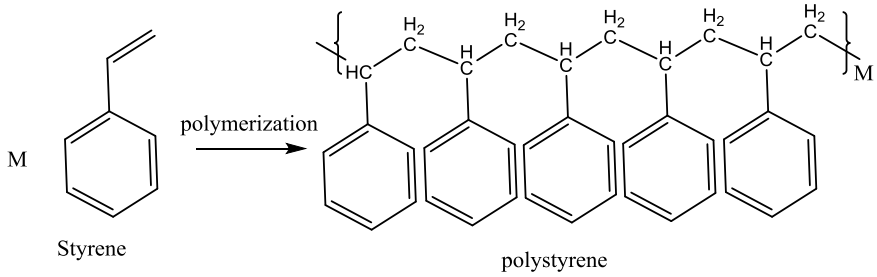

Figure 1.1. Scheme showing polymerization of monomer of styrene under going polymerization reaction to polystyrene chain [5].

Condensation or step polymerizations and addition polymerizations are two types of polymerization reactions [5, 6].

1.1.1. Condensation polymerization

The polymerization via condensation reaction occurred in stages. Throughout a polymerization, a unit monomer reacts with another unit of a monomer to form A polymer whose molecules are made up of a small number of repeated units called oligomers, which have a molecular weight that is less than that of the polymer itself [7]. Those oligomers condense to produce trimer, tetramer, and then a large polymer molecular weight at the completion in the polymerization reaction. The molecules should be able to possessed one or two functional groups (for example amine, carboxylic acid, or alcohol groups). The reaction take place between two same or monomers or different functional groups. It may happen from a dimer and oligomer, a monomer and a dimer or a polymer chain and different polymer chain. Smaller molecules are often combined to create higher weight molecules. The properties of either molecules and functional groups were considered [8, 9]. Figure 1.2 shows polymerization of monomer of styrene under going polymerization reaction to polystyrene chain.

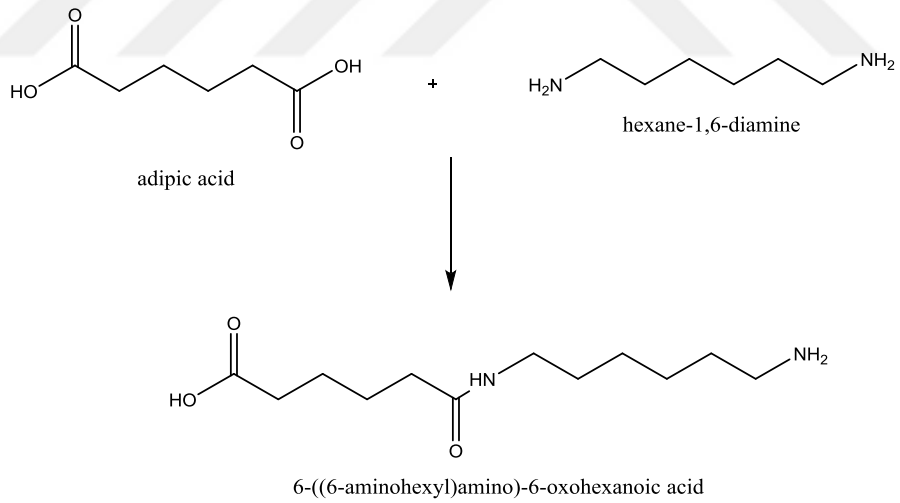

Figure 1.2. Condensation reaction of hexanedioc acid and ethane diol to form a polyester [1]

The condensation product is a linear polymer, if all functional groups are difunctional. The polymer would be crosslinked whether one of the functional groups is tri-functional or tetra-functional. Condensation polymerization is a process in which monomers which possessed functional groups go through condensation reactions forming a polymer chain. Esterification, amidation, urethane formation, and aromatic substitution are examples of such condensation reactions [8, 9]. Ring opening polymerization can also be used to produce condensation polymers

in addition to these reactions. A condensation polymerization reaction can be used in the manufacture of Nylon 66 from hexamethylene diamine and adipic acid [9].

1.1.2. Addition polymerization

The presence of active centers or activated species that may polymerize monomer units characterizes addition polymerization or chain growth polymerizations. This approach can be used to polymerize unsaturated monomers. Activated sites are both free radicals or ions/highly polarized molecules formed via a homolytical scission a kind of organic compound named initiators. These active centers will strike a monomer's double bond and generate a new active center as a result. Initiation is the name for this process [3, 8-10]. Newly formed active centers will target monomer groups, resulting in the formation of more active centers. Propagation is the name given to this process. Further addition reactions involve ionic polymerization, which is initiated and propagated by ions attacking a double bond rather than the free radical. Propagation go on until the active core dies or is terminated. Chain growth polymerization is shown by the conversion of propylene (CH_2]CH(CH_3) to polypropylene ([CH_2=CH(CH_3)]) [3, 8-10]. Generally, 4 types of addition polymerization

- Radical chain growth polymerization

(a) In the initiation stage, involves the use of an initiator, a thermolabile compound that decomposes on heating to produce two active free radicals at the reaction mixture's temperature. Generally, two processs are involved in the initiation process first formation of radical and formation of radical monomer. Note that in radical monomer the free radical initiator attached to the monomer is called end group in the polymer chain. usually in free radical polymerization monomers containing vinyl group or unsaturation such as styrene and acrylonitrile [10].

$$\text{Initiator} \longrightarrow 2I^{\cdot}$$

(b) In the propagation stage the radical monomer (initiator + monomer) react with another monomer to dimer, tetramer and so on, the reaction fallowed head to tail arrangement due to the radical formed is being stabilized by resonance hence electrons are delocalized. Head to head arrangement cannot occur due to the formation local electrons and steric hindrance.

$$I^{\cdot} + M \longrightarrow IM^{\cdot} \quad \text{chain initiation}$$

$$IM^{\cdot} + nM \longrightarrow IMn^{\cdot} \quad \text{propagation}$$

(c) Last stage, the termination stage in this stage, termination can either occur by chain transfer, combination(coupling) and by disproportionation. termination by coupling two growing polymer chains react with each other head to head to form a long polymer chain and this process usually takes place at low temperature. The termination by disproportionation occurs when active polymer radical abstract a proton from another active polymer chain to two dead polymer chains one with saturated end, another with unsaturated end. In termination by disproportionation high temperature is required [10]. The Figure 1.3 shows the termination stage.

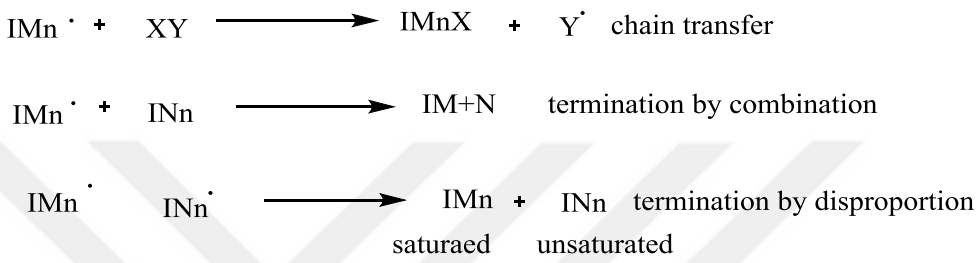

Figure 1.3. The termination stage

- Controlled radical polymerization (CRP) depends on absolutely pure reactions so that no impurities can cause termination. CRP stops only when all the monomer is used. The reaction continues in the presence of an additional monomer. Copolymers (block) are produced using this method. This polymerization can be terminated and start again at any period. This innovative technology facilitates the synthesize of tailored polymers with composition control and macromolecular structure [11]. Figure 1.4 shows the ATRP mechanism.

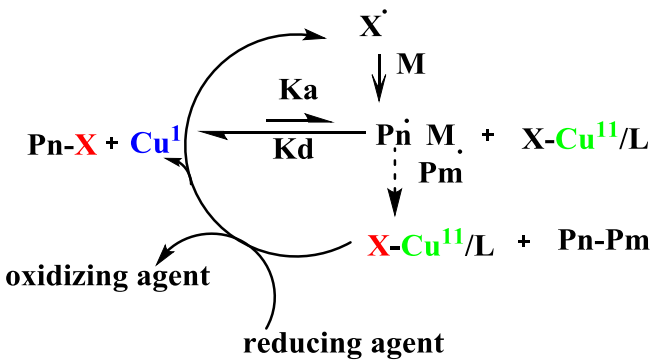

Figure 1.4. Scheme showing the ATRP mechanism [11, 12]

Cationic chain growth polymerization

Cationic polymerization is a method of chain-growth polymerization whereby an initiator (cationic) transfers a charge to a monomer (vinyl) therefore making it reactive. The formed

monomer which is a reactive formed polymer by reacting with other monomers. A lot of vinyl monomers in the presence of a very minute quantity of catalyst of the kind used in Friedel-Crafts reactions freely undergo polymerization. Catalysts of effective important are $AlBr_3$, $AlCl_3$, and BF_3 e.t.c. The aforesaid catalysts are all Lewis acids examples with strong electron-acceptor capability. The presence of co-catalyst is required in other to achieve the effectiveness of the catalyst which are Lewis bases e.g. H_2O and OH [10].

$$AlCI_3 + H_2O \Leftrightarrow H^+AlCI_3OH^-$$

Monomers such as styrene, vinyl alkyl ethers, alpha-methyl styrene polymerize in the presence of the aforementioned catalyst Let X represent the catalyst, co-catalyst by YH, and the monomer by M. Then the kinetics can be shown as follows In the Figure 1.5. below.

$$X + YH \Leftrightarrow H^+XY^-$$

$$H^+XY^- + N \rightarrow HN^+XY^-$$

$$HN_n^+XY^- + N \rightarrow HN_{n+1}^+XY^-$$

$$HN_n^+XY^- \rightarrow N_n + H^+XY^-$$

$$HN_n^+XY^- + N \rightarrow N_n + HN^+XY$$

Figure 1.5. Schematic representation of cationic polymerization

- **Anionic polymerization**

Anionic polymerization is a method of addition polymerization that covers the polymerization of monomers (vinyl) with groups that are strongly electronegative. Entirely, the strong electronegative substituent (monomers), in the presence of carbanions polymerize freely. Certain substituents which are electron-withdrawing that stabilize the negative charge via delocalization of charge and Therefore, allow anionic polymerization consist of cyanide and carboxylic acid e.t.c. Thus, monomers such as styrenes, acrylates, epoxides, and dienes freely go through anionic polymerization. The initiators (electron donors) are strong anions or electron transfer agents. The transfer of an electron from an initiator to the monomer (vinyl) front-runners to the creation of a carbanion known as anion radicals. Nucleophiles or Lewis bases are alkali group metals like lithium or sodium which are typical donors of an electron. Additional examples of strong nucleophilic initiators OH^-, CN^-, organometallic compounds like alkyl and Grignard reagents. Nucleophiles or lewis bases are alkali group metals like lithium or sodium which are

typical donors of an electron. Additional examples of strong nucleophilic initiators OH^-, CN^-, organometallic compounds like alkyl and Grignard reagents [10].

The kinetics of an anionic polymerization comprises of initiation and propagation. Let XMe be an organometallic compound that initiates polymerization and M_n a monomer. The distinct steps can be shown in Figure 1.6 [10].

$$XMe \Leftrightarrow Me^+ + R^-$$

$$R^- + Mn \rightarrow RMn^-$$

$$RMn^- + Mn \rightarrow RMn_2^-$$

$$RM_{n-1}^- + Mn \rightarrow RMn_n$$

Figure 1.6. Schematic representation of anionic polymerization

1.2. Single Chain Polymers

SCT (single-chain technology) is an innovative approach to the creation of smart and autonomous soft nanodevices. Individual polymer chains, known as single-chain polymer nanoparticles (SCNPs), can now be converted into folded/collapsed unimolecular soft nanoparticles using SCT. Synthetic polymer compaction with SCNPs is somewhat close to protein folding close to its native form, but it's also a long way from perfection seen in a natural macromolecules [6]. During the last few years, important A lot of work has been done to provide bioinspired SCNPs with functions that attempt to replicate those present in natural polypeptides (both intrinsically disordered as well proteins folded proteins), for-instance enzymatic function and multi binding activity, selectivity as well as transport properties. First and foremost, a global representation of the conformation properties of SCNPs in solution has been given, spanning the entire concentration continuum from infinite dilution to melt density [6].

1.2.1. Synthesis of single chain polymer

Controlled radical polymerization techniques like ATRP and RAFT had been considered adaptable synthetic methods for preparing a vast variety of linear homopolymer and linear copolymer precursors, which possessed correct molecular weight and composition. Higher molecular weight copolymer structures may be made from living polymers or copolymers. Different intrachain cross-linking reactions have been used to make irreversible SCNPs. The intrachain crosslinking reaction possibly permanent (covalent bonds) either reversible (noncovalent or dynamic covalent bonds) depending on its existence. Reaction of synthesis of

SCP-CoPc, poly(VBOP-*co*-St), $CoCl_2.6H_2O$, phthalonitrile and excess cyclohexanol as solvent. The Figure 1.7 shows reaction synthesis for SCP-CoPc.

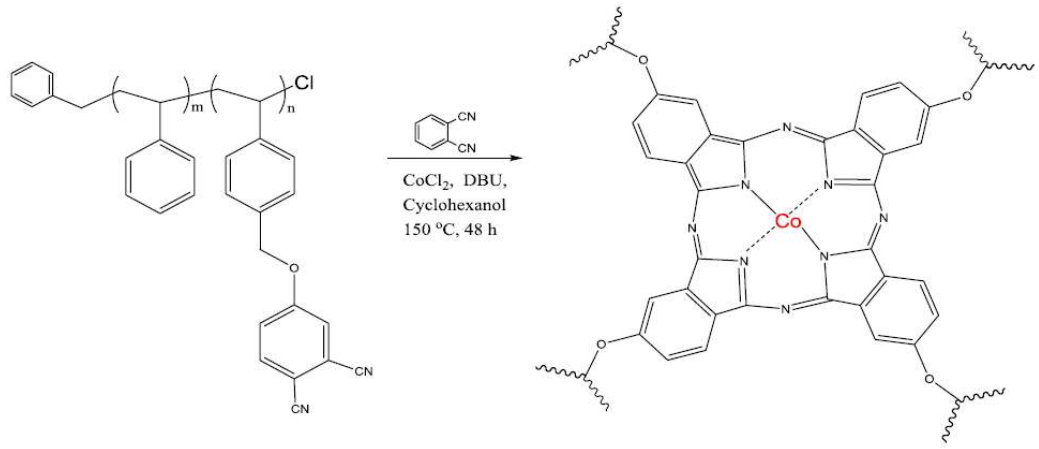

Figure 1.7. Reaction synthesis for SCP-CoPc

The intrachain homocoupling technique was used to synthesize permanent SCNPs under high dilution conditions for the first time. relied for the use of vinyl reactive functional groups in poly(alkyl methacrylate), poly(styrene), and poly(ε-caprolactone) based precursors. Poly(4-N-Boc-aminostyrene) and poly(carbonate)-based SCNPs were also made with unsaturated functional groups. Polymer composites are materials that contain at least two polymeric phases. The polymeric materials combine with material properties both high specific and light weight specific properties or individual constituents retained their separate identities [1].

1.2.2. Properties polymeric composites

The polymeric composites have a lot of useful properties following as:

a. stiffness and strength
b. strong abrasion resistance,
c. high resistance to fracture
d. outstanding impact resistance
e. excellent corrosion resistance
f. a high level of exhaustion tolerance, and
g. low price.

1.2.3. Uses of polymeric composites

a) They are commonly important as construction components in aircraft, electronic packaging for surgical devices, space vehicles, as well as in residential buildings [1].

b) Because of their resilience, stability in terms of temperature, desirable electrical properties and mechanical properties, and potential to stay undamaged or unchanged by unfavorable environmental factors, composite materials have sparked people's interest. Electromagnetic interference insulation, Wire and cable sheathing, and antistatic material are all examples of applications for such composites.

1.2.4. The conductivity of composites

Changing the amount and type of filler in such materials will improve their electrical properties. In some applications, graphite/polymer composites provide an appealing replacement to the metal conductors: Rubber is only seen in its purest form because it is mostly coated with carbon blacks. Carbon blacks are reasonably conductive, whereas filled rubber is generally an insulator. The conductivity of polymer composites can be because of the following factors:

- The polymer/graphite composites conduct electricity only if there is proper dispersion of graphite in a polymer matrix [13]. A specific resistivity of the order of 10-100 $\Omega.cm^{-1}$ was achieved for conductive rubber. As the conductive particles creates a continuous network, the dc electrical conductivity of carbon black filled rubbers reaches a maximum possible value. This connection between filler material and composite conductivity reveals a sudden shift in the dispersal condition of the conducting particles, for examples, particle coagulation to create conducting networks that make electrical conduction across composites easier [14].
- The particles in the composites produced continuous conduction paths. The electrical conductivity of conducting composites is affected by the proportions and structure of loading particles. Commercial graphite fragments, for example, have plate-like forms and a sheet structure. Plate-like particles of graphite and Carbon fibers, talc, and mica were found to be easier to order in a polymer matrix along the mixing-mill direction than spherical particles. There is no doubt that the particle size determines the extent of dispersion of the particles of graphite, and the shape of the conduction cannels in the composite is proportional to size of a particle of a conducting graphite particles.

1.3. Graphite

Graphite, also referred to as plumbago, is a crystalline shape of carbon with atoms arranged in a hexagonal arrangement. It's the most stable source of carbon in normal conditions and exists naturally in this state. It turns to diamond at high temperatures and pressures. Graphite is a mineral that is found in pencils and lubricants. It is a strong heat and energy conductor. It is used in electrical devices due to its high conductivity [15].

1.3.1. Structure

The atoms in each sheet of graphite are arranged in a hexagonal fashion, and the layers are lined in the AB series. As a consequence, a hexagonal unit cell with dimensions of c = 6.71 A and a = 2.46 A has been formed. Figure 1.8 shows graphite structure. A and B in Figure 1.8 represent the four atoms that make up a unit cell. The atoms A and B are on the same layer plane, and the atoms A and B are on a layer plane that is half the crystallographic c-axis spacing, or 3.35 A. The atoms A and A˚ differ from the atoms B and B in that the A and A˚ atoms have neighbors in parallel layer planes immediately above and below them, while the B and B` atoms do not. The crystal structure belongs to the P63/mmc or space group, with the 63 screw axis resulting from the AB stacking. The arrangement has an inversion symmetry center halfway between the atoms A and A`[16].

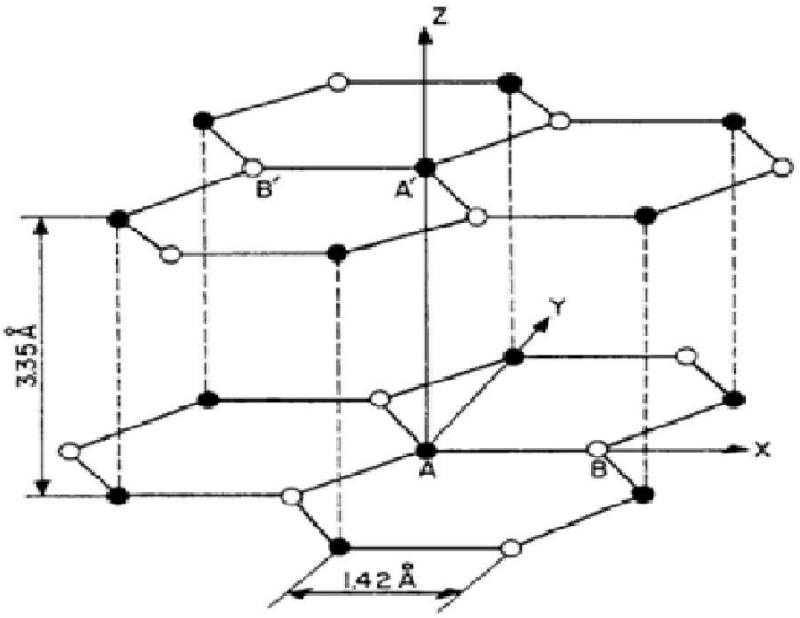

Figure 1.8. Graphite structure [16]

Theoretically and experimentally, the equilibrium temperature and pressure conditions for the transformation between graphite and diamond have been developed. The intensity varies linearly from 1.7 GPa at zero degrees Celsius to 12 GPa at 5000 ^{o}C (diamond/graphite/liquid triple point). The stages, on the other hand, have a large area along this line where they can coexist. The stable form of carbon is graphite at natural temperature 20 °C (293 K) and pressure 1 regular atmosphere (0.10 MPa), yet diamond is metastable and its rate of changing to graphite is marginal [21]. Diamond, on the other hand, quickly transforms to graphite at temperatures above around 4500 K. Speedy conversion of graphite to diamond necessitates well-pressured in excess of the line of equilibrium (A 35 GPa) pressure is expected at 2000 K [15].

1.3.2. Graphite oxide

Graphite oxide is a series of functionalized graphene sheets made up predominantly of oxygen ,carbon, and hydrogen atoms. This substance may be seen as a precursor to graphene. The only difference between graphite oxide and graphite is the oxygenated groups found in Graphite oxide, which bring about the wider distance in the middle the graphene layers. The Figure 1.9 shows carboxyl graphite.

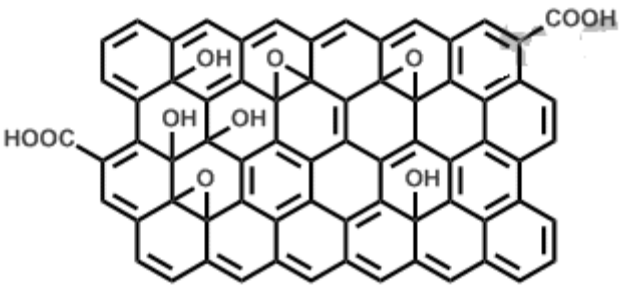

Figure 1.9. Carboxyl graphite

1.3.3. Properties of graphite oxide

The major graphite oxide properties are the following:

- It's an insulator, rather its conductivity changes according to it's own chemical properties and structural properties. GrO can be dispersed in both aqueous medium and organic solvents since it's an amphiphilic in nature.
- GrO has antibacterial characteristics.

1.3.4. Uses of graphite oxide

- ✓ Because of these features, graphite oxide is used in a number of uses. Supercapacitors, for example, are a kind of capacitor that can store large amounts of energy.
- ✓ Manufacture of the transparent conductors, the inhibition of tumorigenesis in a variety of cell lines in biomedical applications, for instance.

1.3.5. Preparation of graphite oxide by the Brodie method

Brodie's technique was used for graphite oxidation as well (GO-B). Finging nitric acid (200 mL) were added at 0 ^{o}C. The 10 g graphite powder was applied to the flask and properly dispersed to prevents agglomeration. Since explosions may occur when adding potassium chlorate, extra caution is needed. Following termination of a reaction, the mixture was dissolved in pure water and filtered under vacuum until the pH of the filtrate were neutral [17, 18].

1.3.6. A modified version of Hummers' process for producing graphite oxide

A modified Hummers system (GO-H) was used to prepare GO for commercial use. This process makes use of additional quantities of $NaNO_3$ and KMnO4 in Hummers' reagents. The mixture containing graphite $NaNO_3$ (7.5 g) was added with concentrated H_2SO_4 (360 mL), as well as mixture was dropped to 0 ^oC in an ice bath**.** To keep a hold on the reaction temperature below 20 ^oC, $KMnO_4$ (45 g) were eventually introduced in small amounts. The solution were heated to a temperature of 35 ^oC for 3 hours while stirring. Then 3 percent H_2O_2 (1.5 L) had been applied slowly. At 98 ℃, 30 minutes were spent stirring the reaction mixture as well as the mixture had been eventually centrifuged for 30 minutes (3700 rpm), then decanted away from the supernatant. Then, the solid material that remains was washed and centrifuged again 600 milliliters (mL) water, repeating this step until the pH level was equal to zero (neutral) [17, 18].

1.3.7. Preparation of graphite oxide via staudenmair method

The graphite oxide was produced adopting a staudenmaier technique. The all reagent grade chemicals was used. Fuming nitric acid, 97% H_2S0_4 and $KCIO_3$ (all Panreac), was oxidized by commercially powdered graphite (40-47 pm; 99.9 percent), made available by Fluka. Along with an ice bath, a 500 ml flask containing 97% H_2SO_4, (175 ml) and fuming nitric acid (90 ml) had been cools off to 273 K. $KClO_3$ had been added to a solution which is under continuous stirring, after adding 10 g of graphite powder into the flask. The addition continued until the addition of 110 g $KClO_3$ was added. The solution of acid containing graphite was transferred to 10-11 ml of distilled water after this process. The solution was filtered immediately and a 5% HCl solution was washed with the graphite oxide filtrate until the sulfates has totally gone, and afterwards with purified water until the chloride ions had disappeared. Samples that produced had been dried for 16 hrs under 323 K in the oven. There were ten samples produced by graphite oxidation at different periods, a period of time ranging from 24 to 240 hours, samples are labeled with a G during which there will be a period of hours of oxidation (for example G120 means 120 hours of graphite oxidized) [19].

1.3.8. Graphite Oxide Synthesis Procedure using Improved Hummers method.

By the Improved Hummers Process, graphite oxide was synthesized. The initial step made up of the graphite oxidation using the oxidizing agent $KMnO_4$. As a result, 360 mL of H_2SO_4 and 40 mL of H_3PO_4 was added with continuous and vigorous shaking into the Erlenmeyer flask. The H_2SO_4/H_3PO_4 mixture was applied gradually to 9 g $KMnO_4$ and 3 g graphite of the ratio (3:1). The reaction mixture was held for 12 hours at 50 °C. The resulting mixture was added after the oxidation stage to the beaker containing 400 g of crushed ice and 3 mL of H_2O_2 to initiate the

reaction system. It was filtered under vacuum by a filter of 10-20 μm. Finally, the compact cake was washed with 200 mL dry diethyl ether, filtrated and dried for 24 hours at 100 °C [20].

1.3.9. Characterization of GO

- **Elemental analysis**

Carbon compounds, hydrogen, and oxygen produced from the elemental analysis of samples are seen as a function of oxidation degree.

- **Thermogravimetric Analysis**

TGA analysis will measure absorbed water since approximately 5 percent by weight of the oxidized sample has a low water content of approximately 5 percent by weight.

- **FT-IR**

A broad band between 3000-3700 cm^{-1} is contained in the samples that have been most oxidized, showing 2 maximum absorptions at around 3190 cm^{-1} and 3403 cm^{-1} and a shoulder at absorption around 3590 cm^{-1}. The existence of free and related hydroxyl groups because of adsorbed, inhibited water and structural hydroxyl groups of graphite oxides are the result of these bands.

- **x-ray**

Graphite oxidation transforms the crystalline structure into another different one, also laminar, but more open than the graphite structure, thus enabling the physical and chemical intercalation of molecules. Alternatively, depending on the techniques employed in the synthesis, air moisture, It is generally known that graphite oxide has a varied interplanar spacing, And other factors [19].

1.3.10. Methods of manufacturing polymer/graphite nanocomposites

The production of nanocomposites requires selecting the appropriate blending technique to meet up proper dispersion of nanofillers (graphite and other forms of nanocomposite material) all across the polymeric matrix.

Silient features for each method along with their limitations (if there are any) are As outlined in the following paragraphs [21, 22].

- **In situ polymerization**

In situ polymerization is a kind of effective technique to contribute proper dispersion of the graphitic fillers all across the polymeric matrix. In this case, in the presence of the filler, the monomer or oligomer polymerizes, and because of this, the in situ compounding method strengthens interactions between the polymeric phase and the reinforcing filler [2, 14, 21].

- **Solution compounding**

During the solution compounding, a solvent is made to dissolve the polymer and in the resulting solution, a filler is dispersed. After the mixing is done, the solvent has been evaporated and after that, the bulk polymer substance comprising the fillers is normally molded to give the composite its shape. This method additionally results in composites of electrical conductivity as well as a low percolation threshold. Nevertheless, a large amount of solvent is used and The related environmental contamination caused by the removal of the solvent has hindered the widespread implementation of this technique for composites production [14].

- **Melt blending**

From the standpoint of an industrial perspective, melt blending seems to be the advantageous compounding process for the production of composites as a result of the fact that it is a direct, method that is both cost-effective and environmentally safe, since no solvents are used in the composite's preparation. Traditional mixing equipment for example internal mixer, extruder, and two-roll mill can be formulated for the melt blending Action and are normally available most of the time in compounding units [14].

1.4. Polymers and Monomers Containing Reactive Phthalonitrile Units as Terminal

Polymers and monomers which are containing reactive phthalonitrile units as side group terminal or group pendants produce high-performance thermoset resins when curing. The additional nitrile group curing process results in hetero aromatic compounds that contribute to their excellent thermal stability phenolic compounds, aromatic amines metals, and their salts are examples of curing agents. and coordinating compounds can speed up the curing step[18]. The most efficient external healing additives for phthalonitrile polymers are found to be aromatic amines; even wt% percent of them may reduce the healing temperature to an acceptable level. But their existence in the polymer network can have an influence on the system's structural excellence [23]. Among the commonly known solutions to mitigate this issue is developing polymers with self-promoting healing behavior. Phthalonitrile polymers that contain amino or hydroxy groups that display self-catalyzed healing actions have been studied already [23]. Figure 1.10 shows the synthesis of phthalonitrile from 4-nitro phthalimide.

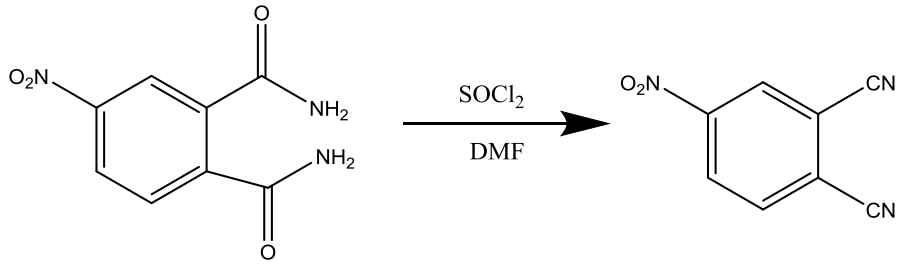

Figure 1.10. Reaction Synthesis of pthalonitrile from 4-nitro phthalimide

1.4.1. Synthesis of 4-nitrophthalonitrile from 4-nitro phthalimide

The 4-nitrophthalonitrile has been synthesized according to the adapted method [24,72]. And, synthesis of pthalonitrile from 4-nitro phthalimide has been indicated in Figure 1.10.

1.4.2. Reaction of phthalonitrile

To accomplish high yields under mild reaction conditions, aromatic nucleophilic replacement of active nitro compounds needs dipolar aprotic solvents like dimethylsulfoxide (DMSO), N,N-dimethylacetamide (DMAc), N,N-dimethylformamide (DMF), N-methylpyrrolidone (NMP), and others [25].

1.4.3. Synthesis of monomer bearing phthalonitrile group, via nucleophilic substitution of nitro group

4-[(4-Vinylbenzyl)oxy] phthalonitrile (VBOP) had been synthesized from the reacting of 4-nitrophthalonitrile along with the suitable 4-hydroxymethyl styrene when there is potassium carbonate and dimethyl formamide (DMF) as solvent dependent on the procedure. For this method, 2 g (14.91 mol) of 4-hydroxymethyl styrene and 2.58 g (14.91 mol) 4-nitrophthalonitrile have been added to the round-bottom flask containing 10 mL anhydrous DMF. The excess 4.14 g, 30 mol of K_2CO_3 was put into a reaction flask, and the reaction mixture was carried out at a temperature of 60 °C. 48 hours later, When the reaction mixture had cooled to room temperature and precipitated in a solution of ethyl alcohol and water in a 4:1 ratio. Finally, the sample product was dried at 40 °C in a vacuum [26]. Figure 1.11 shows a reaction synthesis of 4-[(4-vinylbenzyl)oxy] phthalonitrile (VBOP).

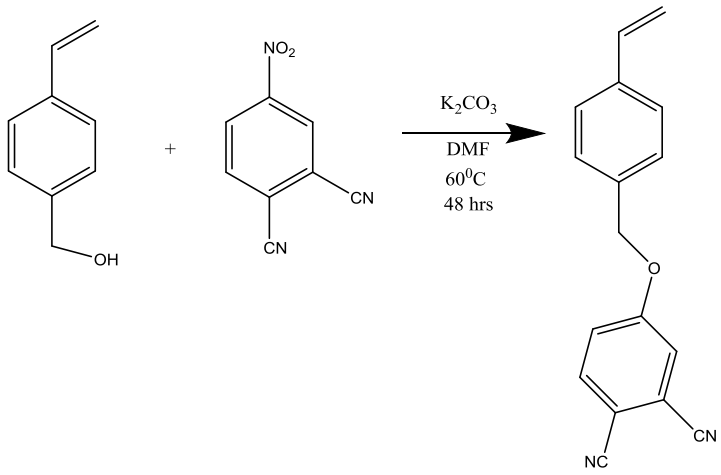

Figure 1.11. Reaction synthesis of 4-[(4-vinylbenzyl)oxy] phthalonitrile (VBOP)

1.4.4. Synthesis of substituted phthalocyanines complex from phthalonitrile compound

A scheme of the tetra substituted phthalocyanine complex has been indicated in Figure 1.12.

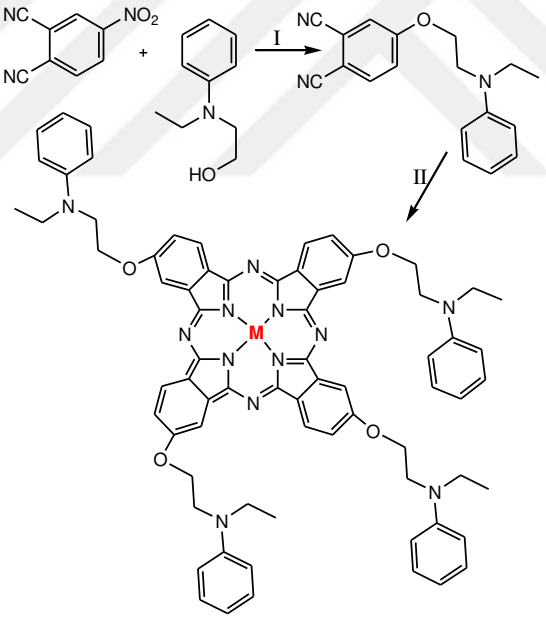

Figure 1.12. The scheme of the tetra substituted phthalocyanine complex [27].

1.4.5. Uses of polymers containing phthalonitrile

Most of polymers which contain phthalonitrile is generally used as:

- Modern aerospace vehicle structures require materials made of polymers with remarkable thermal stability to resist extremes to temperature conditions.

- They give an attractive blend of properties, for example, excellent thermo-oxidative stability, very good mechanical properties, low water absorptivity, and a higher level of flame resistance [25, 28].

1.5. Polymer metal complexes

Another significant category of polymer composition is those polymers developed from coordination with transition metal ions to form polymer-metal complexes. The function of transition metal ion or ligand in the structural perimeter is considered one of the fundamental important factors for the purpose of determining magnitude for polymeric ligand to develop complexes along with metal ion [29]. The term "polymer ligand" refers to a group of substances that make up oxygen, nitrogen, sulfur, and phosphorus whose highest filled atomic or molecular orbital has the higher energy which is generally called donor atoms. Polymer-reinforced ligands are developed as chemically modified with different monomers. These monomers that are modified are important for ion changers since They have the ability to be synthesized to pursued selectivity along with appropriate ionophore reagents. These ligands possessed high chemical and mechanical stability[30]. Those ligands are enormously used for metal ion complexation due to their accessibility, hydrophilicity, and high capacity. These ligands may comprise, amides, hydroxylamines, iminodiacetates, schiff bases, and phosphonates. Figure 1.13 shows the polymer-bounded MC–metal complexes

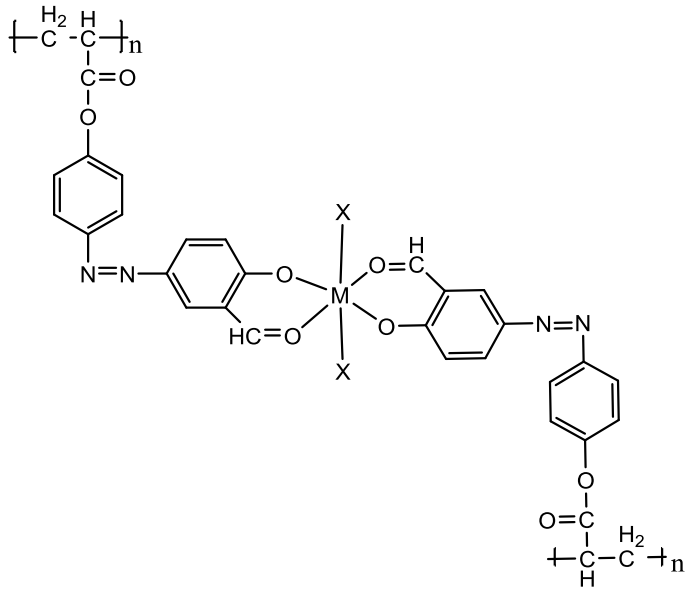

Figure 1.13. Scheme showing the polymer-bounded MC–metal complexes [31].

1.5.1. Preparation of polymer metal complexes

Normally, ligands like these are made by way of modification of crosslinked copolymers of polystyrene, poly(glycidyl methacrylate), poly(vinyl benzyl chloride), and polyacrylic acid. These polymers are of this kind that has a great deal of special practical characteristics. Not long ago, a lot of work in the past carried out on the polymer-metal complexes [30, 31].

1.6. Thermal Methods

The thermal analysis incorporates techniques to determine and record certain physical parameters of the system in relation to temperature (ΔT). Measures according to the dynamic relation involving temperature and mass, reaction heat, and volume [32, 33]. The Table 1.1 shows analytical methods classification. A thermogram of two-stage decomposition weight loss against temperature is indicated in Figure 1.14.

Table 1.1. Analytical methods classification [32, 33]

Name	Property measured	Apparatus Involved
Thermogravimetric Analysis	Weight Change	Thermo balance
Derivative Thermogravimetric Analysis	Rate of Exchange of Weight	Thermobalance
DTA	Heat absorbed or evolved	DTA apparatus

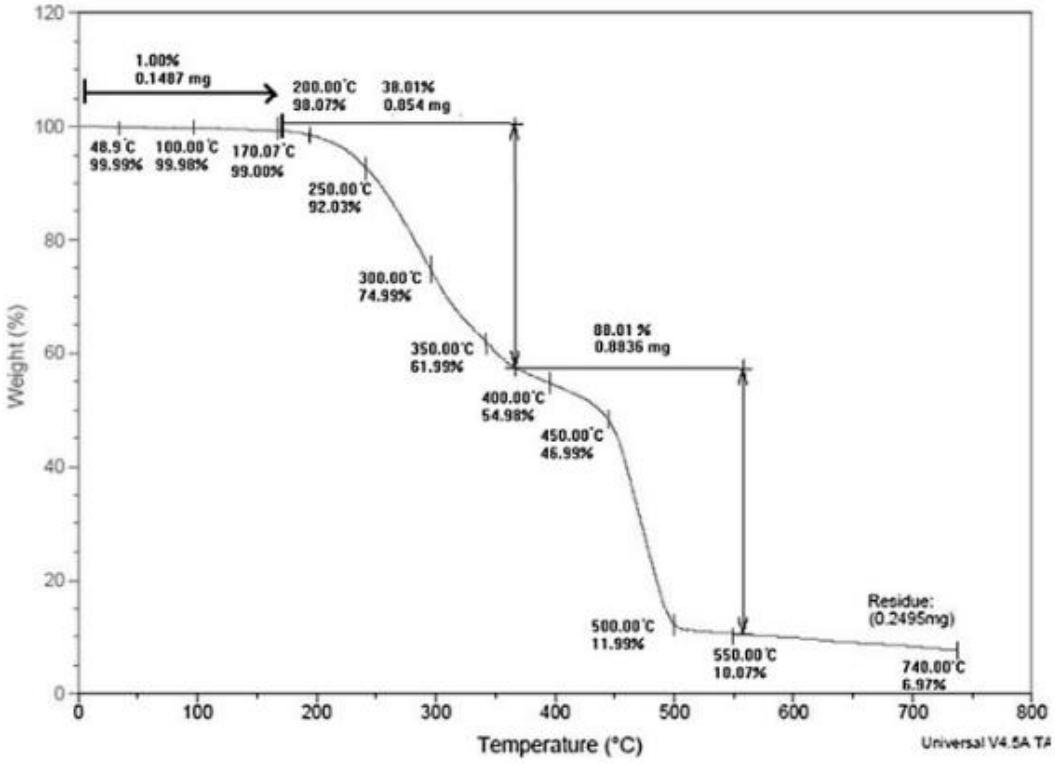

Figure 1.14. A thermogram two-stage indicating weight loss against temperature [32].

1.6.1. Thermogravimetric Analysis (TG)

This is the technique in which the substance's weight, cooled or heated under a controlled rate in an environment, is calculated as a function of time or temperature. There are a lot of chemical substances that decompose upon heating in each case or every occasion or stage and The concept of heating a sample is a novel one to take note of changes in weight is the fundamental principle of TGA. Three TG Types, including Isothermal, Quasistatic TG, and Dynamic TG [32, 33] are used.

- **Principle**

  The underlying principle of the feature can be demonstrated Using a compound weight loss graph.

- **Basic principles of thermal analysis**

  The modern thermal analytical instrumentation is typically divided into four parts [32, 33].

- **Instrumentation**

  There are two techniques of analysis are used such as Dynamic TGA and Isothermal TGA [32, 34].

1.6.2. Differential thermal Analysis

Principle

Differential Thermal Analysis (DTA) consists of the procedure for determining the temperature differential between a sample and a reference material, either as a function of time or as a function of temperature. As a result, the differential thermogram is made up of a record of the temperature differences between the sample and reference temperatures. (ΔT, differential temperature) plotted along with temperature (Ts) function. The substance together with the reference material shall be subject to a temperature regulation [32, 33].

- Emission of heat (exothermic)
- Absorption of heat (endothermic)

Figure 1.15 shows a graph of DTA signal with temperature

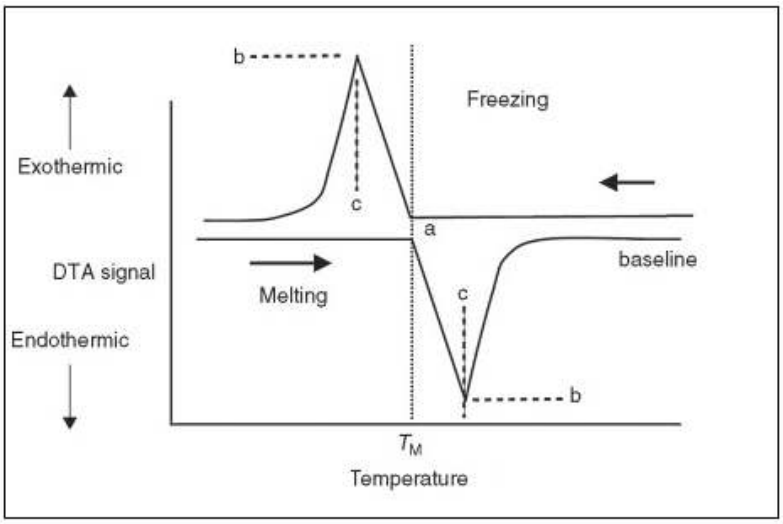

Figure 1.15. DTA [32, 33]

Endothermic peaks with sharp peaks demonstrate changes in processes of crystallinity or fusion while large endosperms mean a reaction to dehydration. Physical change results in endothermal curves while chemical reactions (particularly oxidative ones) give rise to exothermic peaks. DTA allows any chemical or physical change to be detected whether or not it is followed by the weight change [32].

1.6.3. Differential Scanning Calorimeter (DSC)

DSC operating mechanism centered may be divided into 2 (two) types such as Heat flux DSC and Power Compensated DSC. The instrumentation is made up of the Sample Holder, Thermobalance, Sensors, Temperature Controller, and Furnace [33]. Figure 1.16 shows the Heat flux DSC and power compensated DSC and their Differences are shown in Table 1.2.

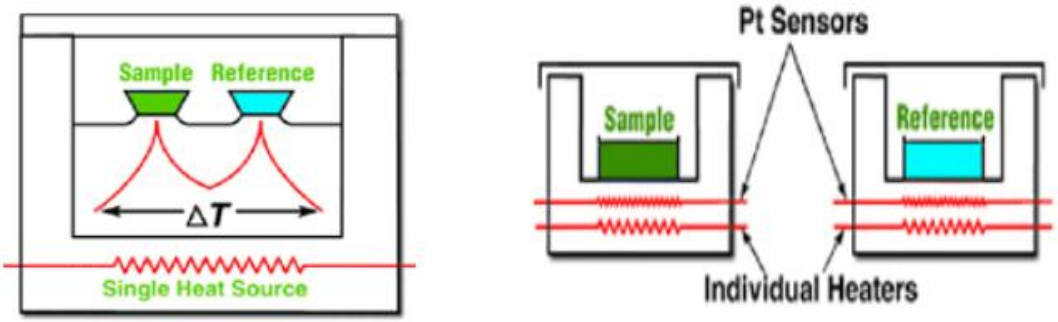

Figure 1.16. Heat flux DSC and power compensated DSC [33]

Table 1.2. Heat flux DSC and power compensated DSC

Heat Flux	Power compensated DSC
Sampleholder: reference and sample are connected by low-resistance heat flow path. Examples are: Aluminium sample pans, stainless sample pans, platium sample pans	Sample Holder: examples are: Aluminium sample pans, platinum sample pans, stainless steel sample pans,
Sensor: Temperature sensors usually thermocouples	Sensor: Pt resistance thermocouples, separate sensors and heaters for reference and sample
Furnace: one block for both sample and reference cell temperature	Furnace: Separate block for both sample and reference cell temperature
Temperature controller: the temperature difference between the sample and reference is measured	Temperature controller: Temperature differential thermal power is supplied to the heaters to maintain the temperature of the sample and reference at the program

The sample temperature would require less heat, by noticing the difference in the flow of heat between the reference and sample, DSC is capable to measure the amount of heat released or absorbed during such transition [33, 34].

Heat Capacity

When Heat is applied to both samples, the difference in heat output between the two heaters will be plotted versus temperature by the computer. Signifies, the heat absorbed by the sample is being plotted against the temperature. where t represents the time, ΔT represents the increase in temperature and q represents the heat [34]. Figure 1.17 shows The DSC Curve has three phases.

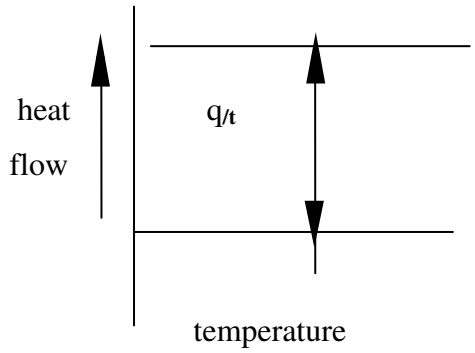

Figure 1.17. The DSC curve has three phases

- The glass transition temperature: A transition which is called endothermic transition which is the transition from solid to less viscous from
- Crystallization: the second transition known as an exothermic transition which shows a sharp negative peaks disorder to determine the amount of latent heat in a glassy solid for example in a polymer

- Melting: lastly a transition called An endothermic transition which shows a sharp positive peak, order to the transition that are disordered transition [33].

Figure 1.18 shows the Tg measurement of amorphous and semicrystalline

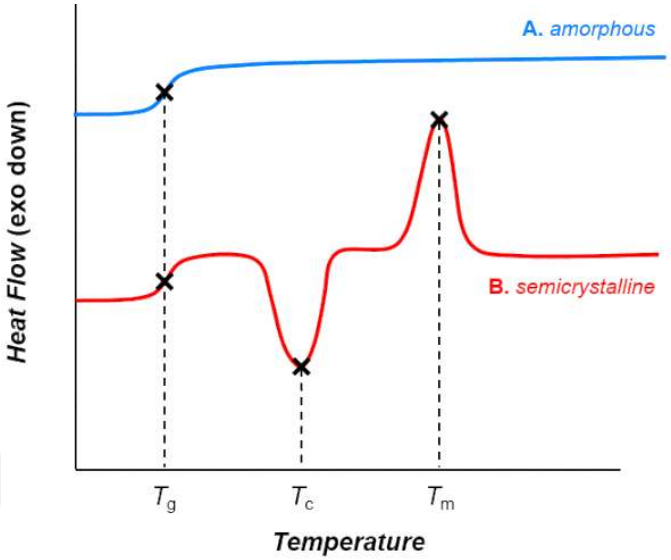

Figure 1.18. The T_g measurement of amorphous and semicrystalline [33].

1.7. MALDI-TOF Mass Spectrometry

1.7.1. MALDI

MALDI is a short form for "Matrix-Assisted Laser Desorption/Ionization." the MALDI sample is homogeneously mixed in a considerable amount of matrix. UV light (nitrogen laser light, 337 nm wavelength) is absorbed by the matrix and converted to heat energy. A little portion of the matrix heats up quickly (in a matter of nanoseconds) and vaporizes with the sample [35]. The Figure 1.19 shows a sample matrix mixture before and after laser irradiation.

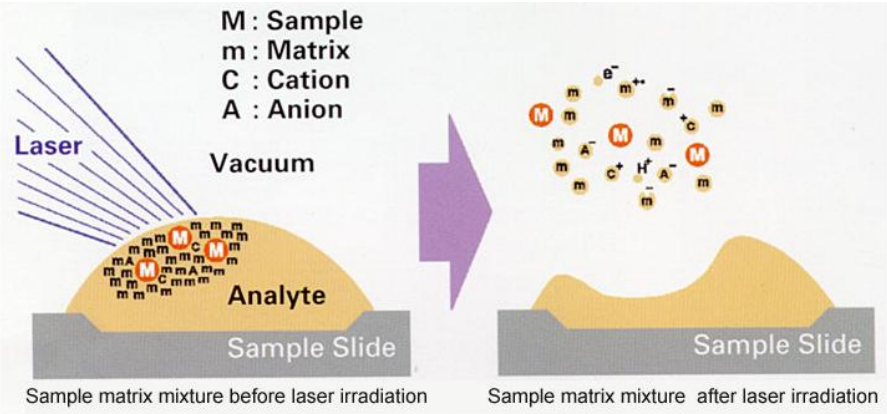

Figure 1.19. Sample matrix miture before and after laser irradiation

1.7.2. TOF-MS

TOF MS is a short form for Time of Flight Mass Spectrometry, the diagram below illustrates how charged ions of different sizes are produced on the sample slide. The following stages:

- Initially, samples are placed in the crystalline matrix and are subjected to laser bombardment after that, the molecules in the samples are vaporized and dispersed in the vacuum, and ionized concurrently
- After that, a high voltage is used to accelerate the charged particle.
- The second step is the time of flight mass spectrometry. After ionization, the particle will impinge on the linear detector in the linear mode within a few seconds. Molecules with a higher mass (high mass) arrive later than those with a lower mass (low molecule).

Time of Flight Mass Spectrometry is a type of mass spectrometry that takes account of these phenomena [35]. The Figure 1.20 shows Time of Flight Mass Spectrometry of the Charged ions of various sizes are generated on the sample slide

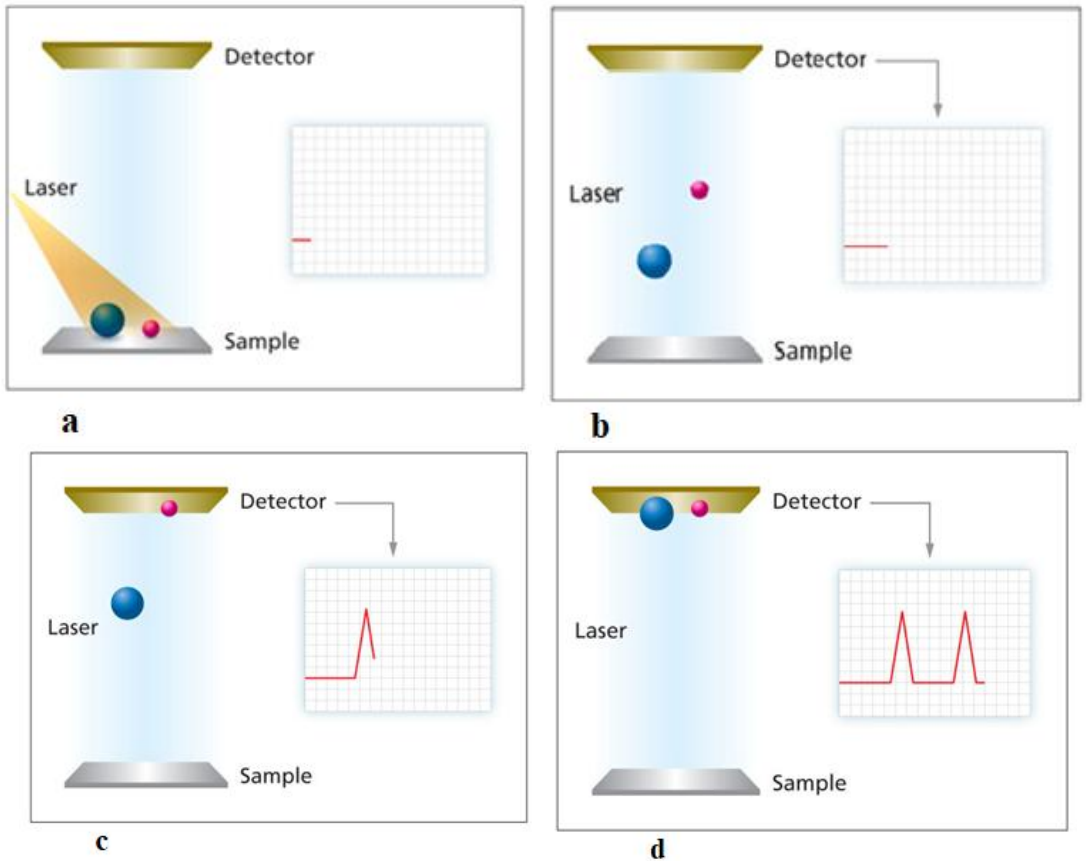

Figure 1.20. Time of Flight Mass Spectrometry of the charged ions of various sizes are generated on the sample slide

1.7.3. Advantages of MALDI-TOF Mass Spectrometry

- Direct measurement of molecules mass distribution
- Sample(maily singly charged ions mucheasily interpreted
- Fast time result (takes few minutes)
- Very high MW species can be analysed, for example Polymers
- Capacity for Insoluble analytes such as Nanoparticles [36]

The Figure 1.21 shows The MALDI-8020 is the latest in a long line of MALDI-TOF products from Shimadzu.

Figure 1.21. The MALDI-8020 is the latest in a long line of MALDI-TOF products from Shimadzu

1.8. Electrical conductivity

Electric conductivity, (σ) (in S/cm), of materials, in general, extends over a wide range, from 10^{-20} to 10^{6} S/cm

- This range is subdivided into conductors (10^{4} –10^{6}),
- semi-conductors(10^{-6} –10^{2}), and
- insulators (10^{-20}–10^{-6}). The tremendous

The transport of charge is referred to as electrical conductivity. The transporting charge may be delivered by unique species or different charge carriers. The Different carriers of charge might possess different masses, may interact differently to their environment, may react differently with changes in the external environments, might face various restrictions in relation to what they're capable of and what they are not. A charge carrier the most frequently found are;

- Electron
- Holes
- and Ions.

This class will be about first look into Why is it important to concentrate our learning on electrical conductivity [37]. We'll noticed that there are different forms of charges carries that carry changed species and these species may display Different behaviors. and in the end We have a good understanding of how conductivity has been measured. When we consider the various device, we can see that devices we regularly utilized on a frequent basis these days, it's simple to realize, many technologies rely on, or take advantage of, electronic properties of the materials. electrical appliances, Toys, and cars are some examples in which electronic devices have taken their place or supplemented some mechanical systems. Previously, when opening and repairing toys were possible because They were built on mechanical principles, when you open today's toys, you're confronted with an electrical chip, and Normally, the process of repair comes to an end. There are many modern cars that possess high-tech electronics that are helpful to them optimize their fuel economy, control the braking process, or regulate the traction of the wheels, etc.[37, 38]. As already stated are only a couple of examples of How pervasive computer has become in modern society.

1.8.1. Conductivity

The property of conductivity is of great interest to us because of a few differences of the electronic properties that a material can display. To begin with, the term "conductivity" is probably the most widely used technologically, in the electronic property both in terms of high-quality wire conductors and Insulation for the wires provided using bad conductors. The second point to consider is, It turns out that the excellent electrical conductors and the poor conductors of electricity, conductivity varies by more than 24 order of magnitude [39, 40]. Silver, silver for example has a conductivity of around 107 Ω^{-1} m^{-1}, The conductivity of teflon is less than 10^{-17} Ω^{-1} m^{-1}. It exists virtually there is nothing else exhibiting such a large difference in its expression in many materials. From the technological standpoint, therefore, the study of electrical conductivity is attractive, because of its vast application, as well as from a scientific point of view, it is fascinating to see if it's possible to categorize theories that can account for such a large variation throughout the property. If we look more deeply at most of the features of conductivity, we can see that it is fundamental to comprehend that electrical conductivity is the carrying of charges in the broadest sense.

1.8.2. Electrical conductivity in polymers

The electrical properties of polymer materials are composed of a wide spectrum. The electrical conductivity of polymer materials, for example, changes from insulators to conductors. These spread across the whole spectrum [41].

1.8.3. Electrical conductivity in Conjugated or Conducting polymers

Insulators are the majority of polymeric materials. The number of polymers containing double bonds that have been conjugated starts to be electrically conducted via treatment with reducing or oxidizing agents. In 1977, a polymer was discovered to be capable of conducting electricity of this type of polymer. Different from or unlike saturated polymers which have no electronic interest because all of their carbon atom valence electrons are paired, conjugated or conductive polymers with one unpaired electron (p-electron) per carbon atom. They contain a p-conjugated system in which the carbon pz orbital overlaps with other orbitals of the successive carbon atoms resulting in electron delocalization along the polymer chain's backbone. Examples are polyaniline, polyacetal, and polythiophene [40]. The Figure 1.22 shows scheme showing conjugated systems in polymers.

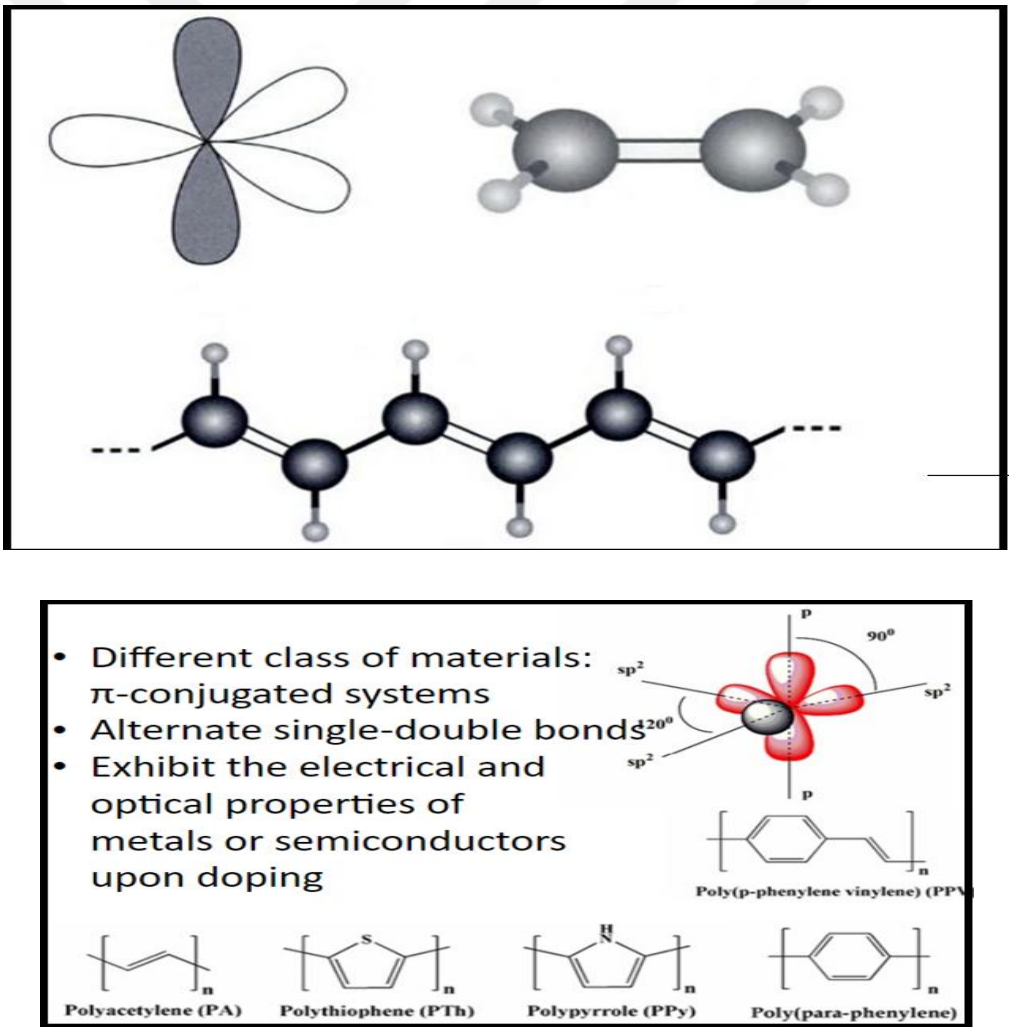

Figure 1.22. Scheme showing conjugated systems in polymers [40].

1.8.4. Electrical conductivity in Saturated polymers

Through incorporating or adding fillers with high conductivity such as graphite, graphene, and carbon nanotubes, the insulating polymers' conductivity can be increased or enhanced to some extent. Such polymers are called polymer composites, the composites' response to an applied electrical field or the material's dielectric properties of the polymer composites are of great importance because of various electrical applications [40, 42].

The ε’ is a significant dielectric property (the material's electrical energy storage capacity). The application of polymers is common in many electrical applications like capacitors, because of their strong dielectric constant values. In the electronic industries, both low and high dielectric constants are needed. The low dielectric constant is mainly used as insulators [38]. They are also passivation materials [42]. Their applications included the separation of signal-carrying conductors from one another, rapid signal propagation, dielectric interlayer in order to reduce resistance-capacity (RC) time delays, high-density crosstalk and power dissipation, and high-speed integration. They actually are important densely packed multi-layered ICs, where it is appropriate to suppress the coupling between very near metal lines in order to avoid system performance degradation [Packaging and encapsulation are part of that function. We detach interlayers in electronic packaging and provide isolated paths in multilayer printed circuit boards for connecting electrical devices. As when the trend towards miniaturization in the manufacture of microprocessors, any reduction in relative permittivity would reduce the deleterious impact of stray and coupling capacities. Additionally, dielectric materials are used to encapsulate the balls that bridged the die and substratum. A distinct encapsulation, which is referred to as underfill assists to protect any circuit failures as well as reduce the thermal mismatch between the layers of the bridges. Small dielectric encapsulation materials are used to insulate the lead frame housings [40, 42].

The most important property in thermal processes is thermal conductivity *k* which helps in quantifying the passage of heat through a substance [41] can be described, as the energy is transported is directly proportionally to the speed of sound. In this case, thermal conductivity according to the relation

$$k_{=} C_p \text{ P.u.l}$$

where u represents sound velocity and *l* represents the molecular separation. The thermal conductivity of amorphous polymers rises as the temperature increases, they're up to *Tg* (glass transition temperature). Over *Tg*, as the temperature rises, the thermal conductivity decreases [42]. Because of the increase in density based on solidification on the semi-crystalline thermoplastics, the solid-state has a higher thermal conductivity than the liquid state. However, when in the liquid stage, the thermal conductivity of semi-crystalline polymers decreases to the

level of amorphous polymers. Moreover, it should come as no surprise that, melt thermal conductivity rises as hydrostatic pressure rises [43, 44].

1.9. Dielectric properties of polymers

When a potential difference (voltage) is applied, the electrons are free to travel, and the flow of current occurs. The main long chain and side groups of polymers, as well as the electrons of the atoms that make them up, are firmly connected to the central long chain and side groups via "covalent" bonding. Because most common polymers can't enable electron mobility due to covalent bonding, they serve considered insulators. Electrons can move about when a potential difference (voltage) is applied, and when electrons can travel freely, current flows [45].

1.9.1. Polar and non-polar polymers

Not every polymer behaves in the same way when voltage is applied and to describe the differences in the behavior of plastics, they might be classed as polar or non-polar. The bonds between polar polymers are not totally covalent. and there is a little distortion in the molecule's electronic charge. This type behavior can be explained in a simple way, which would be the case of H_2O (water molecule). A polar water molecule is typically shown as illustrated in the Figure 1.23.

The two atoms of hydrogen are joined to atom oxygen, and the molecule as a whole is neutral. Actually, Electrons tend to gather around oxygen atoms more than atoms of hydrogen, and This results in a slightly negative charge for oxygen and a little positive charge for hydrogen atoms. This is demonstrated in the image to the right, where the grey areas represent where electrons are found more frequently.

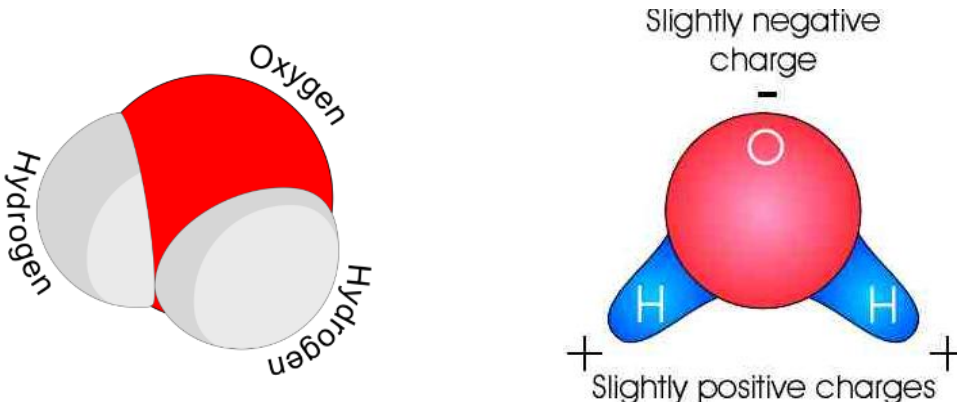

Figure 1.22. A polar water molecule

The water molecule as a whole is electrically neutral and does not carry any charge, but the electron imbalance generates a polar molecule. When there is an electric field present, this 'polar dipole' will move and try to align with the electric field in the exact same manner that the needle of a compass tends to align with the earth's magnetic field [46].

1.9.2. Dielectric Constant (alternating current)

The dielectric constant is a measure of the effect of a dielectric on the capacitance of a condenser. It set on how usefully a substance is used to separate the plates in a capacitor and is explained as "the proportion of an electrode set's capacitance to the dielectric material's capacitance between them to the capacitance of the identical electrodes in the presence of a vacuum. For a vacuum, the dielectric constant is 1, but it is larger than 1 for all other materials [47]. The Figure 1.24 shows a condenser with dielectric constant for a vacuum and Figure 1.25 indicates the condenser with dielectric material.

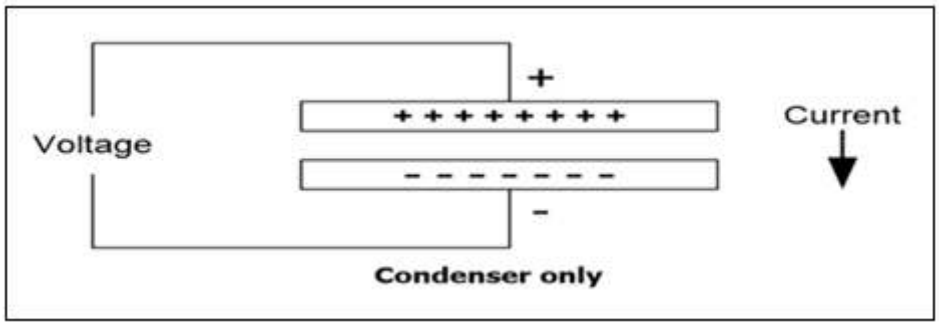

Figure 1.23. The dielectric constant for a vacuum

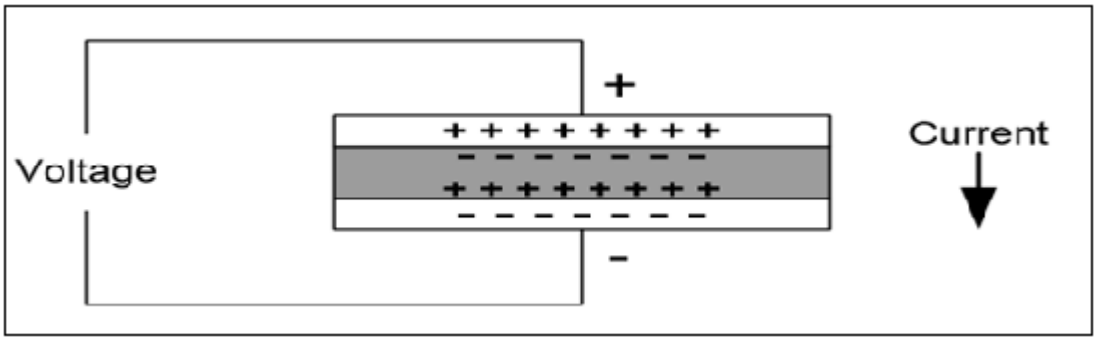

Figure 1.24. The Condenser with dielectric with material

As a polar polymer, the alternating current frequency is a significant factor due to the time it took to line up the polar dipoles. Low-frequency implies the dipoles have the necessary amount of time to line up with the field before it reverses position and It has a high dielectric constant. high-frequency implies, the dipoles don't have enough time to line up before the direction of the field

changes. Hence, the dielectric constant has decreased. In the middle frequency range the dipoles moves, but they haven't completed their move yet. prior to the field changes direction and they are required to realign with the changed field. Plastics that are polar, when the frequency is low (60 Hz) in general have dielectric values ranging from 3 to 9, and operate when the frequency is high (106 Hz). The dielectric constants of most materials are between 3 and 5. For plastics that are non- polar, the dielectric constant is independent in the alternating current frequency as a result, the polarization of electrons occurs almost instantly. Plastic that is non- polar always has dielectric constants of a minimum of 3 [48].

1.9.3. Electrical Property Determination

The capacitance, resistance, dissipation factor (dielectric constant), and dielectric loss factor are all accurately determined with an LCR meter at room temperature by adjusting frequencies. Square samples with a thickness of 3 mm, a length of 10 mm, and a width of 10 mm are commonly used. The samples were held in place by two electrodes.

- The volume resistivity (ρ):

The following equation can be used to compute it from a resistance,

$\rho = RA/t$

so that,

A is the area of the sample's cross-section, R is the resistance of the sample, t is the thickness of sample

The dielectric constant ($\varepsilon^{'}$) :

This equation can be used to compute it from capacitance.

$\varepsilon^{'} = C/\varepsilon_0 A$

so that, ε_0 is the permittivity of air (8.85×10^{-12} Fm^{-1}), C is the capacitance with dielectric [49], A is the area of cross-section of the sample, and t is the thickness of the material or sample.

- The dielectric dissipation factor (tan δ) : As a result, the following can be deduced:

$\tan(\delta) = \varepsilon^{''}/\varepsilon^{'}$ [50]

whereby $\varepsilon^{''}$ is the dielectric loss.

- The dielectric loss factor ($\varepsilon^{''}$) :

can be computed in the following manner::

$\varepsilon^{''} = C/C_0\omega$

so that, C is capacitance of a material, C_0 is the capacitance without dielectric, ω is the angular frequency

1.10. Literature Review

Phthalocyanine-containing polymers [26, 51, 52] can be taken into account as strong and materials that can be processed in which the relative orientation of the constituent Pc units in control by strong covalent bonding. Because of this, the introduction of Pcs into macromolecules is a really effective tool to produce the latest materials possess excellent properties [53, 54]. Polymers containing PC can be identifiable by the manner in which the macrocycle is incorporated within the macromolecular structures, Specifically, as a side group, in the main chain, or in the formation of a polymeric network. [55]. Pcs can be used as side groups of a main polymeric chain [26, 56]. There are two approaches for achieving this goal. One of them involves the polymerization (or copolymerization) of unsymmetrically substituted Pcs, i.e., holding reactive sites at one of the isoindole subunits. The second one requires the preparation of a polymer with side functional groups that can react in a further step with an appropriately functionalized Pc. The integration of a polymer chain might affect the organization of various phthalocyanine molecules. Phthalocyanines and their metal complexes have been incorporated into macromolecular structures as a side group, in the main chain or in a polymeric network [57]. The distance between the two Pc units may affect the degree of interactions between the rings [58]. However, there have been reported a few examples of the polymers containing a terminal and side phthalocyanine group. McKeown and co-workers have reported on the liquid crystalline properties of asymmetric phthalocyanines with one poly(ethylene glycol) chain [59]. The electronic properties of ball-type Pcs can change dramatically depending on the bridging compounds or the central metal [60,61].

In this paper, we describe the syntheses, thermal and dielectric properties of new peripherally substituted ball type cobalt phthalocyanine complexes via integration of Pcs into a single-chain polymer structure. The precursor linear copolymers prepared by free radical polymerization method were amphiphilic poly(PNDEAMSt-*co*-St) random copolymers containing PNDEAMSt units in the ratio of 2 and 6% by mol. According to our literature investigations, it has indicated that there is almost no information about ball type Pcs via integration of Pcs into a single-chain polymer molecule. Therefore, the objective of this investigation is to characterize and to develop a new single-chain polymeric system So, this study is an original study. The above gaps are partially filled with our current research. Thus, the Co(II)-mediated single-chain collapse of the precursor was carried out in the cyclohexanol being a good solvent for linear precursor copolymers prepared from DEAMSt and St monomers. Average apparent activation energies of the thermal degradation of SCP-ball type CoPc2 calculated by three model-free methods in a period of α = 0.07–0.90 have been estimated. The ac dielectric measurements of the precursor linear copolymer2, SCP-ball type CoPc2 were

investigated at room temperature between 100 and 2 kHz depending on the alternating current conductivities.

2. MATERIAL AND METHODS

2.1. Materials

- 4-Nitrophthalonitrile
- Anhydrous sodium carbonate
- Cobalt(II)acetate tetrahidrat
- Styrene was purchased form Sigma–Aldrich
- Dimethylformamide (DMF)
- Tetrahydrofuran (THF)
- Diethanolamine was obtained from Saarchem

All solvents were dried and purified. All the other reagents were used as received

2.2. Characterization

- Furier-Transform Infrared (FT-IR) analyses were conducted on a Perkin Elmer Spectrum One FT-IR spectroscopy. Infrared (FT-IR) spectroscopy were used to characterize all the samples.
- ^{1}H and ^{13}C-NMR spectra by means of a Bruker Avance III 400 spectrometer were recorded using $CDCI_3$ and DMSO-d_6 as solvent. ^{1}H and ^{13}C-NMR(400 MHz) spectra in presence of $CDCl_3$ containing tetramethylsilane in the ppm level were recorded
- The glass transition temperatures (Tg) the linear copolymer precursor, SCPM-ball type CoPc and their composites were measured using a Shimadzu Differential Scanning Calorimetry (DSC-50) instrument. The measurements were performed using virtually 5 mg of sample at 20 ^{o}C/minute rate depending on increase in temperature up to 200 ^{o}C.
- The T_g values were estimated from a midpoint of transition range. Thermogravimetric (TG) behaviors were investigated up to 500 ^{o}C using a thermogravimetric analyzer system under 10 ml/min argon flow (Shimadzu model, TGA-50). The dynamic weight loss measurements were conducted on a Shimadzu TGA-50 thermogravimetric analyzer (TGA). All the measurements were carried out in an argon gas flow (10 ml/min) using sample weights of 5 mg from 25^{o}C to 500 ^{o}C at a scan rate of 10 ^{o}C/min.
- UV–Vis absorption and diffuse reflectance spectra were obtained using a Aurora 4000 TG-UV-NIR, UV–Vis–NIR spectrophotometer.
- Mass spectra were recorded on a Rapiflex MALDI-TOF-MS. In the MALDI-TOF-MS experiments, 3 mg polymeric sample was dissolved in 1 ml THF. For the MALDI matrix solution, 20 mg of DCTB MALDI matrix was dissolved in 1ml methanol. Then, MALDI matrix solution and sample solution was mixed each other in 5:1 ration and finally 1 mL

from final solution was deposited onto the MALDI target and analyzed in MALDI-TOF-MS. Mass calibration of MALDI-TOF-MS was performed by the peptide mixture standard solution (Bruker Daltonics, Bremen-GERMANY).

- The dielectric and electrical behaviors of the polymer and composite materials were performed on tablets prepared under a pressure of four tons. For dielectric measurements, a QuadTech 7600 LRC Impedance Analyzer from 100 Hz up to 2 kHz was used. The electrical characterization measurements were carried out using the FYtronic Electric Characterization device.

2.3. Experimental

2.3.1. Modification of 4-chloromethyl styrene with diethanolamine to formed DEAMSt Monomer

4-Chloromethyl styrene was modified in accordance with the method adapted from the literature [62] 15 g (0.098 mol) of the CMS was added to the 250 mL flask, followed adding in 10mL THF and 20mL DMF. Diethanolamine 11.36 g (0.108 mol) and $NaHCO_3$ 12 g (0.143 mol) were put to the mixture. The reaction mixture was refluxed for one day. The reaction mixture was then filtered and the filtrate was evaporated to remove the solvent (THF and DMF). A reddish brown solution was obtained (DEAMSt). The modified monomer (DEAMSt) was shown in Figure 2.1. FT-IR, ^{1}H-NMR, and ^{13}C-NMR methods were used to determine the structure of DEAMSt monomer. The Figure 2.1 shows the reaction of 4-chloromethyl styrene and diethanolamine to formed DEAMSt Monomer. Also, DEAMSt and St monomers were copolymerized by free radical polymerization method in presence of 1,4-dioxane at 60 ^{o}C. Reaction scheme of P(DEAMSt-co-St) was indicated in Figure 2.1.

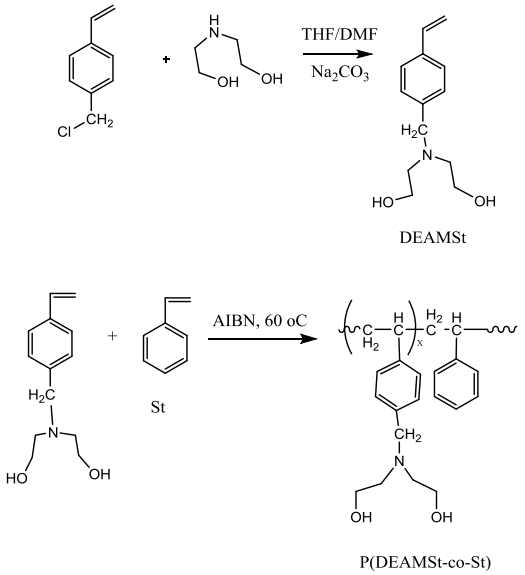

Figure 2.1. Synthesis of DEAMSt monomer and P(DEAMSt-co-St)

2.3.2. Synthesis of 4,4'-((((4-vinylbenzyl)azanediyl)bis(ethane-2,1diyl))bis(oxy))

Diphthalonitrile (PNDEAMSt)

The target precursors were prepared by reaction of 4-nitrophthalonitrile and 4-diethanolaminomethyl styrene. For this purpose, 4-diethanolaminomethyl styrene (1.05 g, 0.00475 mol) and 4-nitrophthalonitrile (1.65 g, 0.0095 mol) were added with stirring to dry dimethyl formamide (DMF, 20 mL). The mixture was passed with nitrogen gas flow. The reaction was carried out at 70°C for 24 h. The reaction during it was added Na_2CO_3 (1.51 g, 0.0142 mol) to the mixture over a period of 6 h. The solution was filtered. After this one, it was then poured into 200 mL of ice-water mixture and it was stirred for about 10 min. The precipitated PNDEAMSt in the aqueous mixture was filtered. Then, the PNDEAMSt was dried on air. The brown solid was soluble in chloroform, tetrahydrofuran (THF), dimethyl formamide (DMF) and dimethylsulfoxide (DMSO). Figure 2.2 shows the preparation of PNDEAMSt monomer and poly(PNDEAMSt-co-St).

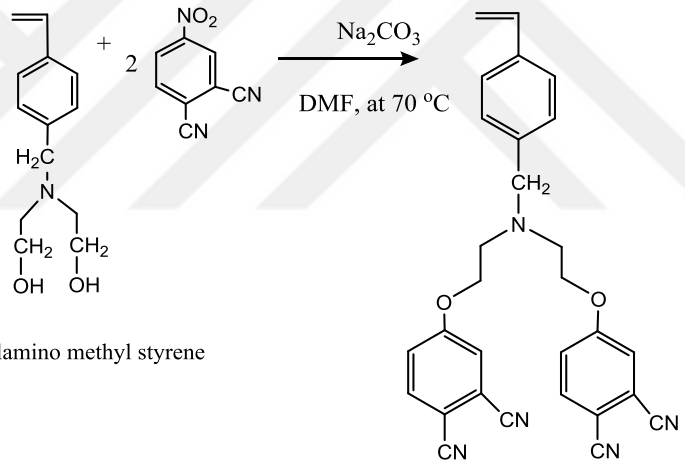

4-Diethanolamino methyl styrene

(PNDEASt)

4,4'-((((4-vinylbenzyl)azanediyl)bis(ethane-2,1-diyl))bis(oxy))diphthalonitrile

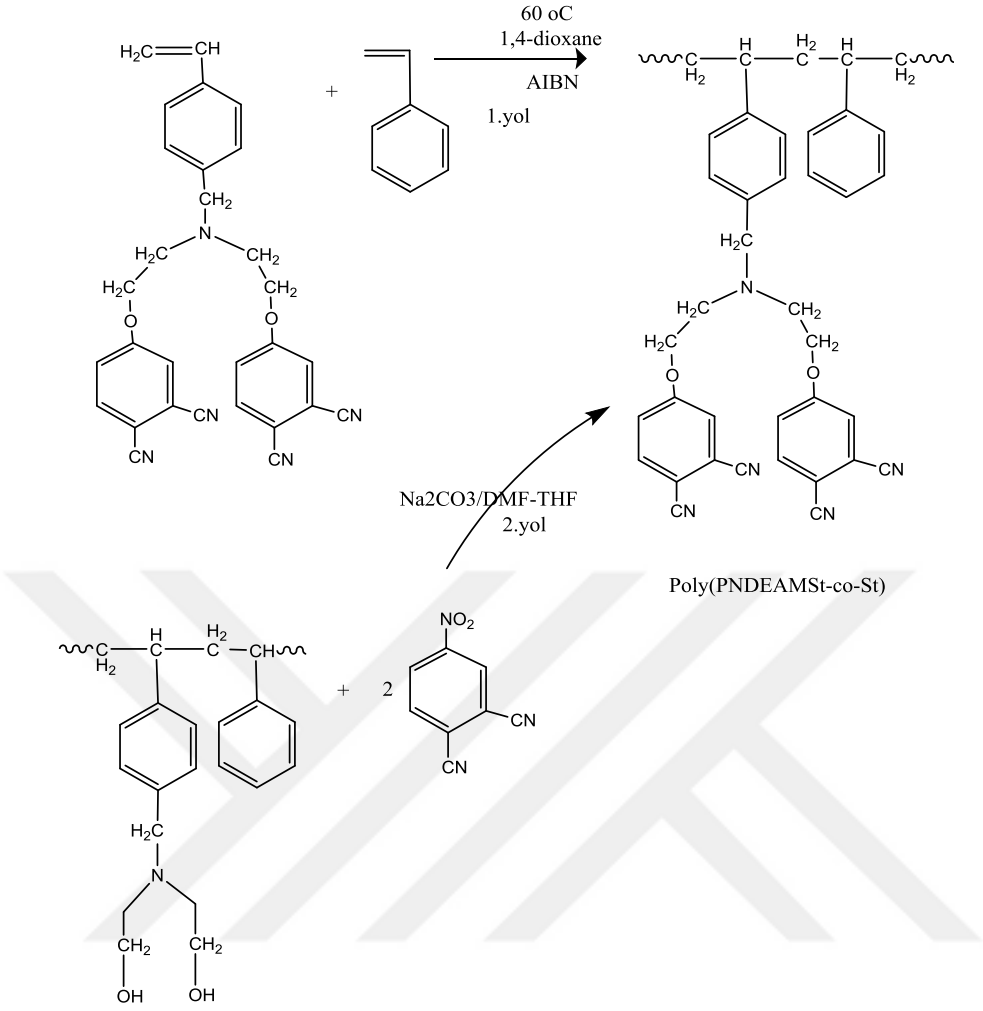

Figure 2.2. Synthesis of PNDEAMSt monomer and poly(PNDEAMSt-co-St)

Mechanism of nucleophilic aromatic substitution reaction as a result of elimination of NO_2 group on aromatic ring bearing nitril or nitrils was indicated in Figure 2.3.

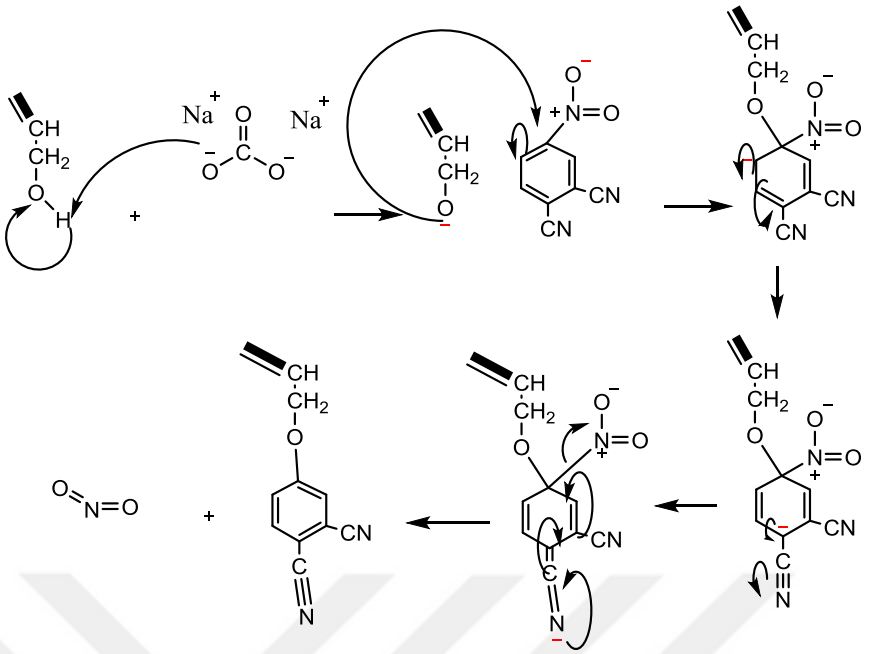

Figure 2.3. Mechanism of nucleophilic aromatic substitution reaction

2.3.3. Free radical copolymerization of PNDEAMSt and Styrene

The copolymerization of PNDEAMSt and styrene was carried out at 60 ^{o}C in presence of 1,4-dioxane using AIBN as initiator. PNDEAMSt and styrene monomers, AIBN and 1,4-dioxane as solvent were mixed within two different polymerization tube. The mixture was passed from argon gas about 5 minutes, and then it was incubated in a preheated oil bath to 60 ^{o}C. After a desired time, the mixture of polymerization was cooled to about 25 ^{o}C. The prepared copolymers were isolated by precipitating within excess ethyl alcohol and purified by reprecipitation, and later the copolymer systems were dried under vacuum at 40 ^{o}C for one day.

Figure 2.4. shows the copolymerization of PNDEAMSt and styrene to produced poly(PNDEAMSt-co-St).

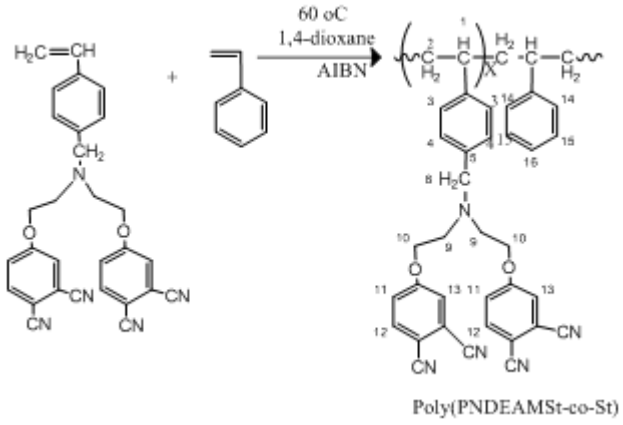

Figure 2.4. Copolymerization of PNDEAMSt and styrene to produced poly(PNDEAMSt-co-St)

2.3.4. Synthesis of Intramolecular Ball-Type Cobalt Phthalocyanine Complexes with Single-Chain Polymer Structure (SCP-ball-type CoPc2)

The precursor copolymer, poly(PNDEAMSt6%-co-St), (320 mg, 0.156 mmol), $Co(CH_3COO)_2.4H_2O$ (19.6 mg, 0.078 mmol), phthalonitrile (116.8 mg, 0.91 mmol) and 150 ml cyclohexanol as solvent were added to a reaction flask. The mixture was refluxed by adding 2 drops of DBU between 140-150 °C for 36 h under argon atmosphere. In addition, the SCP-ball type CoPc1 was synthesized using precursor copolymer, poly(PNDEAMSt2%-*co*-St), under similar conditions. The after cooling to room temperature, the reaction mixture was precipitated into excess cooled ethyl alcohol. The product was filtered, and the greenish products was dried under vacuum at 40°C. The Figure 2.5 and Figure 2.6 show the synthesis and representation of SCP-ball type CoPc.

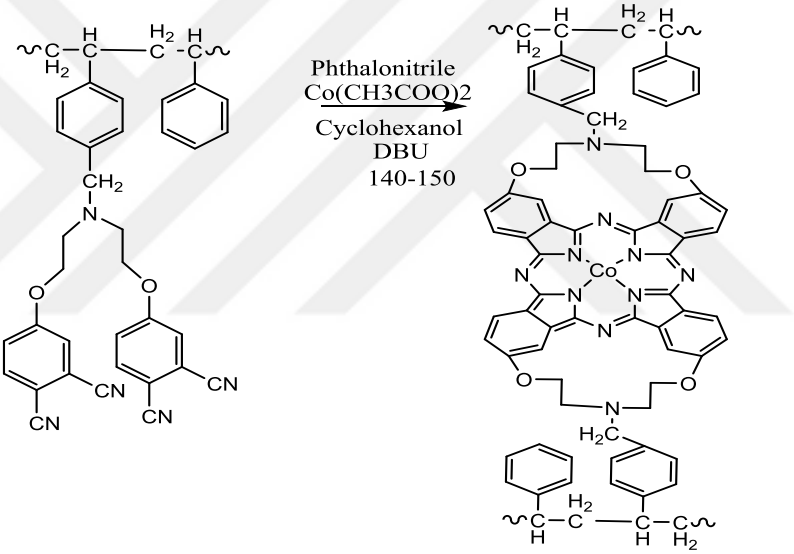

Figure 2.5. Synthesis of SCP-ball type CoPc

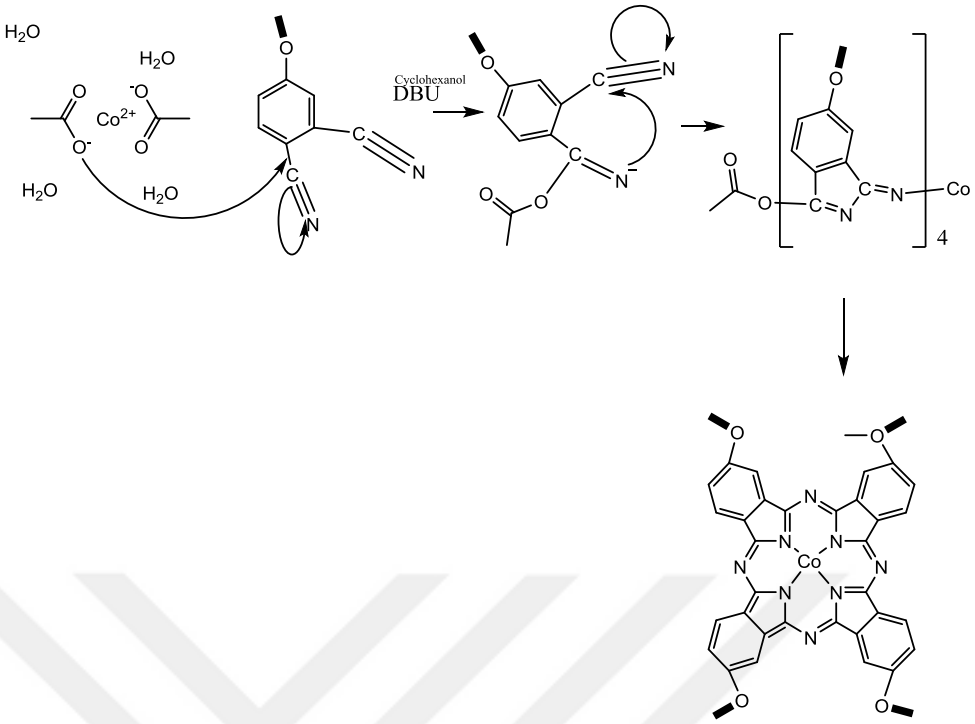

Figure 2.6. Mechanism of phthalocyanine formation [63]

Synthesis scheme of intramolecular ball-type cobalt phthalocyanine complexes with Single-chain polymer Structure (SCP-ball-type CoPc) was illustrated in the Figure 2.7.

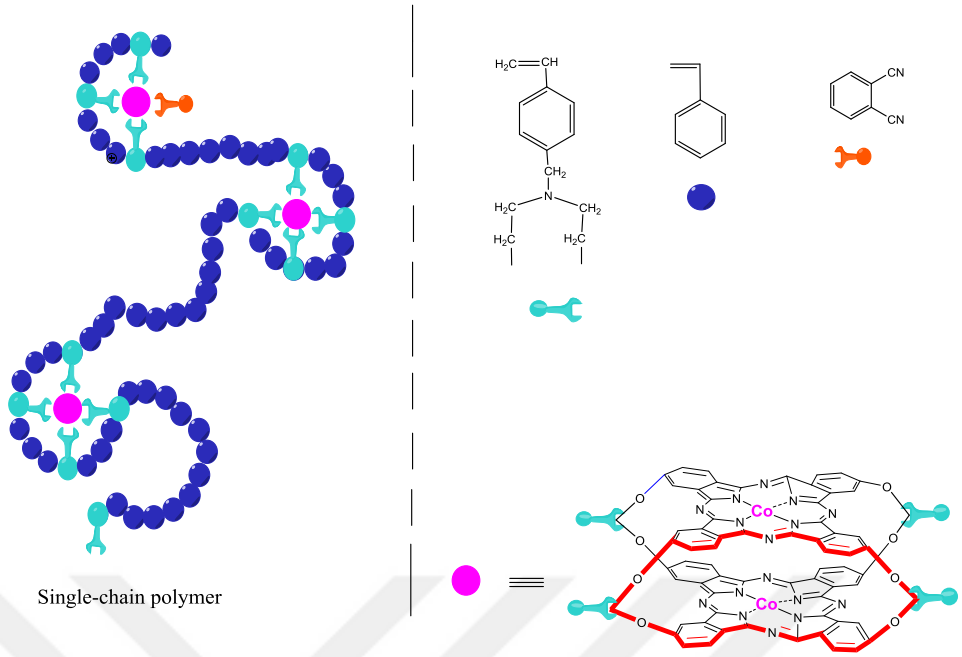

Figure 2.7. Representation of SCP-ball type CoPc

2.3.5. Preparation of linear copolymer precursor [P(PNDEAMSt 12%-co-Styrene)]

PNDEAMSt (280 mg, 0.59 mmol) and styrene (1980 mg, 19 mmol) were copolymerized using AIBN as the initiator in the presence of 1,4-dioxane. Within about 10 minutes, the solution was passed from argon gas and then incubated to 60°C in a preheated oil bath. The polymerization mixture was cooled to room temperature after the required time. The produced copolymer was separated by precipitating in excess ethyl alcohol, and then the linear copolymer precursor was dried in vacuum for one day at 40 °C.

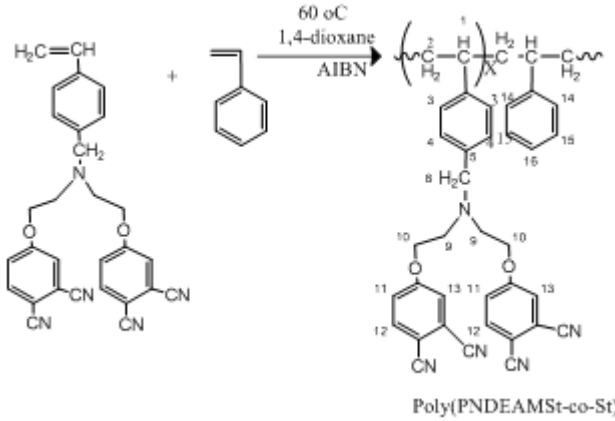

Figure 2.4 shows the copolymer structure of PNDEAMSt and styrene.

2.3.6. Synthesis of SCPM-ball type CoPc

SCPM-ball type CoPc was prepared according to procedure as follow: the linear copolymer precursor, poly(PNDEAMSt12%-co-St), (400 mg, 134 mmol), $Co(CH_3COO)_2{\cdot}4H_2O$ (50.0 mg, 0.20 mmol), phthalonitrile (200 mg, 1.56 mmol) and 140 ml of cyclohexanol was added to the reaction flask as a solvent. The mixture was refluxed at 140-150 ^oC for 34 h under the argon atmosphere in 1,8-diazabicyclo[5.4.0]undec-7-ene (DBU) (2-3 drops). The reaction mixture was cooled to room temperature, and it was slowly precipitated within cooled excess ethyl alcohol. The greenish polymer was filtered and dried under vacuum for 24 hrs at 40 ℃. The Figure 2.8 shows structure of; A) linear copolymer precursor B) SCPM-ball type CoPc.

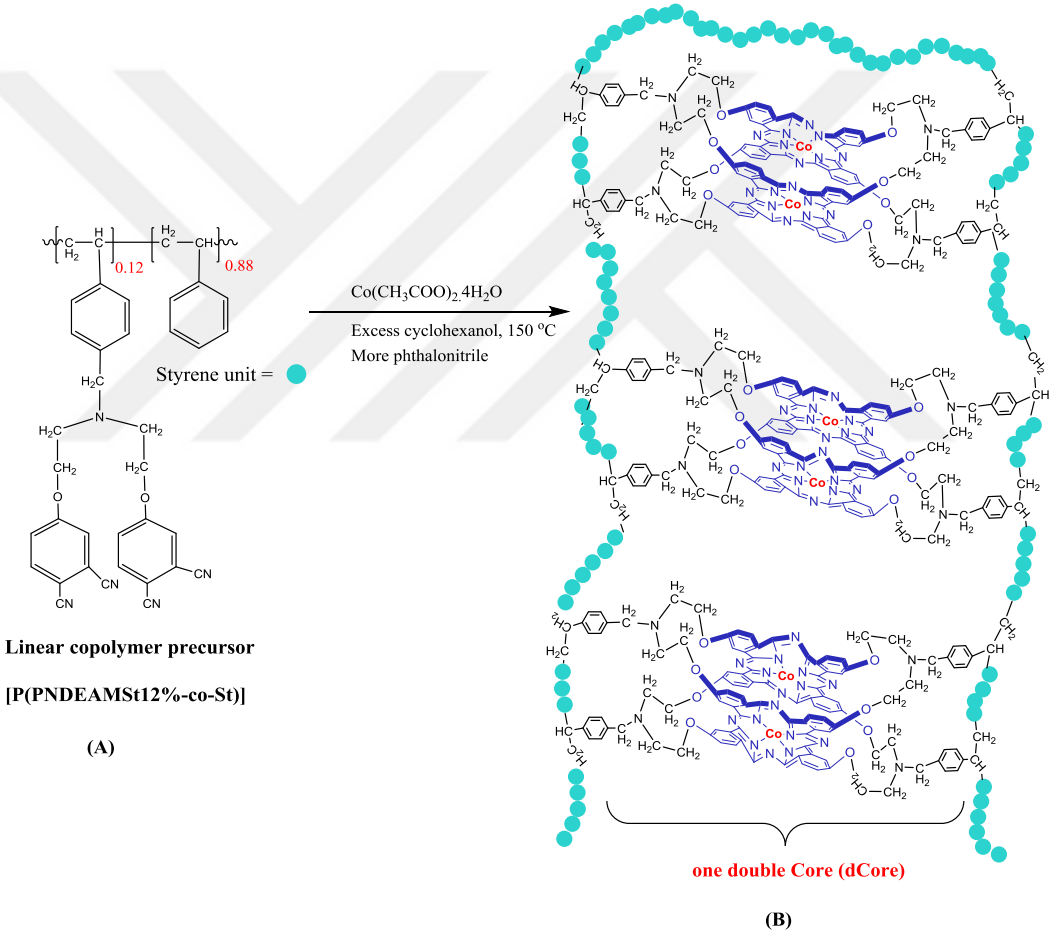

Figure 2.8. The structure of A) linear copolymer precursor B) SCPM-ball type CoPc

2.3.7. Synthesis of Graphite Oxide

Flakes of graphene oxide, Danubia NanoTech has produced, the method was adapted from Hummer's method (Han and coworkers) [64]. For this purpose, graphite (1 g) was treated with mixture of HNO_3:H_2SO_4 (1:3; v/v) (25mL). Refluxing took place for 10 minutes, with the vigorous evolution of NO_2. Next, upon reaching room temperature (2 hours), the oxidized

graphite was filtered off. Finally, graphite oxide was rinsed thoroughly with water to a pH=7.0. The graphite oxide was dried at a temperature of 85 ^{o}C for 12 hours. Figure 2.9 shows synthesis scheme graphite oxide prepared by Hummer's method.

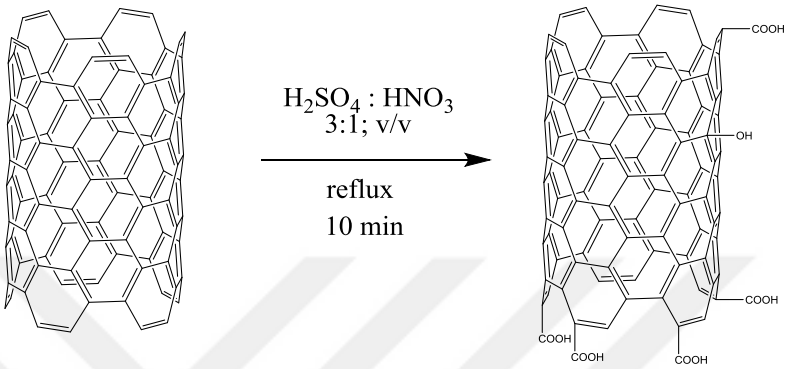

Figure 2.9. Synthesis of Graphite Oxide

2.3.8. Preparation P(PNDEAMSt 12%-co-St)/GO and SCPM-ball type CoPc/GO composites

The preparation of P(PNDEAMSt12%-co-St)/GO and SCPM-ball type CoPc/GO composites was as follows. Initially, the dispersion of graphite oxide was carried out in the CGOLDENWALL Ultrasonic Homogeniser Sonicator Processor 300 W-500 mL Cell Distruptor Mixture for 3 hours at 50 W. The graphite oxide filler in the required amount was added into every of polymer matrix the predissolved in dichloromethane and mixed mechanically at a ratio of 3.6 wt%, 4.5 wt %, 6.5 wt% and 14 wt%. After this process, the mixture was subjected to ultrasonic dispersion for 5 minutes for a proper filler dispersion. The dichloromethane was removed from the polymer composites. Then, the composites were dried for 24 h under vacuum to constant weight at 40 ^{o}C.

3. CHAPTER RESULTS

3.1. Linear Copolymer Precursor1, P(PNDEAMSt2%-*co*-St)

The characterization of copolymers was carried out using FT-IR and ^{1}H-NMR analysis.

3.1.1. Characterization of P(DEAMSt2%-*co*-St)

The FT-IR spectrum of linear copolymer precursor1 or P(DEAMSt2%-*co*-St). The FT-IR spectrum of poly(DEAMSt2%-co-St) is indicated in the Figure 3.1 and evaluated in Table 3.1.

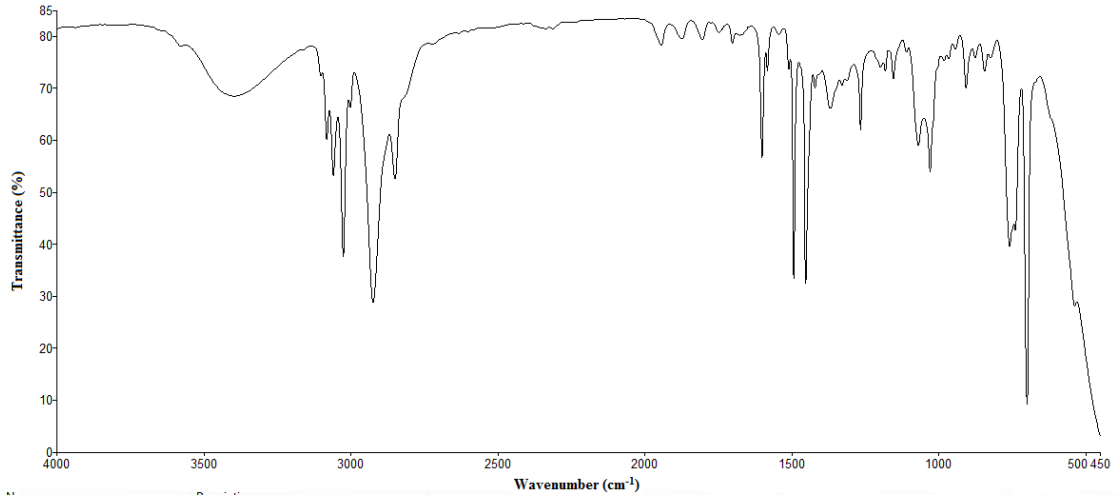

Figure 3.1. FT-IR spectrum of poly(DEAMSt2%-co-St)

Table 3.1. FT-IR spectrum evaluation of poly(DEAMSt2%-co-St)

Wavelength (cm^{-1})	Vibration Type
3400	O-H stretching
3025-2924	C-H stretching on the aromatic and aliphatic groups
1601	C=C stretching
1265	C-O stretching
699	C-N stretching

The Figure 3.2 shows the ^{1}H-NMR spectrum of poly(DEAMSt2%-co-St) or linear copolymer precusor and evaluated in Table 3.2.

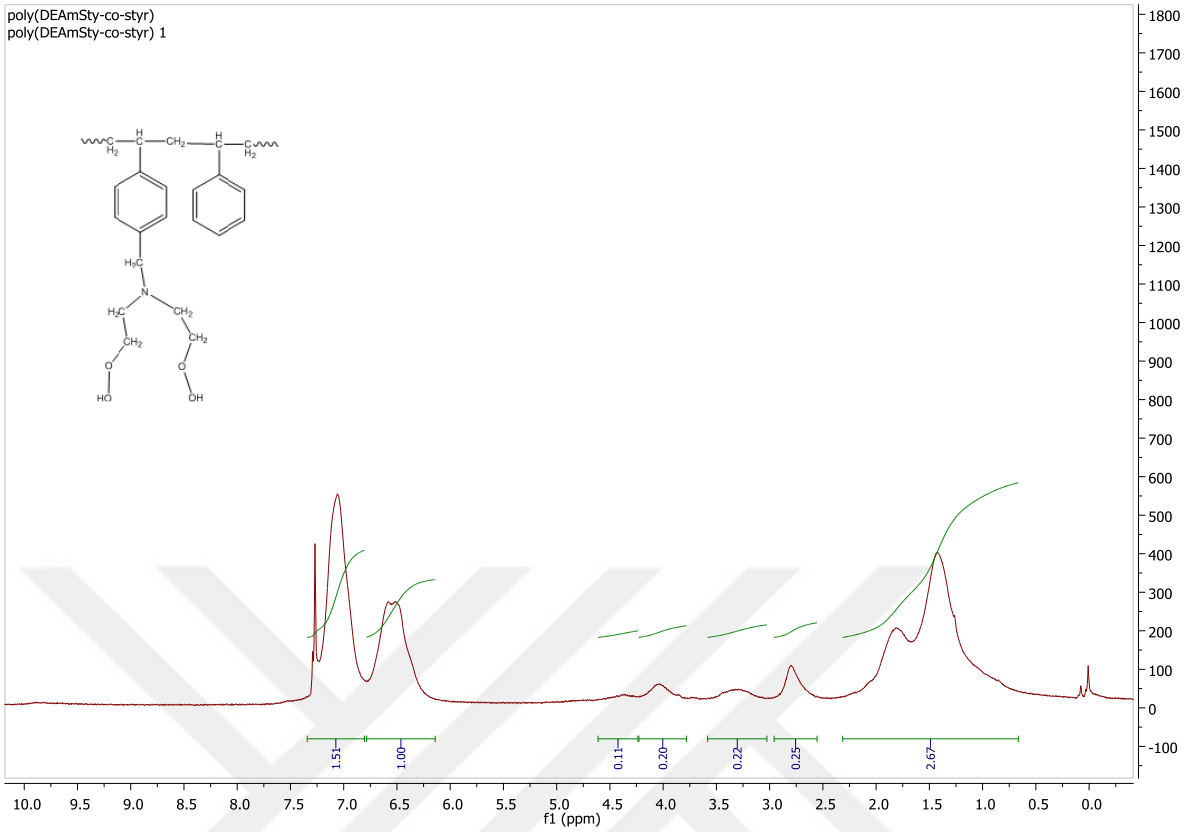

Figure 3.2. ^{1}H-NMR spectrum of poly(DEAMSt2%-co-St)

Table 3.2. ^{1}H-NMR spectrum evaluation of poly(DEAMSt2%-co-St)

Chemical Shift (ppm)	Signal Type
1.25-1.9	CH_2-
2.75	CH_2N-
3.42	CH_2O-
4.12	OH

3.1.2. Characterization of P(PNDEAMSt2%-*co*-St)

The IR spectrum of linear copolymer precursor 1 P(DEAMSt2%-*co*-St) is given in Figure 3.3 and its IR spectrum is evaluated in Table 3.3.

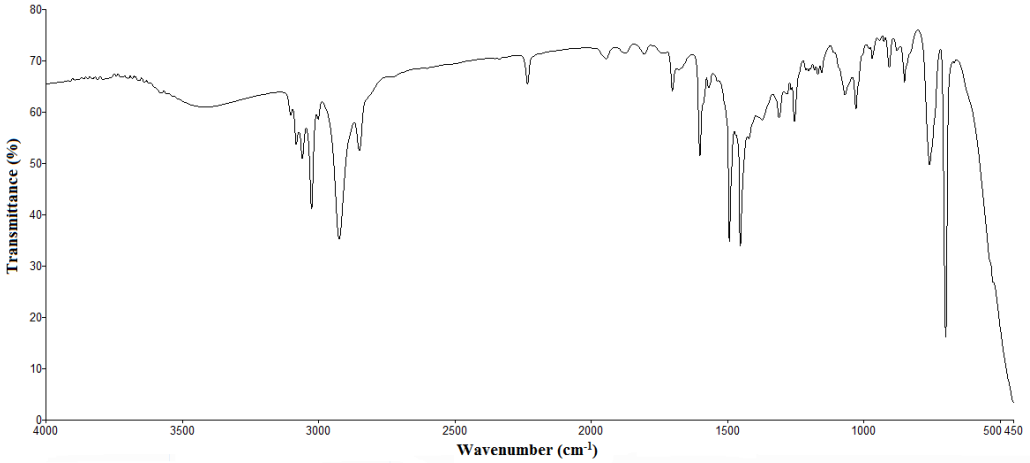

Figure 3.3. FT-IR spectrum of P(PNDEAMSt2%-*co*-St)

Table 3.3. FT-IR spectrum evaluation of P(PNDEAMSt2%-*co*-St)

Wavelength (cm^{-1})	Vibration Type
3025,2924	C-H stretching on the aromatic and aliphatic groups
2233	CN stretching
1601	C=C stretching
1452	C-C stretching
1254	C-O stretching
699	C-N stretching

The ^{1}H-NMR spectrum of P(PNDEAMSt2%-*co*-St) is given in Figure 3.4 and evaluated in Table 3.4

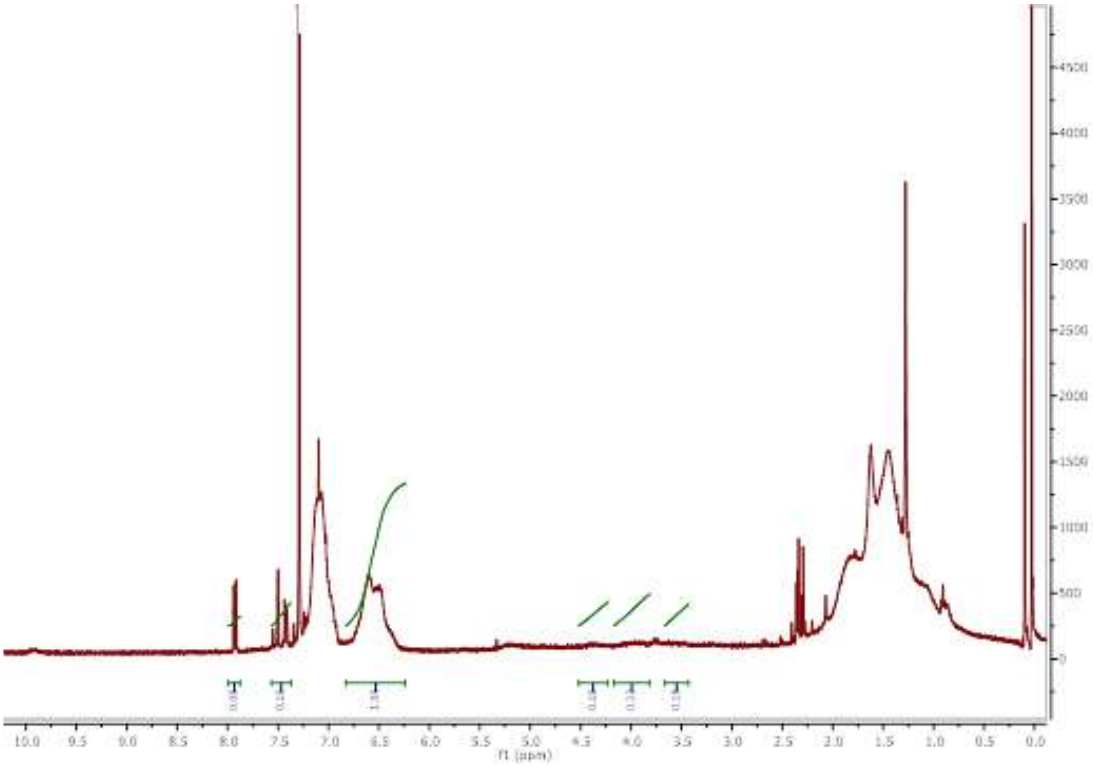

Figure 3.4. ^{1}H-NMR spectrum of P(PNDEAMSt2%-*co*-St) (Solvent: $CDCl_3$)

Table 3.4. ^{1}H-NMR spectrum evaluation of P(PNDEAMSt2%-*co*-St)

Chemical Shift (ppm)	Signal Type
1.25-1.9	CH_2-
2.75	CH_2N-
3.42	CH_2O-
1.25-1.9	CH_2-

3.2. SCP-ball type CoPc1

The IR spectrum of SCP-ball type CoPc1 and P(PNDEAMSt2%-co-St) is given in Figure 3.5 and its IR spectrum is evaluated in Table 3.5 and Table 3.6.

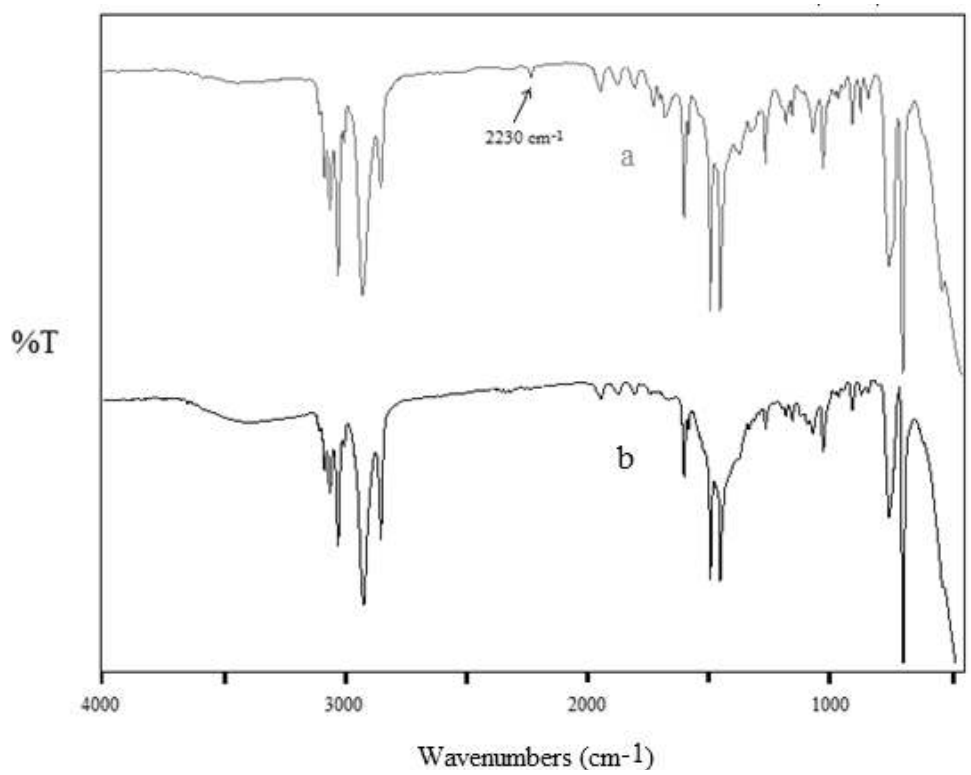

Figure 3.5. FT-IR spectrum of a) P(PNDEAMSt2%-co-St) b)SCP-ball type CoPc1

Table 3.5. FT-IR spectrum evaluation of P(PNDEAMSt2%-co-St)

Wavelength (cm^{-1})	Vibration Type
3025,2924	C-H stretching on the aliphatic CH_2
2230	CN stretching
1601	C=C stretching
1452	C-C stretching
1254	Ar-O-Ar stretching
699	C-N stretching

Table 3.6. FT-IR spectrum evaluation of SCP-ball type CoPc1

Wavelength (cm^{-1})	Vibration Type
3025,2924	C-H stretching on the aromatic and aliphatic groups
1601	C=C stretching
1452	C-C stretching
1254	Ar-O-Ar stretching
699	C-N stretching

3.2.1. UV-Vis spectroscopy Analysis of SCP-ball type CoPc1 and Scp-ball type CoP2

The UV-Vis spectroscopy Analysis of SCP-ball type CoPc1 is given in Figure 3.6 and the UV-Vis spectroscopy analysis is evaluated in Table 3.7.

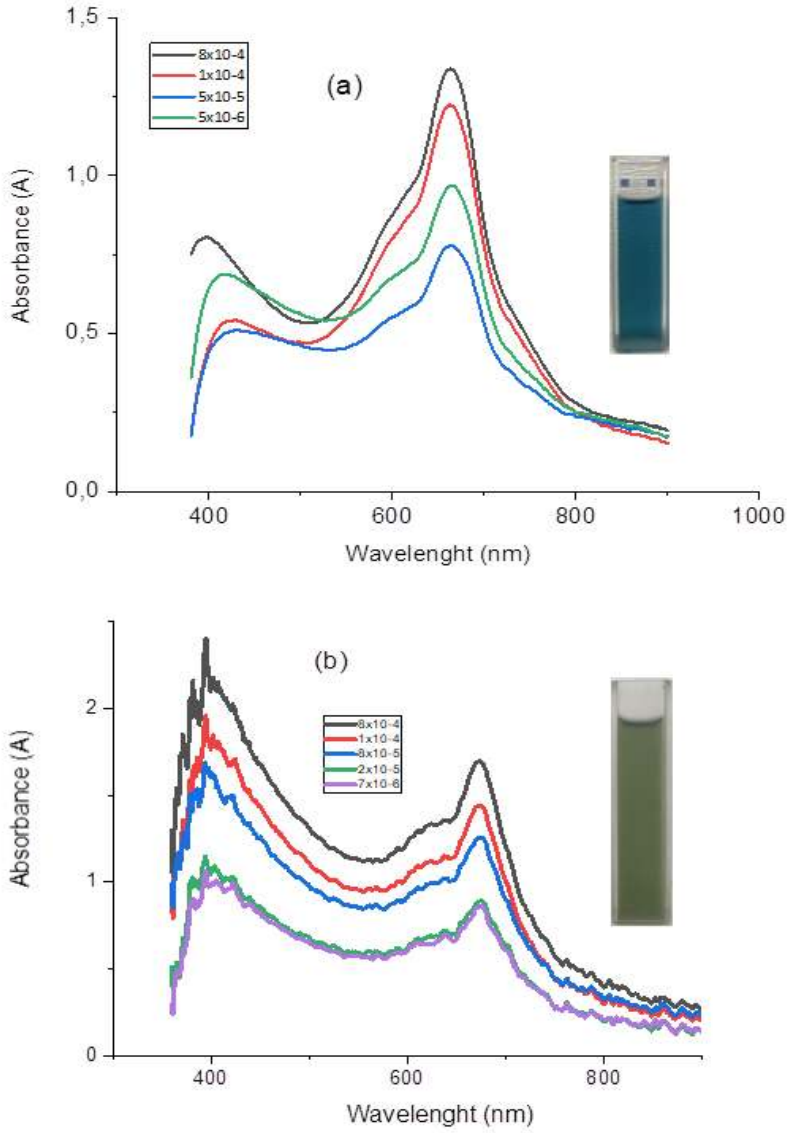

Figure 3.6. UV-Vis spectroscopy interpretation of SCP-CoPc1 and SCP-CoPc2

Table 3.7. UV-Vis spectroscopy interpretation of CoPc1

Absorption bands	Wavelength	Region
B-bands	320-350	UV
Q-bands	600-700	Visible region

3.2.2. MALDI-TOF-MS Characterization of SCP-ball type CoPc1

The MALDI-TOF-MS analysis of SCP-ball type CoPc1 is given in Figure 3.7 and evaluated in Table 3.8.

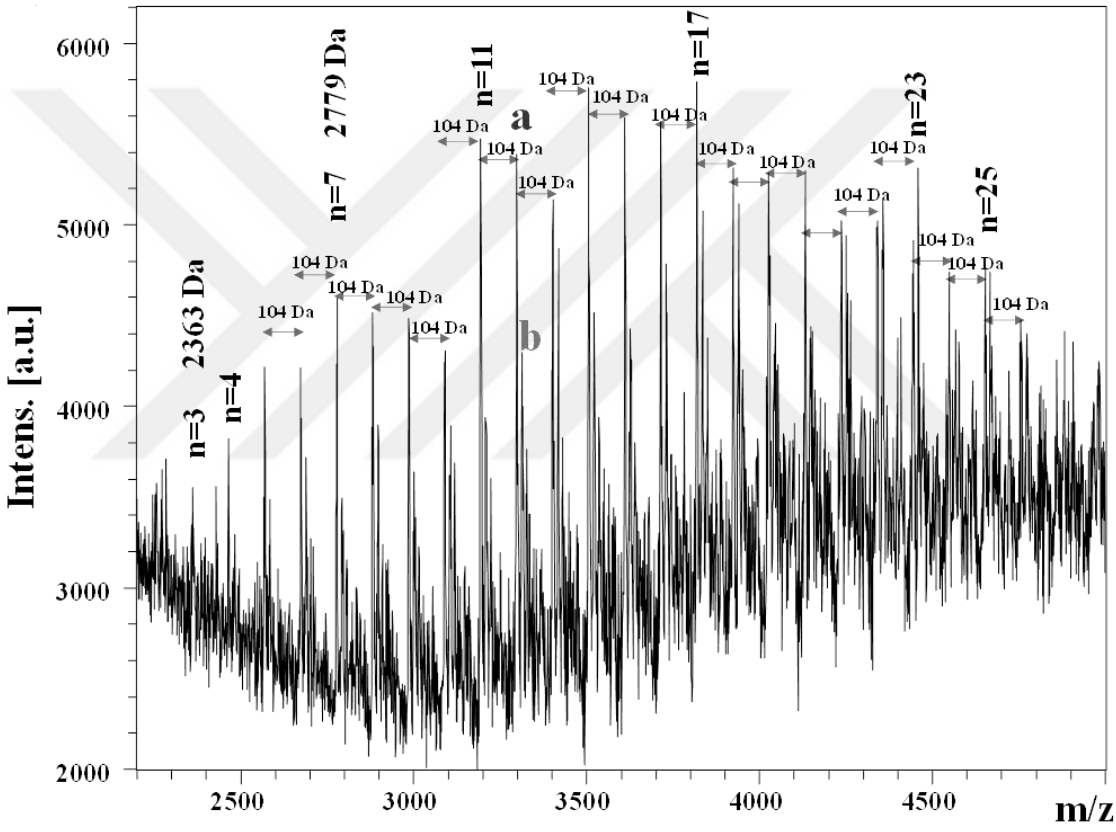

Figure 3.7. MALDI-TOF-MS Analysis of of SCP-ball type CoPc1

Table 3.8. MALDI-TOF-MS analysis of SCP-ball type CoPc1 is evaluated

Spacies	Chemical Formula	MW
a and b	H and OH	16 Da
Repeating Unit	Styrene	104 Da
Pendent group	Phthalocyanine	2010 Da

3.2.3. DSC measurements of SCP-ball type CoPc2

DSC curves of SCP-ball type CoPc2 and pure polystyrene (PSt) prepared by free radical polymerization method were recorded at heating rate of 20 ^{o}C/min. The Figure 3.8 shows DSC curves of SCP-ball type CoPc2 and pure polystyrene (PSt) and evaluated in Table 3.9.

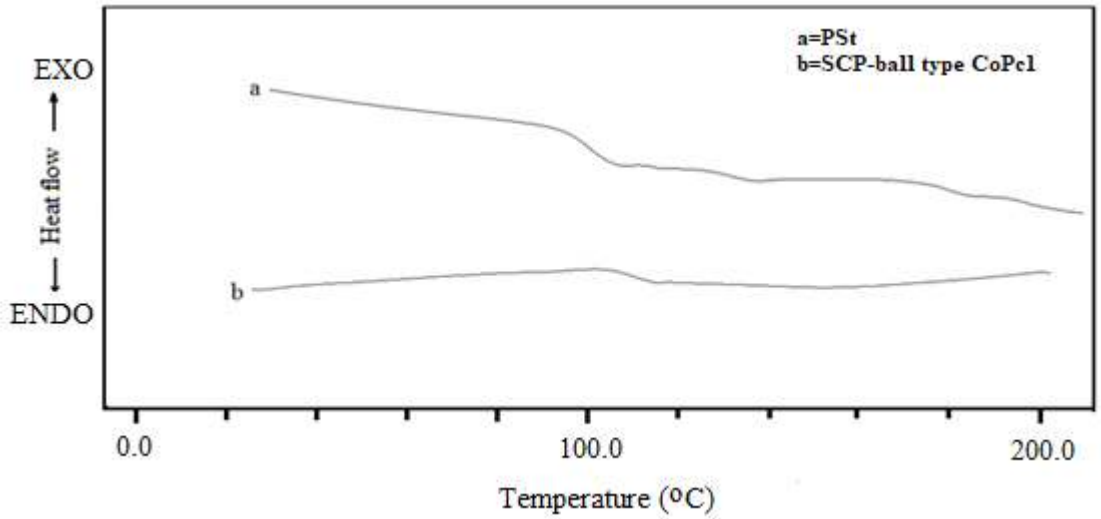

Figure 3.8. DSC curves of SCP-ball type CoPc2 and pure polystyrene (PSt)

Table 3.9. DSC evaluation

Polymer	T_g (^{o}C)
PSt	84.2
SCP-ball type CoPc1	75.8

3.2.4. Thermogravimetric measurements and analysis of residue

Thermal decomposition temperatures of pure PSt, P(PNDEAMSt6%-co-St)2, SCP-ball-type CoPc1 and SCP-ball-type CoPc2 were estimated by thermogravimetric analysis. The Figure 3.9 shows a TGA Analysis of pure PSt, P(PNDEAMSt6%-co-St)2, SCP-ball-type CoPc1 and SCP-ball-type CoPc2 and evaluated in Table 3.10.

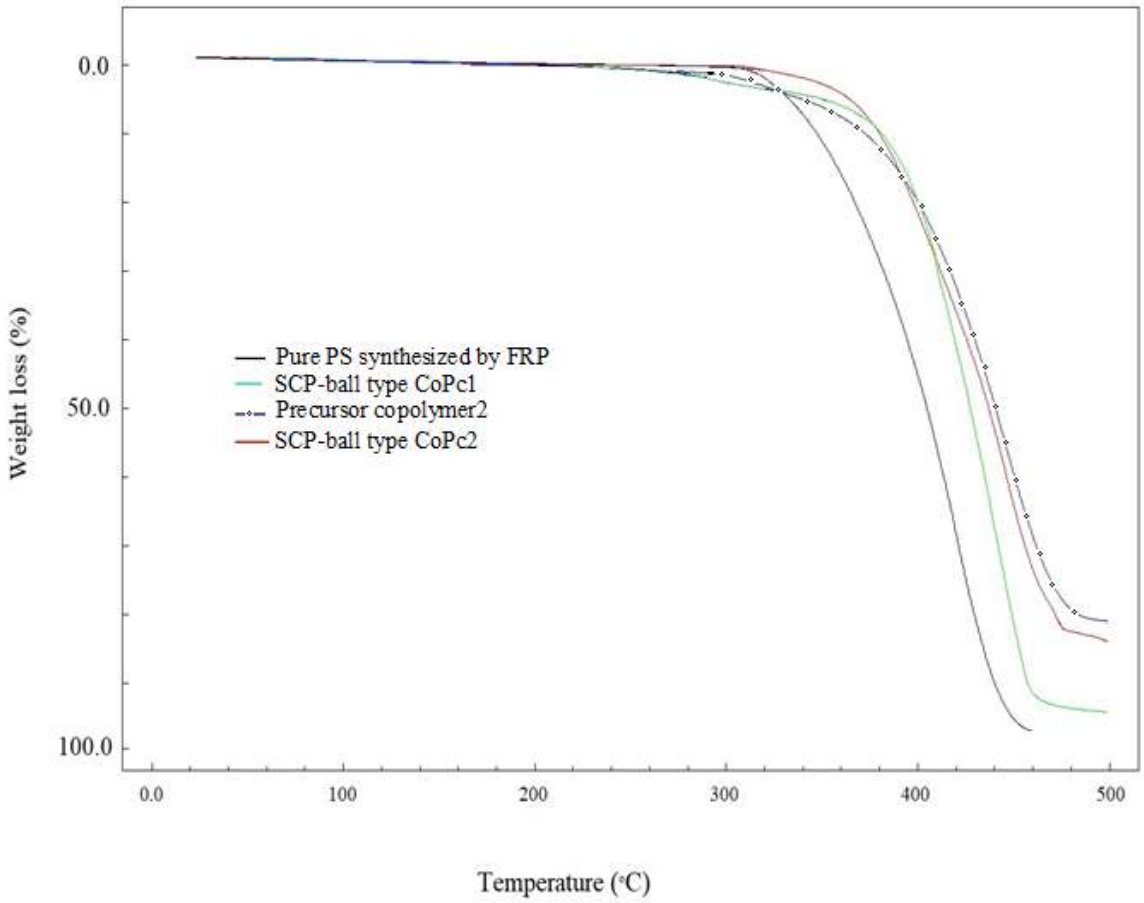

Figure 3.9. TGA Analysis of pure PSt, P(PNDEAMSt6%-co-St)2, SCP-ball-type CoPc1 and SCP-ball-type CoPc2

Table 3.10. TGA Evaluation

Sample	Tg/°C	T_i^a /°C	$T_{\%50}$ /°C	%Residue
Pure PS synthesized by FRP	102	305	402	2
SCP-ball type CoPc1	106	224	424	6
Precursor copolymer2	105	303	442	18
SCP-ball type CoPc2	116	312	438	16

3.2.5. FT-IR analysis for residue of SCP-ball type CoPc1

FT-IR spectrum was recorded in presence of KBr for residue of SCP-ball type CoPc1 heated to 600 °C. The Figure 3.10 shows FT-IR spectrum of residue for SCP-ball type CoPc1 heated to 600 °C and evaluated in Table 3.11.

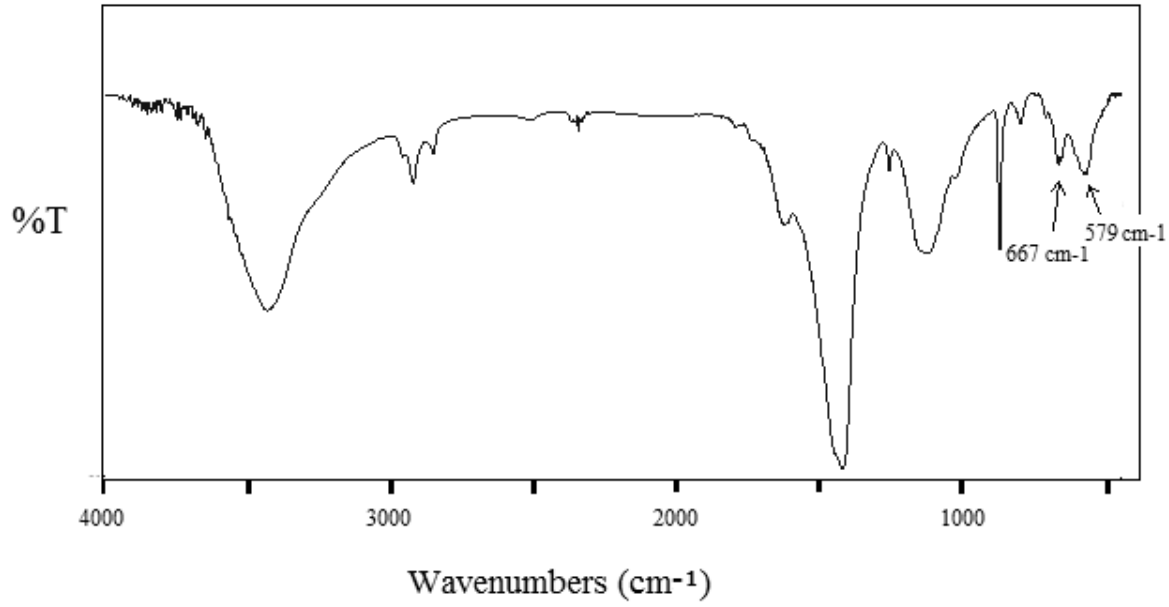

Figure 3.10. FT-IR spectrum of residue for SCP-ball type CoPc1 heated to 600 ^{o}C

Table 3.11. FT-IR evaluation

Wavelength (cm^{-1})	Vibration Type
2995-2924	C-H stretching on the aliphatic CH_2
1625	C=C stretching
1424	C-C stretching
667,579	Co-O stretching in the Co_3O_4
3430,1630	H_2O bending and stretching vibration

3.2.6. The kinetic analysis of SCP-ball type CoPc1

The kinetic analysis of the degradation of samples was performed by utilizing the thermograms obtained from the TGA. For this purpose, the dynamic thermal degradation measurements on SCP-ball type CoPc1 were performed at temperature range from room temperature to 600 ^{o}C, under a nitrogen flow (10 ml/min), at different heating rates (5.0, 10.0, 15.0, 20.0, 25.0 and 35.0 ^{o}C/min). The Figure 3.11 shows TGA of SCP-ball type CoPc1), at different heating rates (5.0, 10.0, 15.0, 20.0, 25.0 and 35.0 ^{o}C/min).

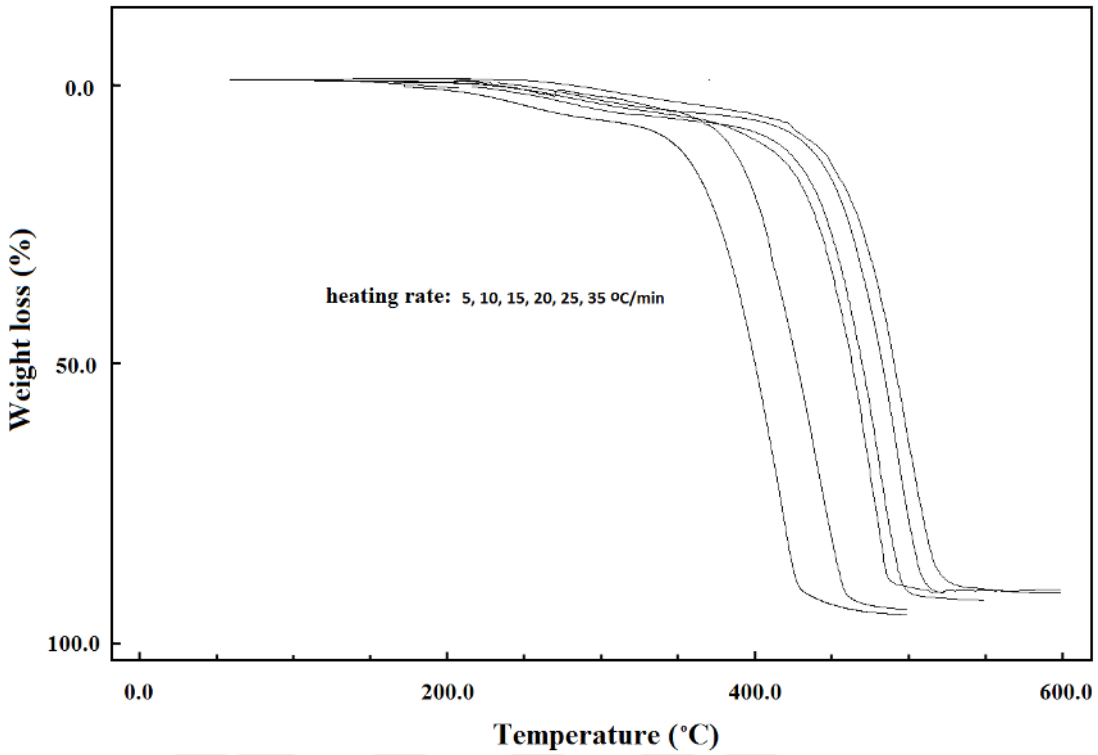

Figure 3.11. TGA of SCP-ball type CoPc1 at different heating rates (5.0, 10.0, 15.0, 20.0, 25.0 and 35.0 °C/min)

Figure 3.12 shows graph kinetic analysis using the specific results of application of Ozawa's method for all type CoPc1 decomposition in argon gas flow.

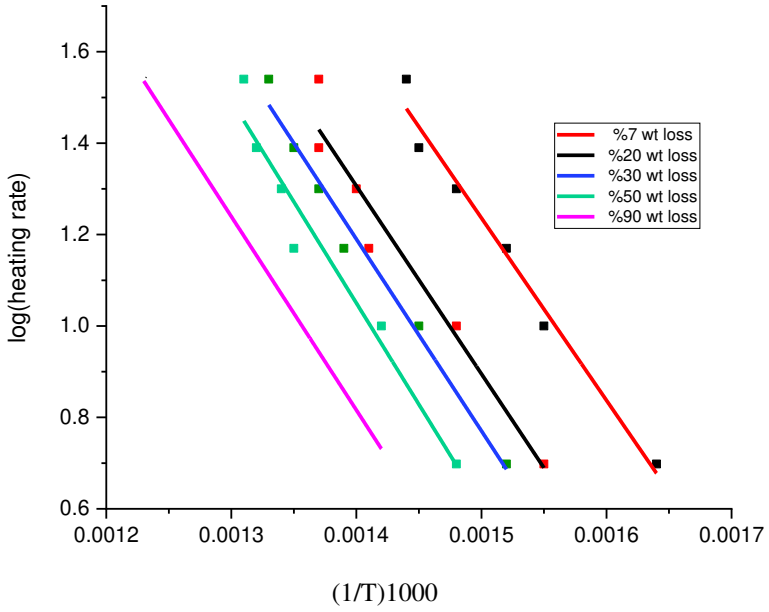

Figure 3.12. shows graph kinetic analysis using the specific results of application of Ozawa's method for all type CoPc1 degradation in argon gas flow

Table 3.12 shows the average apparent activation energy of the thermal degradation of SCP-ball type CoPc1 calculated by three model-free methods in a period of α = 0.07–0.90 (weight loss (%).

Table 3.12. Average apparent activation energy of the thermal degradation of SCP-ball type CoPc1 calculated by three model-free methods in a period of α = 0.07–0.90

Weight loss (%)	Activation energies (Ea), kJ/mol
7	33,156
20	34.178
30	34.877
50	35.425
90	56.726

Figure 3.13 shows the plots of activation energy as a function of conversion for extent of conversion.

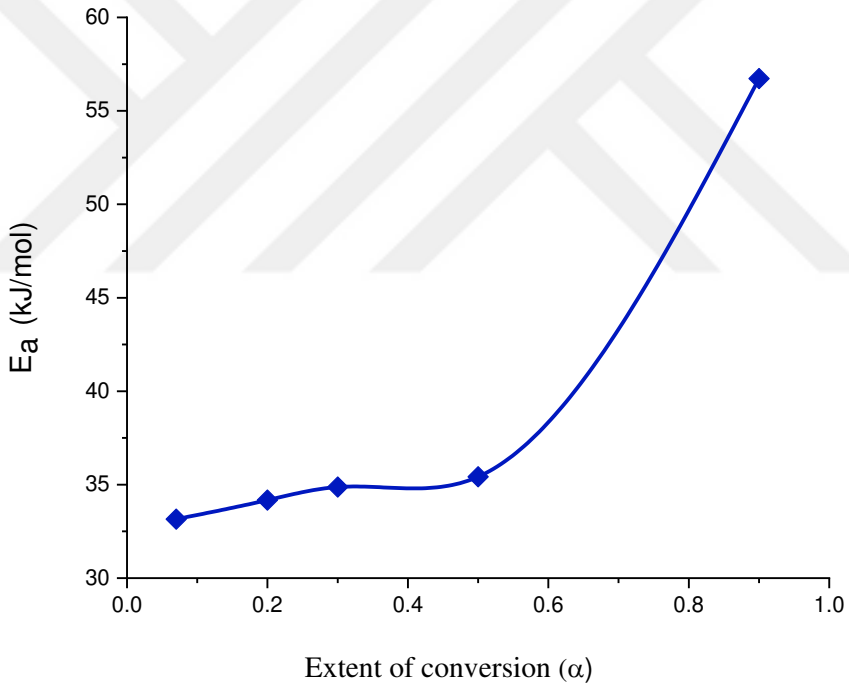

Figure 3.13. Plot of activation energy as a function of extent conversion

3.2.7. Optical and Dielectric behaviors for the SCP-ball type CoPc1

Figure 3.14 shows refractive index, n, for the SCP-ball type CoPc1 as a function of wavelength and evaluated in Table 3.13.

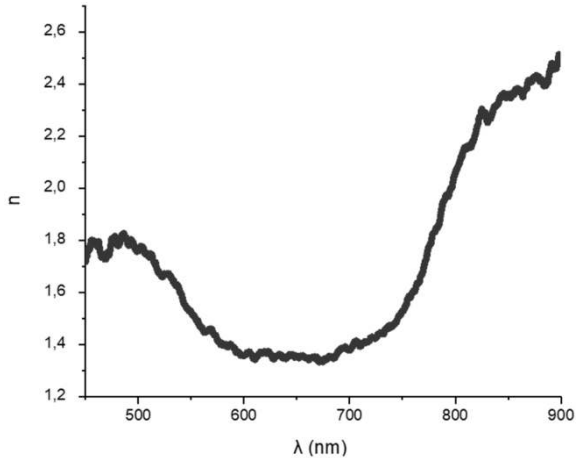

Figure 3.14. Plot of refractive index, n, for the SCP-ball type CoPc1 as a function of wavelength.

Table 3.13. Wavelength and Region for SCP-ball type CoPc1

Refractive index	Wavelength(nm)	Region
B-bands	488-600	UV
Q-bands	600-700	Visible region

3.2.8. Dielectric behavior investigation of precursor copolymer2

The Figure 3.15 shows graphs of a) ε', b) ε", c) tanδ and d) $\ln\sigma_{ac}$ versus frequency for precursor copolymer2.

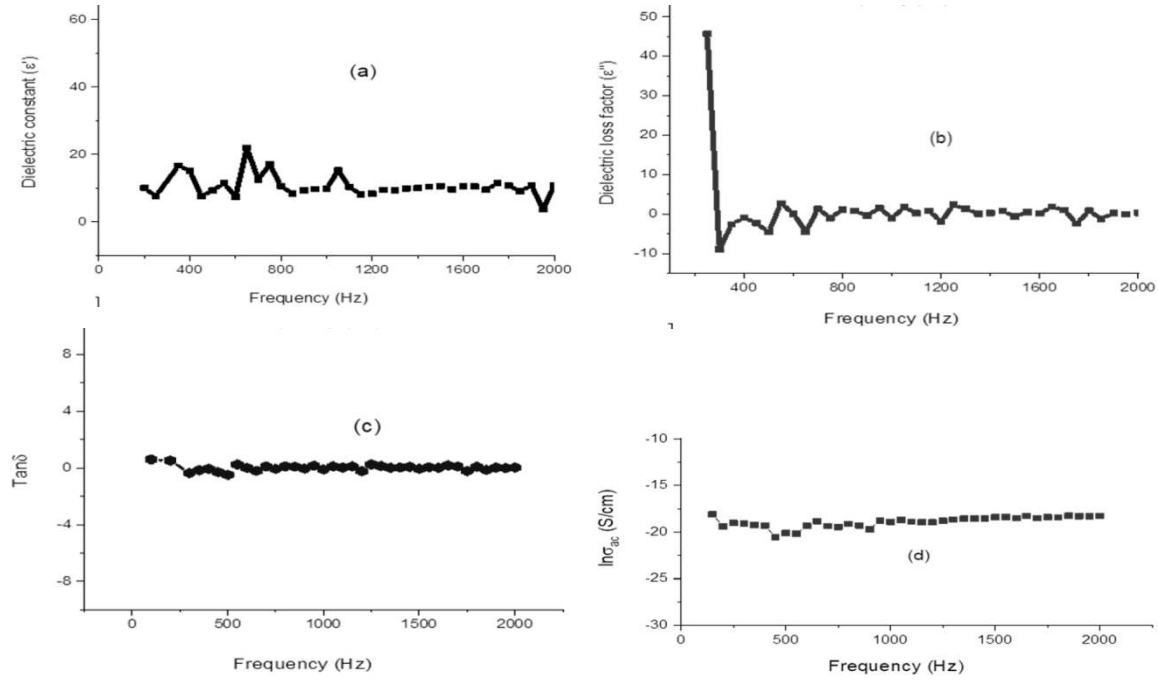

Figure 3.15. Graphs of a) ε', b) ε", c) tanδ and d) $\ln\sigma_{ac}$ versus frequency for precursor copolymer2

3.2.9. Dielectric behaviors of SCP- ball type CoPc2

Figure 3.16 shows graphs of a) ε', b) ε", c) tanδ and d) $\ln\sigma_{ac}$ versus frequency for SCP-ball type CoPc2.

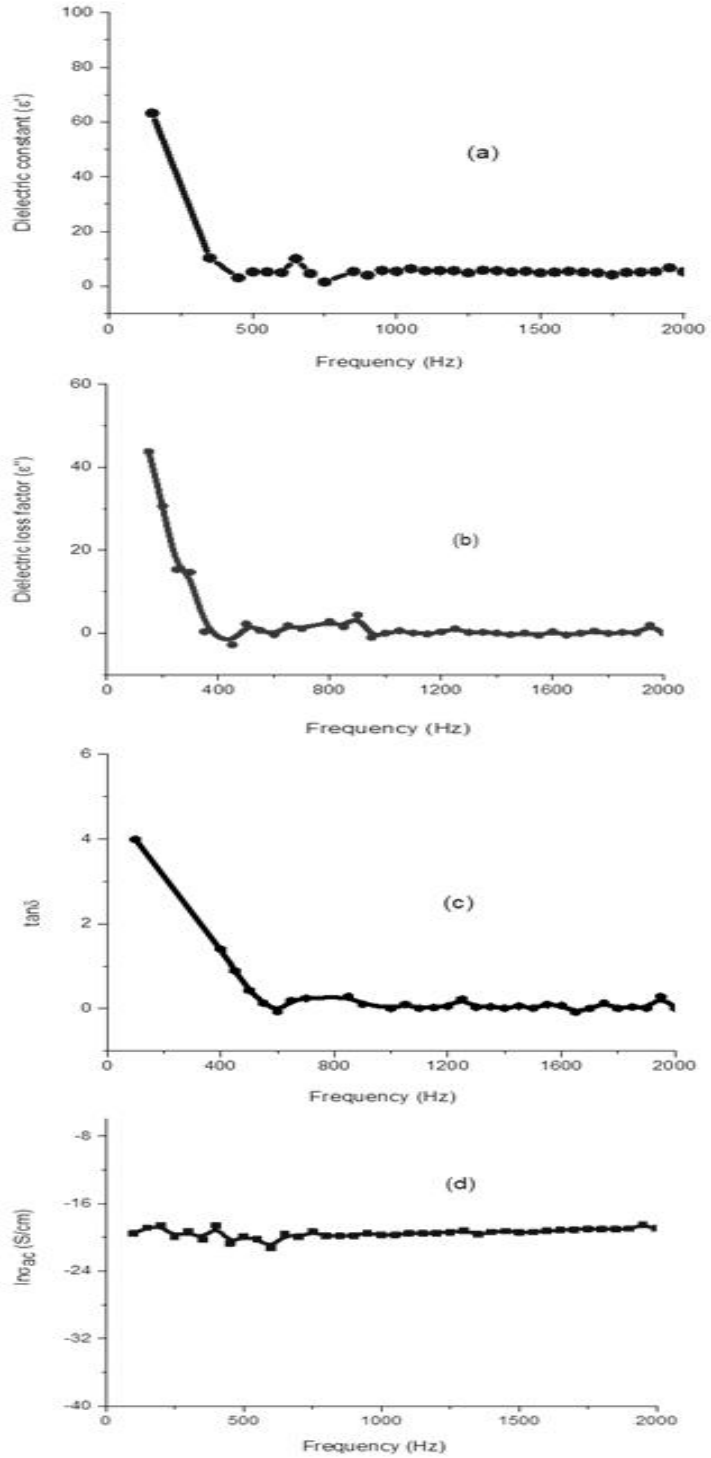

Figure 3.16. Graphs of a) ε', b) ε", c) tanδ and d) ln σ_{ac} versus frequency for SCP-ball type CoPc2

3.3. Characterization of P(DEAMSt12%-*co*-St)

The IR spectrum of linear copolymer precursor or P(DEAMSt12%-*co*-St) is given in Figure 3.17 and the IR spectrum is evaluated in Table 3.14.

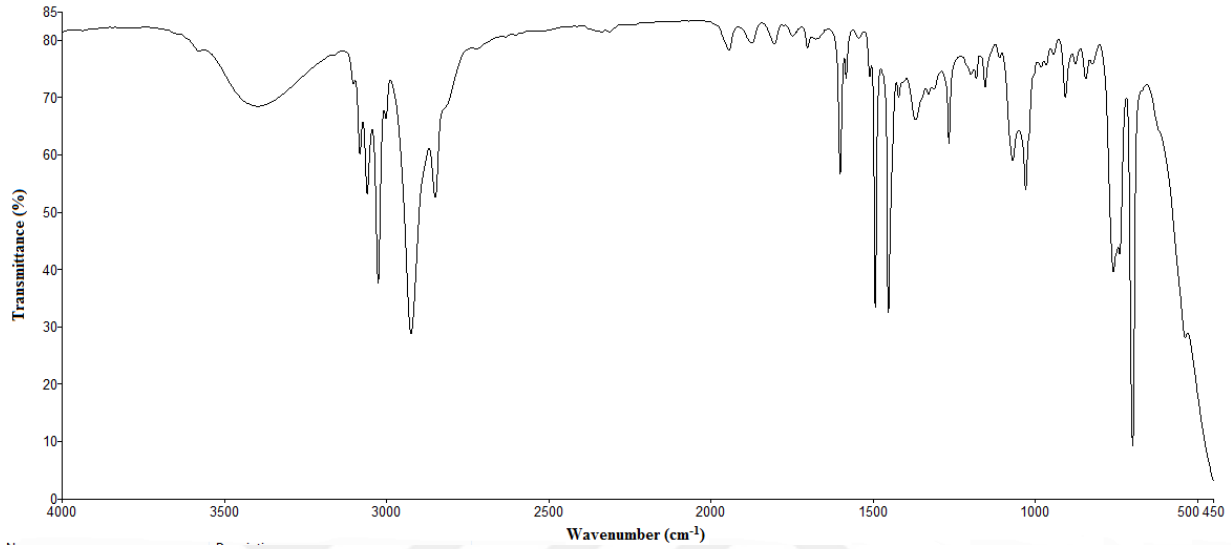

Figure 3.17. FT-IR spectrum of poly(DEAMSty12%-co-St)

Table 3.14. FT-IR spectrum evaluation of poly(DEAMSt12%-co-St)

Wavelength (cm^{-1})	Vibration Type
3400	O-H stretching
3025,2924	C-H stretching on the aliphatic CH_2
1601	C=C stretching
1265	C-O stretching

Figure 3.18 shows ^{1}H-NMR spectrum of poly(DEAMSt12%-co-St) and evaluated in Table 3.15.

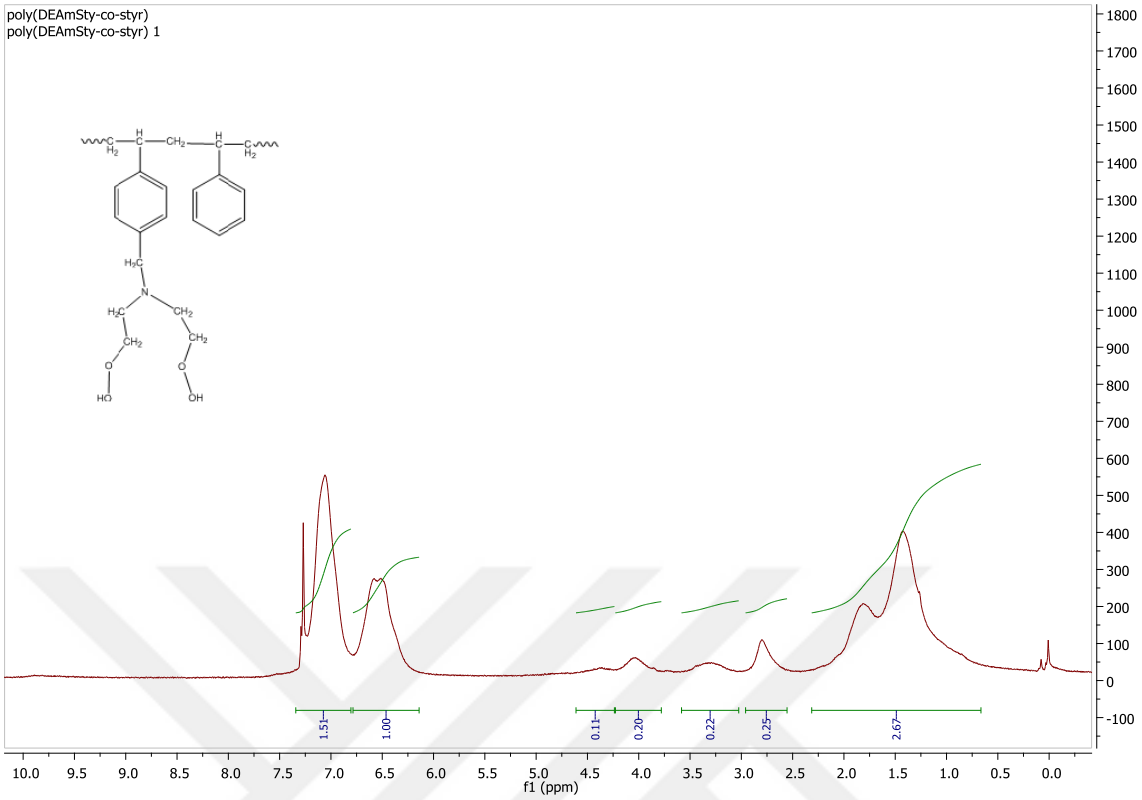

Figure 3.18. ^{1}H-NMR spectrum of poly(DEAMSt12%-co-St)

Table 3.15. ^{1}H-NMR spectrum evaluation of poly(DEAMSt12%-co-St)

Chemical Shift (ppm)	Signal Type
1.25-1.9	CH_2-
2.75	CH_2N-
3.42	CH_2O-
4.12	OH

3.3.1. Characterization of P(PNDEAMSt12%-*co*-St)

The FT-IR spectrum of linear copolymer precursor or P(PNDEAMSt12%-*co*-St) is given in Figure 3.19 and evaluated in Table 3.16.

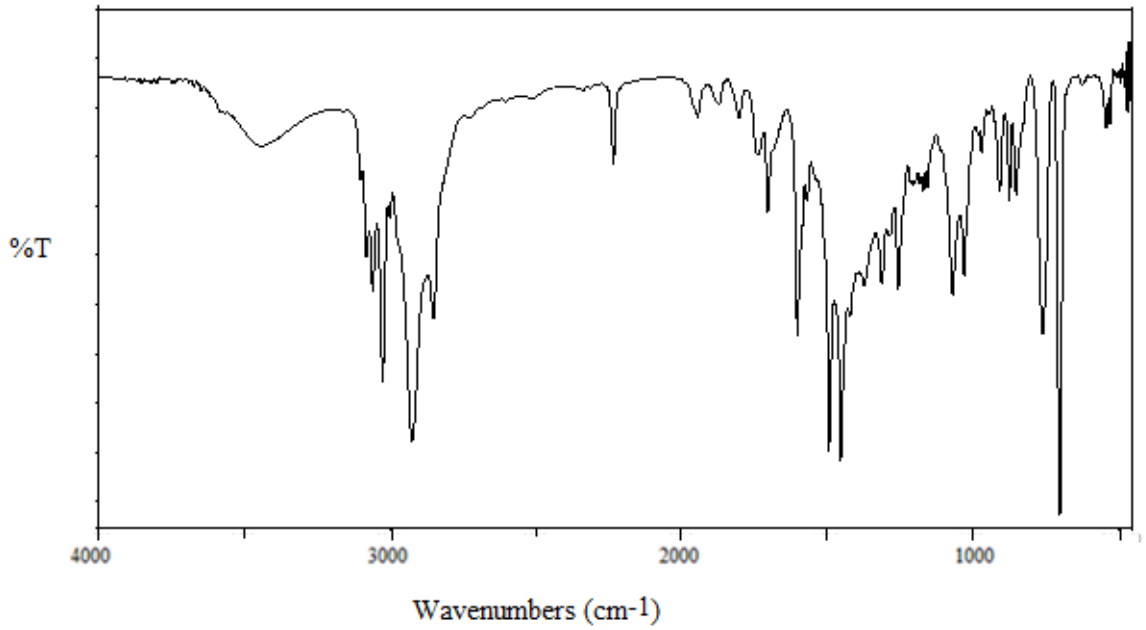

Figure 3.19. FT-IR spectrum of P(PNDEAMSt12%-*co*-St)

Table 3.16. FT-IR spectrum evaluation of P(PNDEAMSt12%-*co*-St)

Wavelength (cm^{-1})	**Vibration Type**
3025,2924	C-H stretching on the aliphatic CH_2
2233	CN stretching
1601	C=C stretching
1452	C-C stretching
1254	C-O stretching
699	C-N stretching

The ^{1}H-NMR spectrum of P(PNDEAMSt12%-*co*-St) is given in Figure 3.20 and evaluated in Table 3.17.

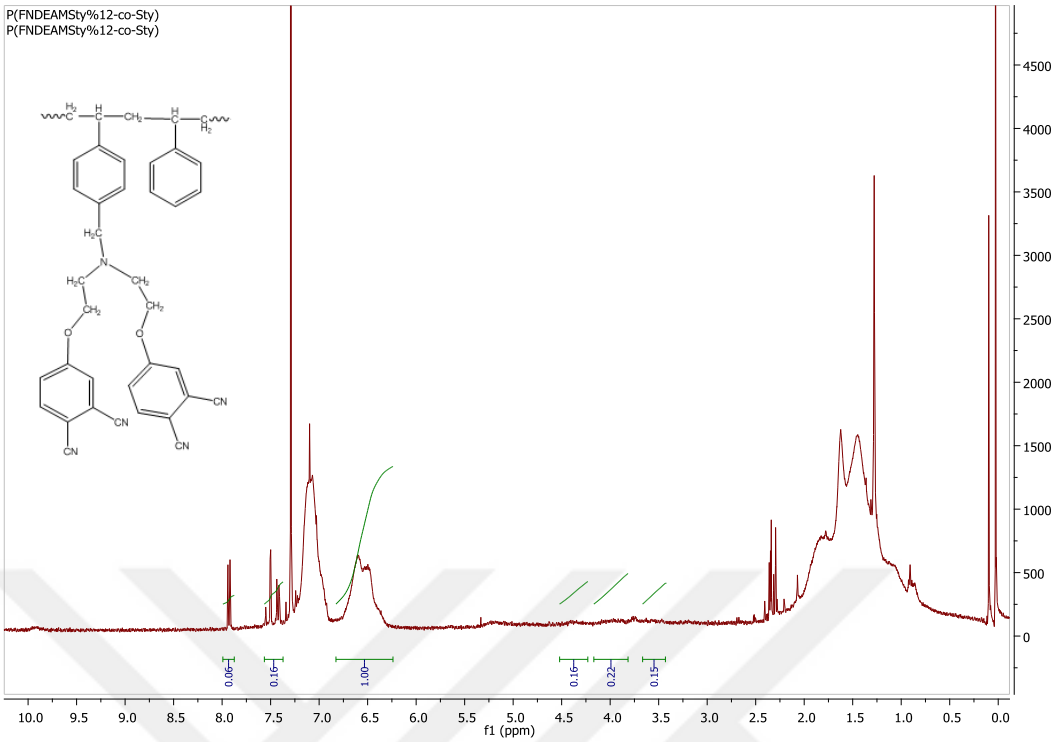

Figure 3.20. ^{1}H-NMR spectrum of P(PNDEAMSt12%-*co*-St) (Solvent: $CDCl_3$)

Table 3.17. ^{1}H-NMR spectrum evaluation of P(PNDEAMSt12%-*co*-St)

Chemical Shift (ppm)	Signal Type
1.25-1.9	-CH_2-
2.75	-CH_2N-
3.42	-CH_2O-
1.25-1.9	-CH_2-

3.4. SCP-ball type CoPc3

3.4.1. The IR spectrum of SCP-ball type CoPc3 and P(PNDEAMSt12%-co-St)

The FT-IR spectrum of SCP-ball type CoPc3 is given in Figure 3.21.

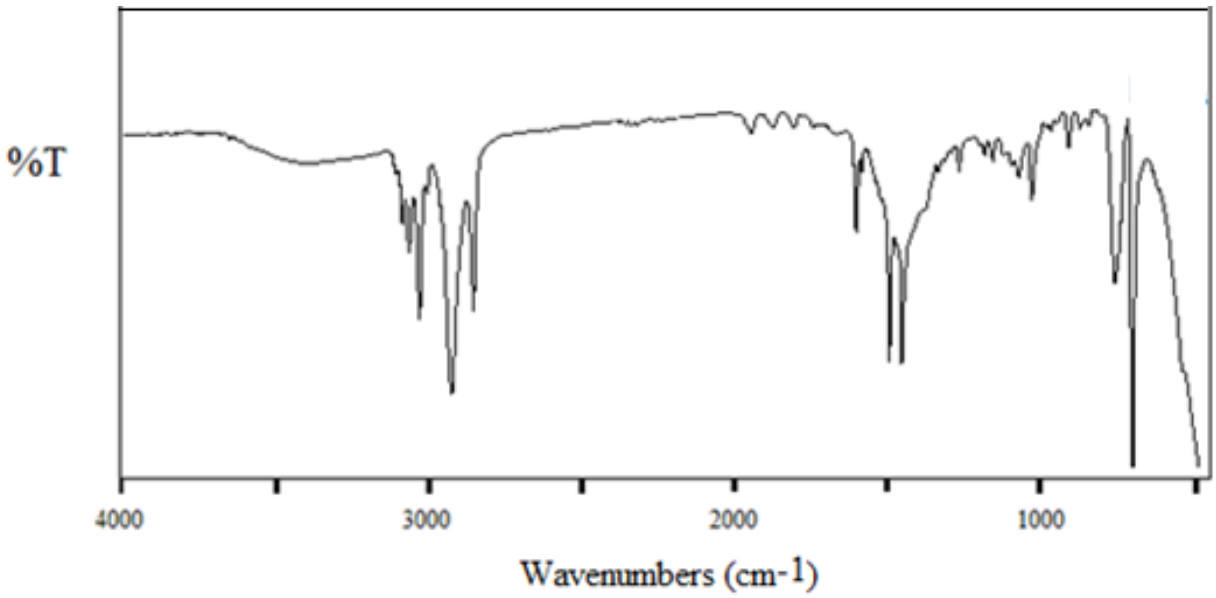

Figure 3.21

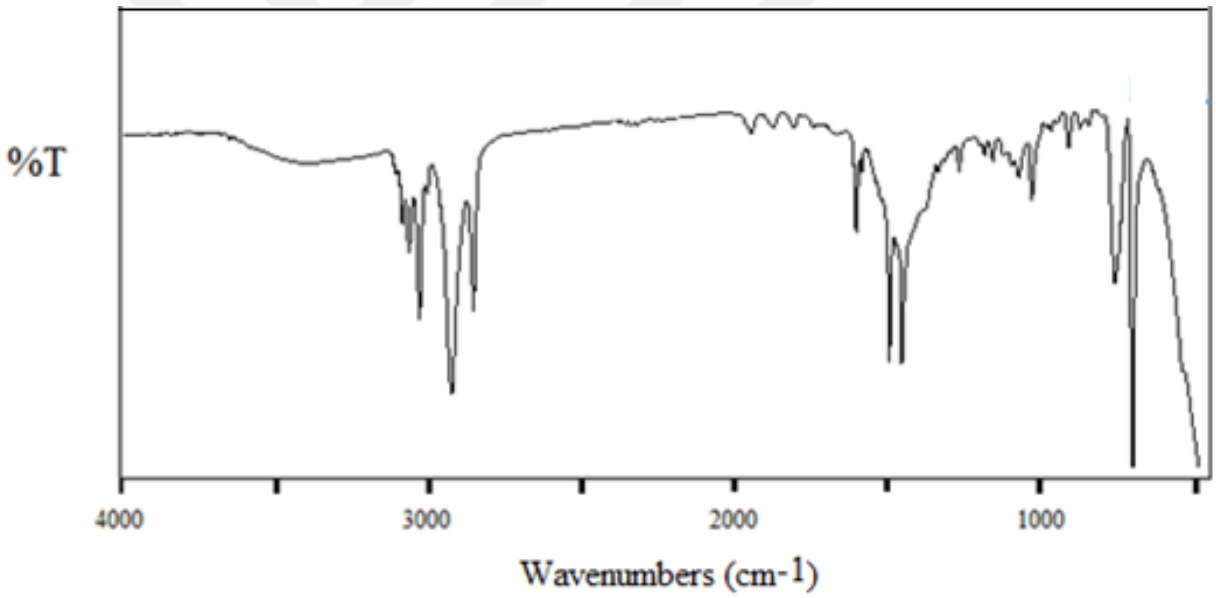

Figure 3.21. FT-IR spectra of SCP-ball type CoPc3

3.4.2. MALDI-TOF-MS of the SCPM-ball type CoPc3

The SCPM-ball type CoPc3 structure having two double core or more double core phthalocyanine was confirmed by MALDI-TOF-MS in positive ion and reflection mode. The spectrum is indicated in Figure 3.22 and characterized in Table 3.18.

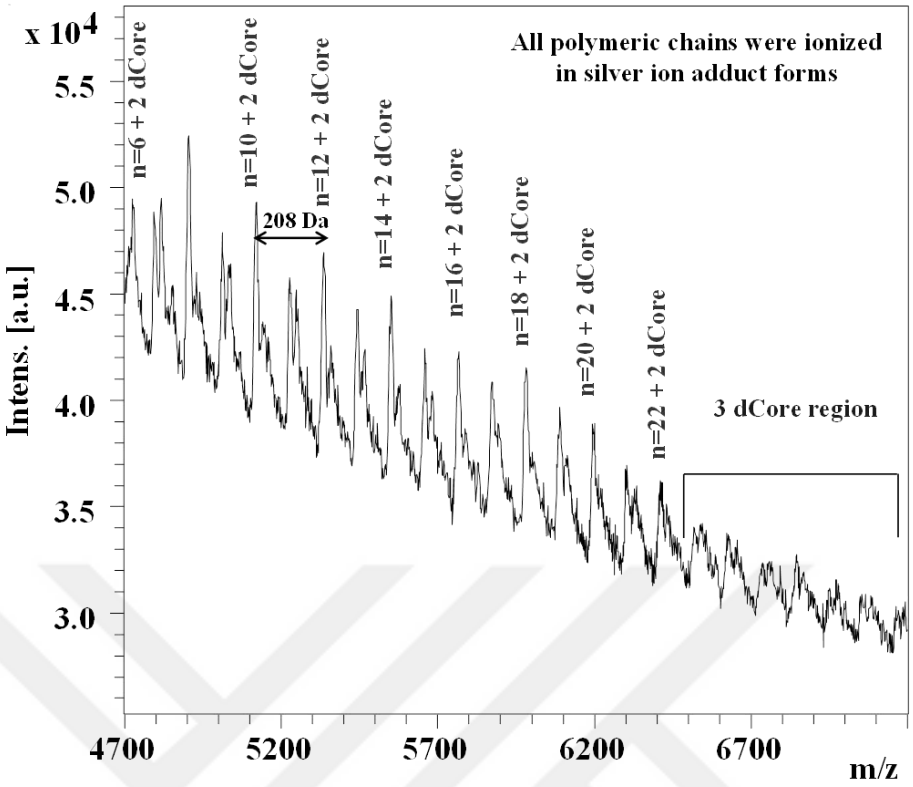

Figure 3.22. MALDI-TOF-MS spectrum of SCP-ball type CoPc3 sample acquired in positive ion mode. All the species are ionized in silver adduct forms

Table 3.18. MALDI-TOF-MS spectrum of SCP-ball type CoPc3

Spacies	Chemical Formula	MW
a and b	H, and OH	16 Da
Repeating Unit	Styrene	104 Da
Pendent group	Phthalocyanine	2010 Da

The Figure 3.23 shows the FT-IR spectra of a) poly(PNDEAMSt12%-co-St) and b) SCP-ball type CoPc3 as comparison.

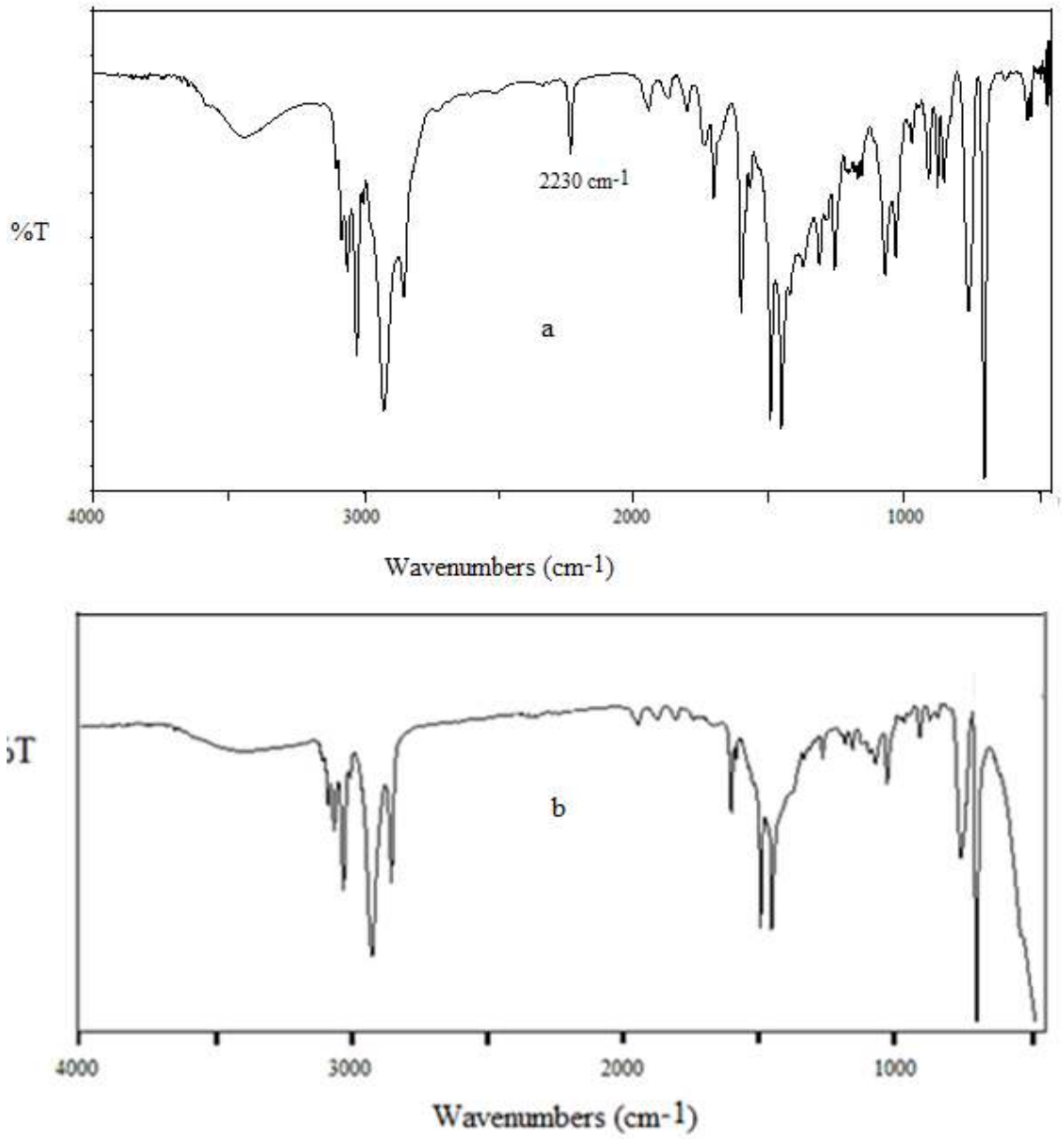

Figure 3.23. FT-IR spectra of a) poly(PNDEAMSt12%-co-St) and b) SCP-ball type CoPc3

3.4.3. UV-vis spectrum of SCP-ball type CoPc3

The UV-vis spectrum having two broad peaks at 598 nm and 660 nm of SCPM-ball type CoPc3 is indicated in Figure 3.24 and evaluated in Table 3.19.

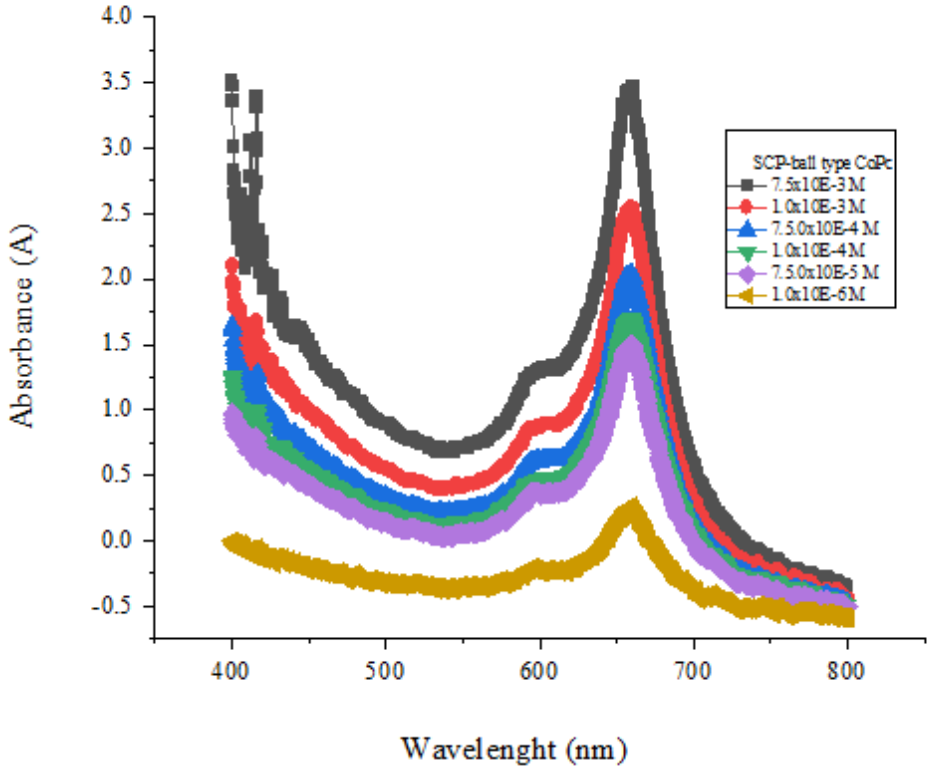

Figure 3.24. UV-vis spectrum of SCP-ball type CoPc3

Table 3.19. UV-vis spectrum of SCP-ball type CoPc3 characterization

Absorption bands	Wavelength	Region
B-bands	320-350	UV
Q-bands	600-700	Visible region

3.4.4. SEM Analysis of SCPM-ball type CoPc3

The Figure 3.25 shows a SEM micrograph of the plan view in the different magnitudes of SCPM-ball type CoPc3.

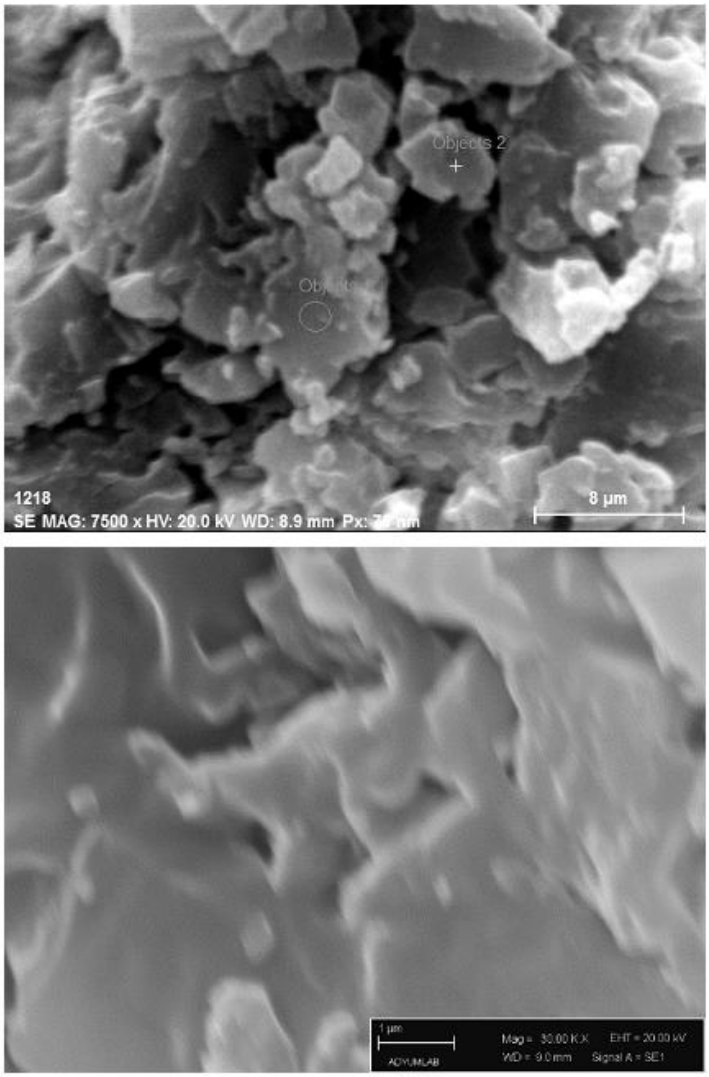

Figure 3.25. SEM images of the SCPM-ball type CoPc3 structure at different magnifications

3.4.5. DSC curves of SCPM-Ball Type CoPc3 and P(PNDEAMSt12%-co-St) GO Composites

The DSC curves of P(DEAMSt12%-co-St), P(PNDEAMSt12%-co-St), P(PNDEAMSt12%-co-St)/GO 3.6% (by wt), P(PNDEAMSt12%-co-St)/GO 4.5% (by wt) and SCPM-ball type CoP were indicated in Figure 3.26.

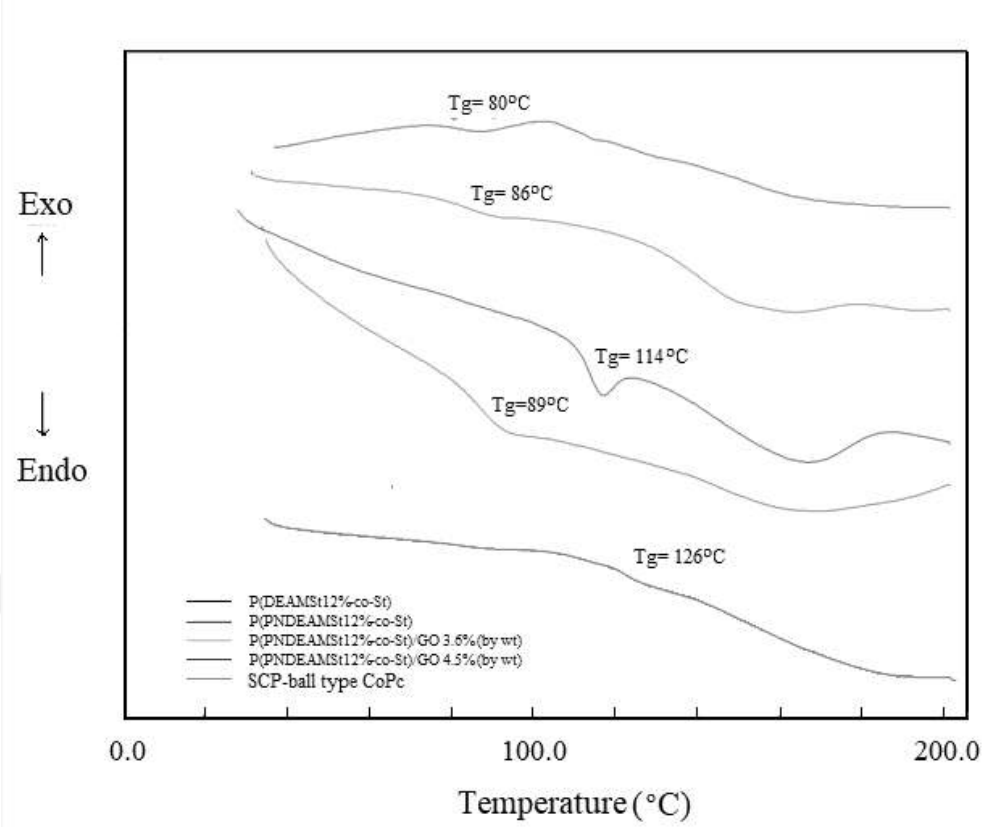

Figure 3.26. DSC curves of P(DEAMSt12%-co-St), P(PNDEAMSt12%-co-St), P(PNDEAMSt12%-co-St)/GO 3.6% (by wt), P(PNDEAMSt12%-co-St)/GO 4.5% (by wt) and SCPM-ball type CoPc

3.4.6. Thermo-Gravimetry (TG) of SCPM-ball type CoPc3 and P(PNDEAMSt12%-co-St)

Thermal stabilities of P(DEAMSt12%-co-St) and linear copolymer precursor and SCPM-ball type CoPc were investigated, and their TG curves were showed in Figure 3.27 and Figure 3.28 and are evaluated in Table 3.20.

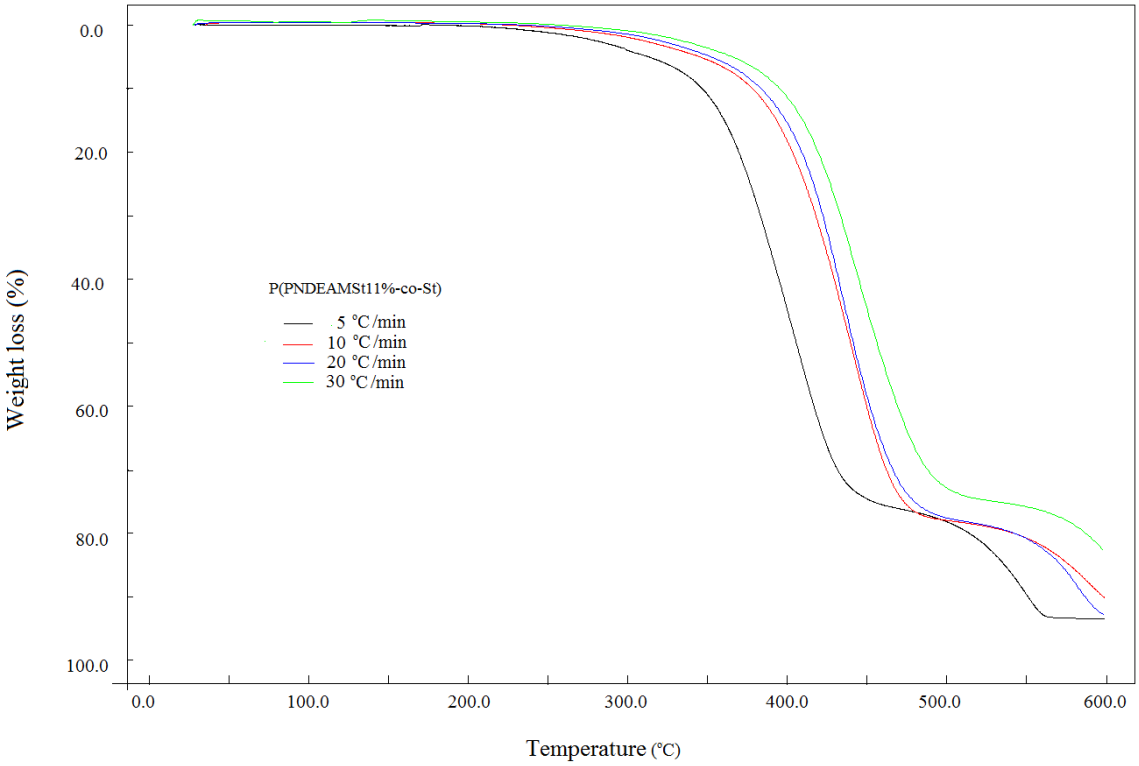

Figure 3.27. TGA curves of P(DEAMST12%-co-St) at different heating rate

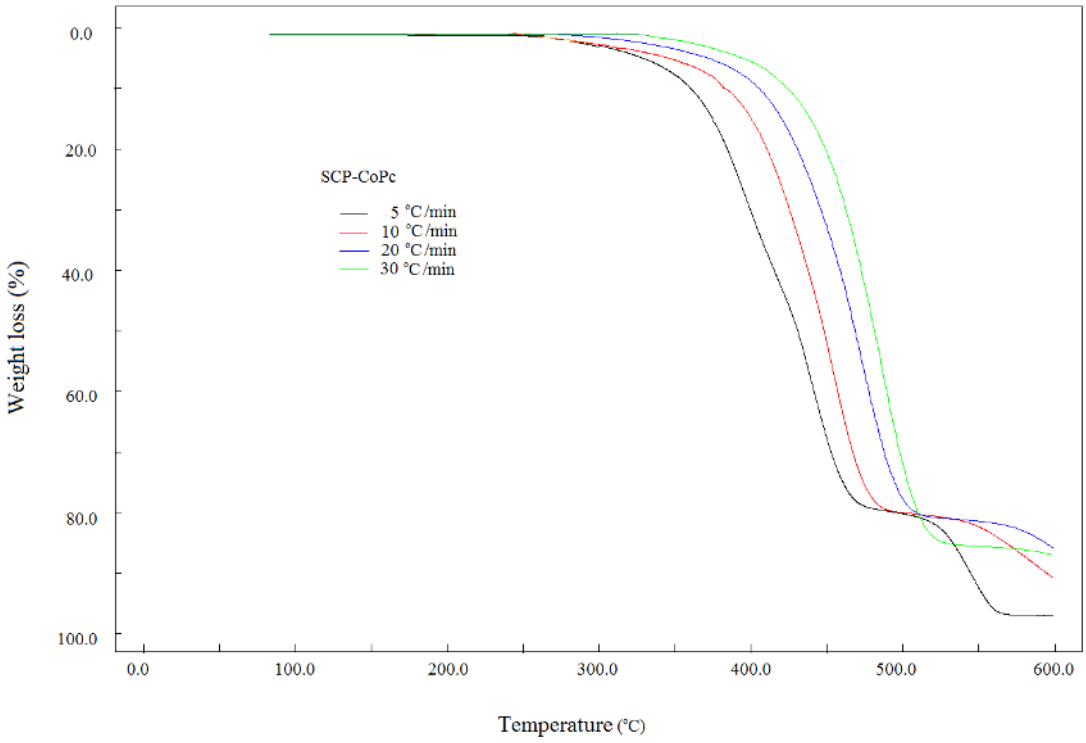

Figure 3.28. TGA curves of SCP-ball type CoPc measured at different heating rate

Table 3.20. TGA results of TGA data for P(DEAMSt12%-co-St), lineer copolymer precursor and SCP-ball type CoPc

Sample	$T_{initial}$ (°C)	$T_{\%50}$ (°C)	T_f	% Residue at 500°C
P(DEAMSt12%-co-St)	243	437	480	8
P(PNDEAMSt12%-co-St)	300	382	500>	25
SCPM-ball type CoPc	298	440	500>	22

3.4.7. Kinetic Analysis

The kinetic properties of decomposition of the linear copolymer precursor and SCPM-ball type CoPc were revealed by calculating the activation energy (E_a) by the FWO and KAS models, which are iso-conversional methods. The Figure 3.29 and Figure 3.30 show the determination of the activation energy of the SCPM-ball type CoPc calculated by the methods; (a) FWO and (b) KAS, respectively.

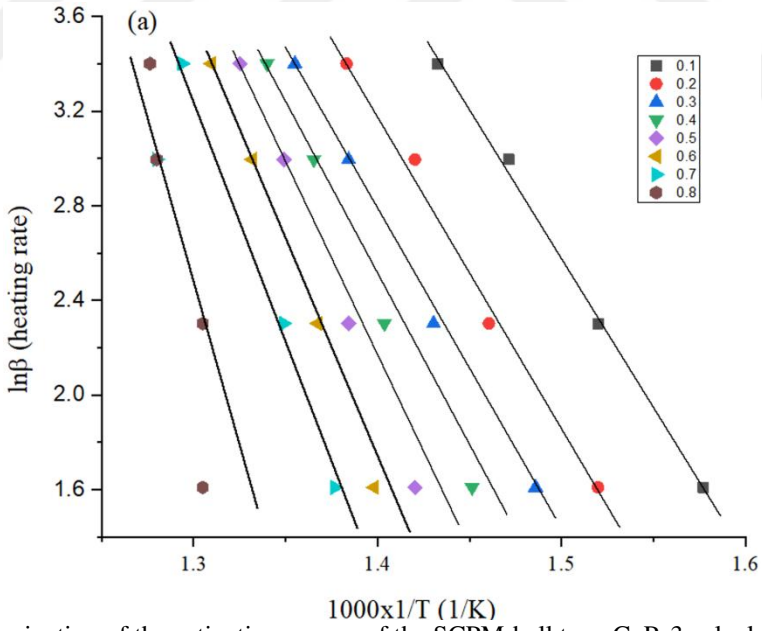

Figure 3.29. Determination of the activation energy of the SCPM-ball type CoPc3 calculated by the methods (a) FWO and (b) KAS methods

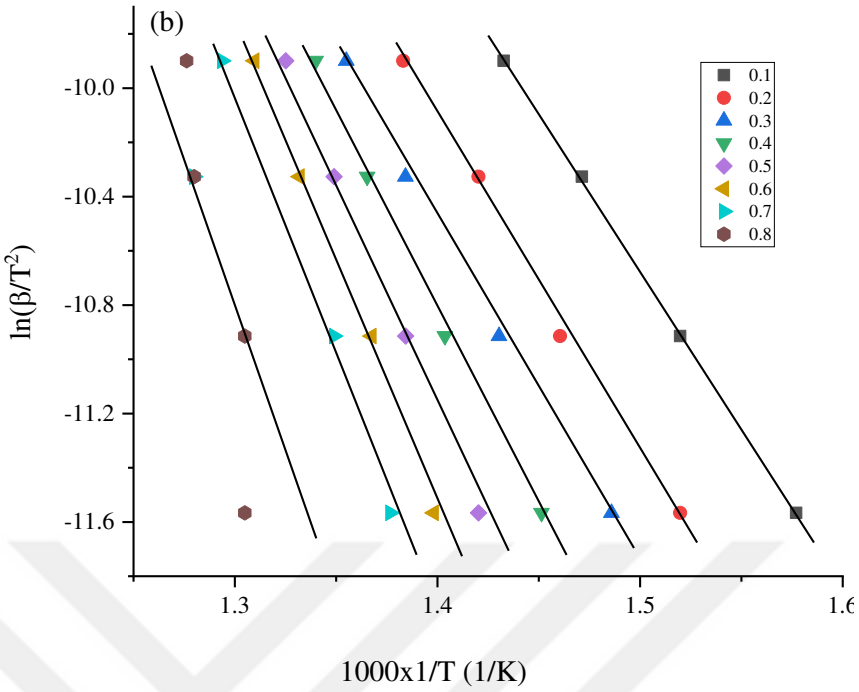

Figure 3.30. Determination of the activation energy of the SCPM-ball type CoPc3 calculated by the methods (a) FWO and (b) KAS (Continue)

The Figure 3.31 shows the activation energy variation versus conversion plots for F-W-O and KAS methods for P(PNDEAMSt12-co-St) and SCPM-ball type CoPc values of E_a are evaluated in Table 3.21 for each conversion.

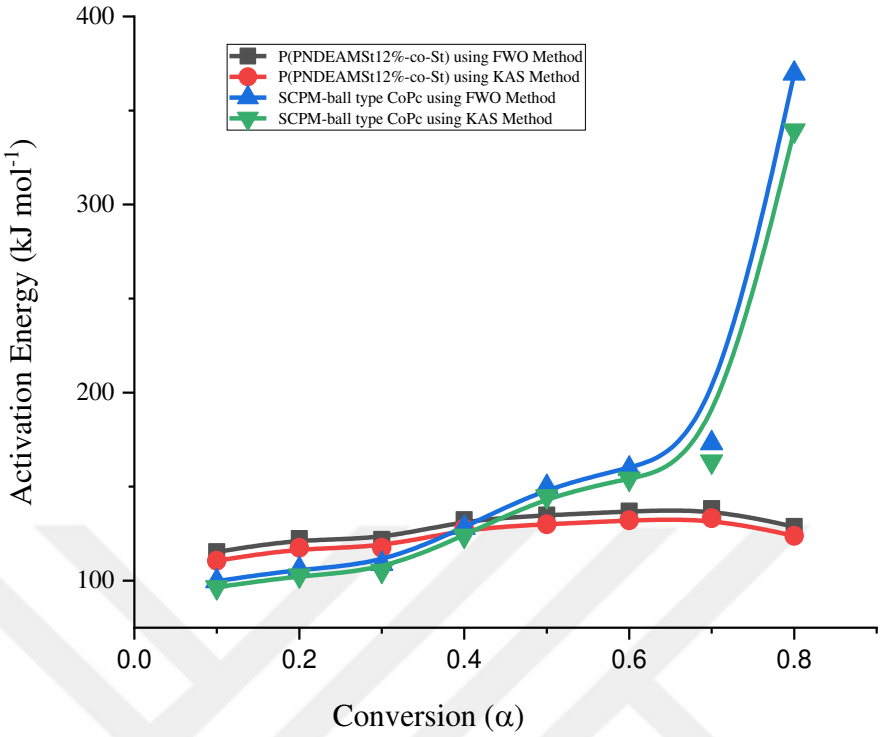

Figure 3.31. Activation energy variation versus conversion plots for F-W-O and KAS methods.

Table 3.21. Values of E_a for each conversion for F-W-O and the KAS methods

	Linear copolymer precursor		**SCP-ball type CoPc**	
α	Ea (kJ/mol) (F-W-O)	Ea (kJ/mol) (KAS)	Ea (kJ/mol) (F-W-O)	Ea (kJ/mol) (KAS)
0.1	99.73	110.57	99.73	96.52
0.2	106.13	117.47	106.13	102.76
0.3	108.90	117.47	108.90	105.25
0.4	128.18	127.70	128.18	123.96
0.5	149.84	130.03	149.84	144.91
0.6	159.64	132.10	159.64	154.30
0.7	173.15	133.19	173.15	163.37
0.8	369.62	123.87	369.62	339.37
Average	128.77	124.05	161.90	153.80

3.4.8. Electrical Characterization of Linear Copolymer Precursor P(PNDEAMSt12%-co-St) 5% by wt loaded GO

Figure 3.32, Figure 3.33 and Figure 3.34 show frequency dependence of dielectric constant, dielectric loss factor and tanδ at different temperatures (40, 90 and 130°C), P(PNDEAMSt12%-co-St) 6.5% (by wt) loaded GO.

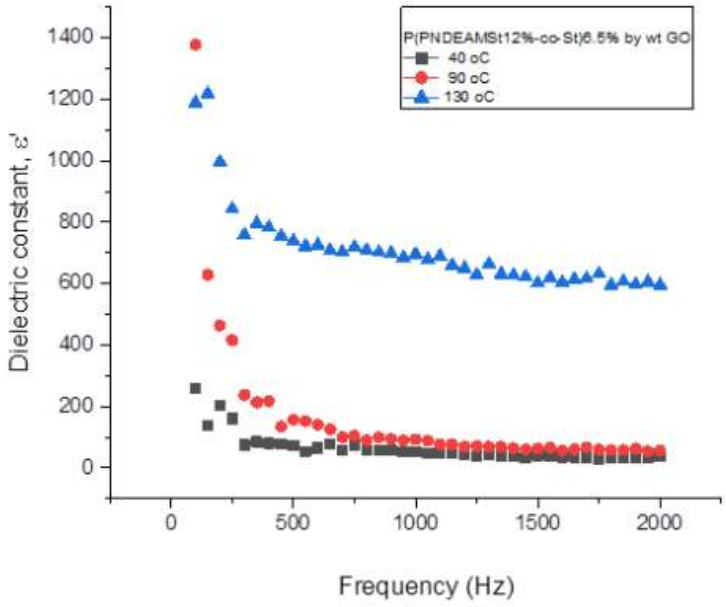

Figure 3.32 Frequency dependence of dielectric constant, at different temperatures (40, 90 and130 °C), P(PNDEAMSt12%-co-St) 6.5% by wt loaded GO.

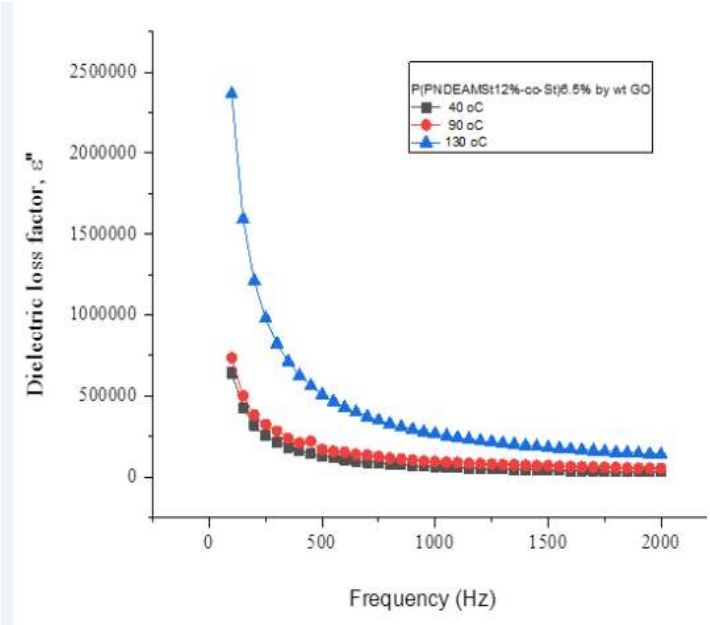

Figure 3.33. Frequency dependence of dielectric loss factor, measured at different temperature (40, 90 and130 °C), for P(PNDEAMSt12%-co-St) 6.5% by wt loaded GO.

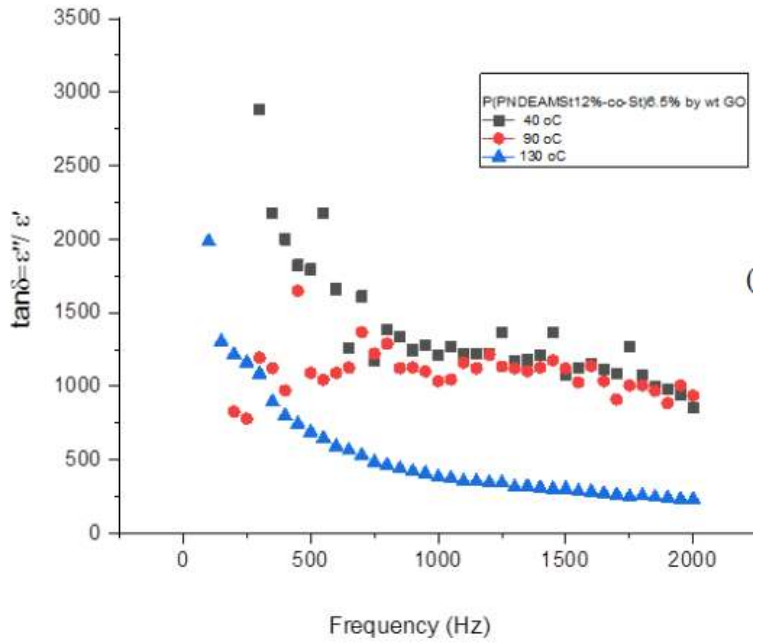

Figure 3.34. Frequency dependence of tanδ measured at different temperature (40, 90 and130 ^{o}C), for P(PNDEAMSt12%-co-St) 6.5% by wt loaded GO.

3.4.9. Electrical Characterization of SCP-ball Type CoPc3 Loaded GO

Figure 3.35 and Figure 3.36 show frequency dependence of dielectric loss factor and tanδ at different temperatures (40, 90 and 130 ^{o}C), for SCP-ball type CoPc3 14 wt % GO composite.

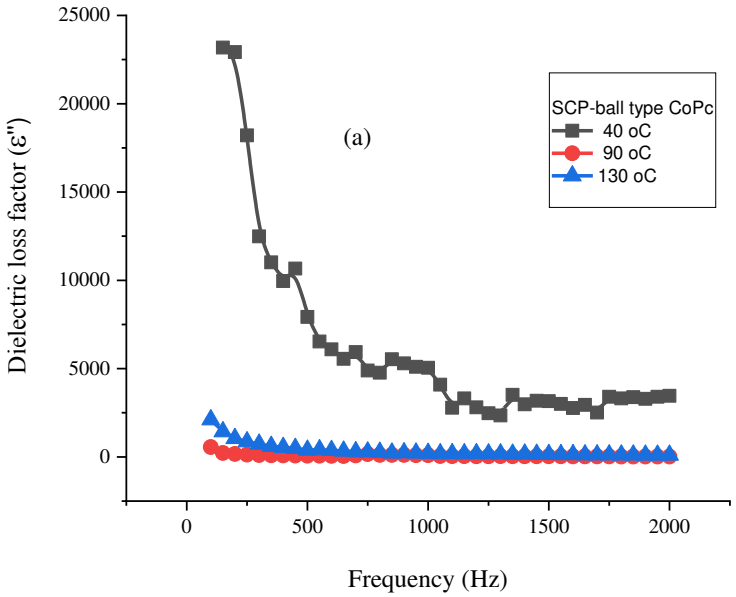

Figure 3.35. Frequency dependence of dielectric loss factor, measured at different temperature (40, 90 and 130 ^{o}C), for SCP-ball type CoPc3 14% wt GO composite.

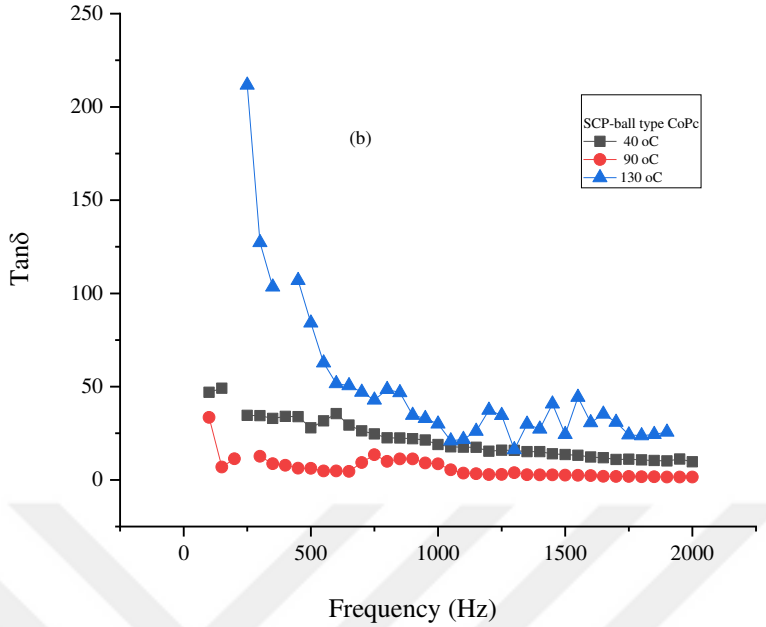

Figure 3.36. Frequency dependence of tanδ measured at different temperature (40, 90 and 130 ^{o}C), for SCP-ball type CoPc/14 wt% GO composite

The Figure 3.37 shows the ac conductivity versus frequency at two different temperature of linear copolymer precursor 6.5% by wt GO and SCP-ball type CoPc14% by wt GO composites.

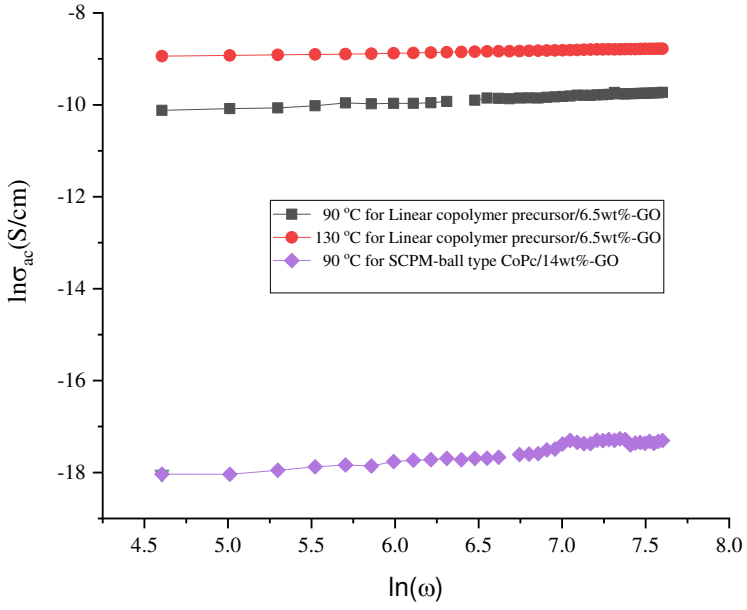

Figure 3.37. Ac conductivity versus frequency at two different temperature of linear copolymer precursor 6.5% by wt GO and SCP-ball type CoPc314% by wt GO composites

The Figure 3.38 shows dc conductivity dependence of temperature for linear copolymer precursor 3.6% by wt GO.

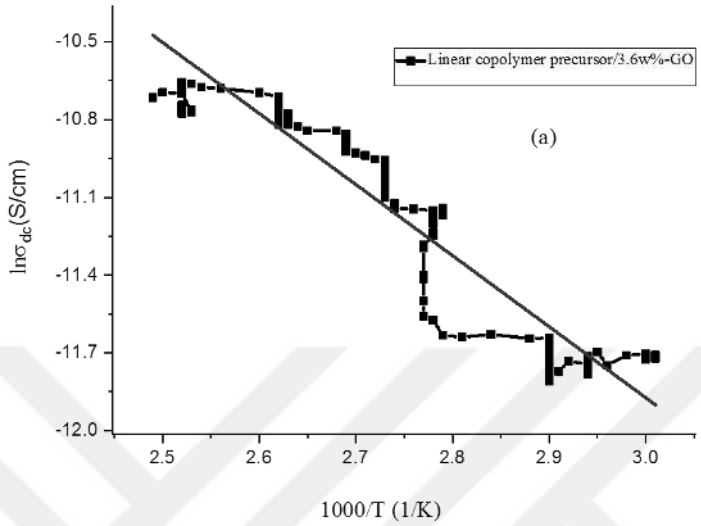

Figure 3.38. Dc conductivity dependence of temperature for linear copolymer precursor 3.6% by wt GO.

The Figure 3.39 shows dc conductivity dependence of temperature for linear copolymer precursor 4.5% by wt GO

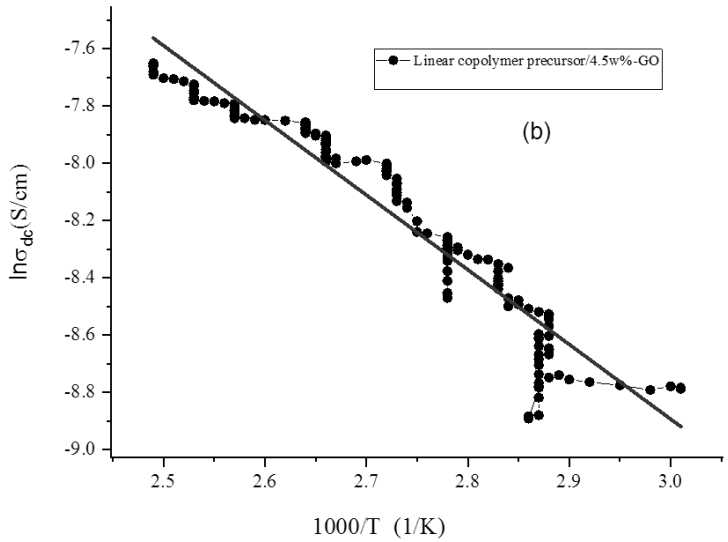

Figure 3.39. Dc conductivity dependence of temperature for linear copolymer precursor 4.5% by wt GO

Figure 3.40 shows dc conductivity dependence of temperature for linear copolymer precursor 6.5% by wt GO.

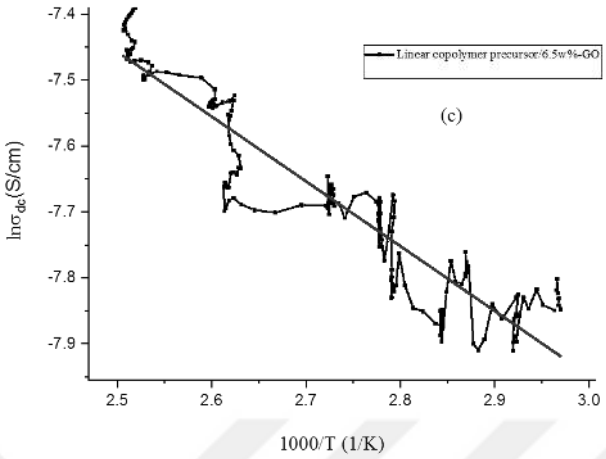

Figure 3.40. Dc conductivity dependence of temperature for linear copolymer precursor 6.5% by wt GO

The Figure 3.41 shows dc conductivity dependence of temperature SCP-ball type CoPc3 14% by wt GO composites.

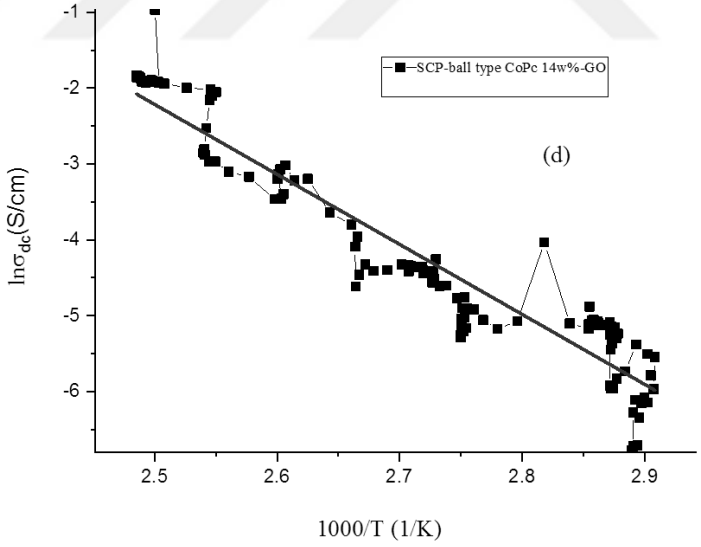

Figure 3.41. Dc conductivity dependence of temperature SCP-ball type CoPc3 14% by wt GO composites

The Figure 3.42 shows graph of current versus voltage linear copolymer precursor composites.

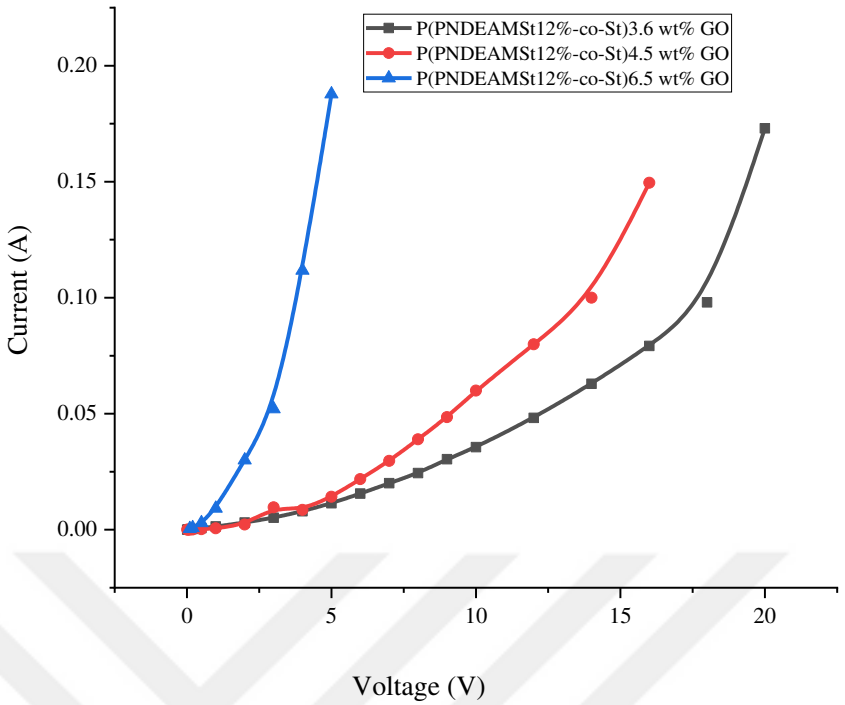

Figure 3.42. Graph of current versus voltage linear copolymer precursor composites

4. DISCUSSION

SCP-ball type CoPc prepared from three different linear copolymer precursors carrying phthalonitrile pendant groups (prepared by free radical polymerization) followed by macrocyclization of the pendant groups to form CoPcs.

4.1. Linear copolymer precursor 1 and 2, SCP-CoPc 1 and 2

The styrene monomer containing phthalonitrile group [4,4'-((((4-vinylbenzyl)azanediyl) bis-(ethane-2,1diyl)) bis(oxy))diphthalonitrile, (PNDEAMSt) was synthesized via a nucleophilic aromatic substitution reaction according to the synthetic route (as shown in Figure 2.2) between 4-diethanolaminomethyl styrene and 4-nitrophthalonitrile in presence of Na_2CO_3 at 70 ^oC. The some important signals as to structure of PNDEAMSt synthesized are summarized following as: FT-IR (cm^{-1}) 3115, 3083, 3046 (aromatic C-H stretching), 2833-2948 (aliphatic C-H stretching, 2230 (C≡N stretching), 1628 (C=C stretching in the CH_2=CH-) 1598 (C=C stretching on the aromatic ring), 1253 (C-O stretching on the aryl group). ^{1}H-NMR (ppm) : 3.11 (two CH_2 next to nitrogen), 3.83 (CH_2 between phenyl and nitrogen atom), 4.13 (two CH_2 next to -O-aryl), 5.28 (cis H in the CH_2=CH-phenylene-), 5.77 5.28 (trans H in the CH_2=CH- phenylene-), 6.63 (CH_2=C<u>H</u>-phenylene-), 7.13-7.29 (another aromatic protons), 7.69 (aromatic ring protons (4H) adjacent to CN group).^{13}C-NMR (ppm) : 53.28 3.11 (<u>C</u>H_2 next to nitrogen), 59.5 (<u>C</u>H_2 between phenyl and nitrogen atom), 68.04 (CH_2 next to -O-aryl), 114 and 115 (C in the C≡N).

Two different copolymers prepared with PNDEAMSt and styrene were synthesized by free radical polymerization method at 60 ^oC (as shown in **Figure 2.4.**)

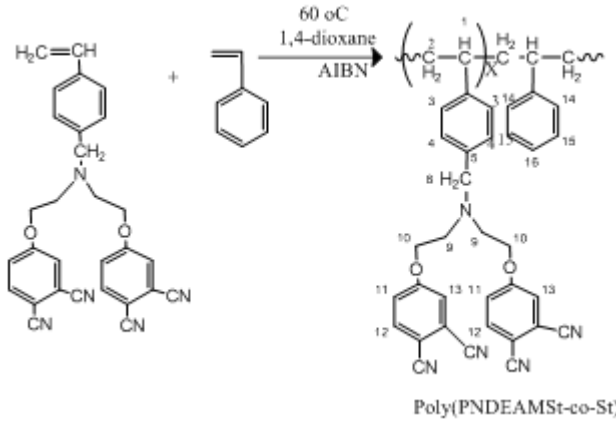

Poly(PNDEAMSt-co-St)

New binuclear, SCP-ball-type CoPcs were prepared by the reaction of poly(PNDEAMSt2-*co*-St) and poly(PNDEAMSt6-*co*-St) with $Co(CH_3COO)_2.4H_2O$ in presence of excess pthalonitrile under diluted conditions. The structure and purity of the ball-type SCP-ball type CoPcs were confirmed by UV–Vis, FT-IR and MALDI-TOFF-MS. The both of SCP- ball-

type CoPcs were well soluble in most of routine organic solvents such as dichloromethane, tetrahydrofuran, DMSO, THF and $CHCl_3$. The composition of copolymers synthesized by free radical copolymerization of PNDEAMSt and St at 60 ^oC were estimated via ^1H-NMR spectra (as shown in Figure 3.4). The characteristic peaks of the PNDEAMSt were observed for protons being next to etheric oxygen (δ = 3.0 ppm) and aromatic proton (δ =7.8 ppm) in the ^1H-NMR spectrum. ^1H-NMR spectra of poly(PNDEAMSt-co-St)1 and poly(PNDEAMSt-co-St)2 showed a characteristic some broad signal at 7.8 ppm, which is assigned to four protons the peripherally positioned proton (12 and 13 numbered protons on the Figure 2.4) on the CN-Ar-H moiety. Also, 11 numbered proton overlaps with other aromatic protons. In ^1H NMR spectrum of poly(PNDEAMSt-co-St)2 the total integration height of protons 12 and 13 numbered is 0.12. Mol number of PNDEAMSt moiety was estimated as 0.03 (0.12/4), and those of 11 and total aromatic protons are 2.60. PNDEAMSt moiety has 0.06 for 11 numbered protons and 0.21 for its aromatic protons, those integral height (0.06 and 0.21) 0.27 was removed from 2.6 and estimated 2.33. Here, mol number of styrene moiety estimated as 0.466 (2.33/5). In this context, mol fractions of PNDEAMSt and St in the precursor copolymer2 was found as 6% and 94%, respectively. In similar fashion, in ^1H NMR spectrum of precursor copolymer1, mol fractions of PNDEAMSt and St were estimated as 2% and 98%, respectively. Green colored SCP-ball type CoPc1 and SCP-ball type CoPc2 were prepared by cyclotetramerization of precursor copolymer1 and 2 with $Co(CH_3COO)_2$ and phthalonitrile in cyclohexanol. Structure of green colored SCP-ball type CoPc has been showed in the Figure 2.5 The precipitated polymers occured during reaction. For the efficient formation of CoPcs in SCP, the phthalonitrile was added to the reaction medium. The use of excess of solvent in the reaction was considerably required to minimize intermolecular coupling reactions of SCP-ball type CoPcs resulting in insoluble impurities. Before the reaction, although the mixture is colorless the color of the solution changed from light yellow to greenish together the macrocyclization step. Any precipitant not occured at end of reaction. This behavior implies that intermolecular coupling reactions are not occured due to excesses used cyclohexylalcohol and added phthalonitrile. The vibronic peaks of the nitrile groups in FT-IR spectra of the PNDEAMSt unit after copolymerization (as seen in the Figure 3.5) were observed at 2230 cm^{-1} and the precursor copolymers showed Ar-O-Ar vibrational band bands at 1254 cm^{-1} in the FT-IR spectrum. To confirm the formation of SCP-ball type CoPcs, it was characterized using FT-IR and UV-Vis spectroscopy. FT-IR spectra of green colored SCP-ball type CoPc1 and SCP-ball type CoPc2 indicate that the peak corresponding to the C≡N vibrational peak at 2230 cm^{-1} completely disappeared and a new band (-C=N- for imine group) appeared at 1720 cm^{-1} after cyclotetramerization (Figure 3.5 a and b). FT-IR spectra of both SCP-ball type CoPcs indicated a imin (-C=N-) band at 1720 cm^{-1}. Those data confirmed the formation of the desired green colored SCP- SCP-ball type CoPc complexes. The phthalocyanines show typical electronic spectra with

two significant bands (B-bands) in the UV region (320–350 nm) and the visible region (600–700 nm, the Q-band). A strong intermolecular interaction between the Pc rings in ball-type CoPc complexes is expected to result in a splitting of the molecular orbitals. The UV–Vis spectra of SCP-ball type CoPc1 and SCP-ball type CoPc2 complexes in CH_2Cl_2 are in accordance with the trend found in the literature, as indicated in the Figure 3.5a and b. The characteristic Q-band transition of metallophthalocyanines is observed as a single band of high intensity in the visible region. Aggregation in metallophthallocyanines is understood by broadened or split Q band. A well-defined band between 600 nm and 675 nm in ball type phthalocyanines is due to exciton coupling between the two Pc rings [65-67]. The copolymers SCP-ball type CoPc1 and SCP-ball type CoPc2 showed characteristic absorptions around 601 and 673 nm in the Q band region. As expected, well splitting of the Q band in the spectrum of SCP-ball type CoPc1 and SCP-ball type CoPc2 was observed. It was found that the shape of their Q bands changed considerably in comparison with the SCP-ball type CoPc1 and SCP-ball type CoPc2 complexes. The spectral changes consist of a shift in the Q-band from 663 to 673 nm. The UV-Vis spectrum of SCP-ball type CoPc1 complex as indicated in the Figure 3.6a showed some broad band in the 663 nm region, which could be a combination of vibronic bands and the band due to exciton coupling between the two rings. Whereas, that of SCP-ball type CoPc2 illustrated in Figure 3.6b was 673 nm. This can be attributed to strong intramolecular interactions between the Pc rings in the SCP-ball type CoPc2 complexes, probably due to the ball-type cofacial structure and aggregation. The absorption spectrum provided information about the type of aggregated structure, such as cofacial (face-to-face)[68]. The p-p stacking among the cofacial phthalocyanine groups provides a driving force for self-organization of polymers. In addition, the another bands revealing as result splitting of the Q band for SCP-ball type CoPc1 and SCP-ball type CoPc2 are 601 nm and 622 nm, respectively. The spectra of complex SCP-ball type CoPc1 in dichloromethane shows bands in the 601 nm region, which could be a combination of vibronic bands and the band due to exciton coupling between the two rings. That of SCP-ball type CpPc2 complex was 622 nm. This can be attributed that β substitution results in blue shifting of the spectra in metallo Pcs, this is due to the electron density decrease caused by the substitution at the peripheral position. Also, as expected for ball type structures, SCP-ball-type CoPc1 and SCP-ball type CoPc2 complexes have broad spectra. A well-defined absorption at 622 nm in ball type phthalocyanines at our study has been associated with exciton coupling between two Pc rings, and it can be attributed to intramolecular interactions [69-71].

The synthesized SCP-ball type CoPc1 having double core phthalocyanine was analyzed by MALDI-TOF-MS in reflectron mode and the spectrum is given in Figure 3.7. MALDI-TOF-MS spectrum showed a polymeric distribution following 104 Da mass difference that have styrene repeating unit used in synthesis of phthalocyanine containing polymer. Mass of cobalt complex of

double core phthalocyanine without monomer units was 2010 Da nominal mass. When each peak mass was evaluated, it was noticed that the polymer having cobalt complexed phthalocyanine core was initiated with hydrogen and ended again by hydrogen. Also, each polymeric species was ionized by potassium adduct. All peak masses corresponded these phenomena. On the other hand, each peak followed another repeating peak which have 16 Da mass higher than the intense peaks. These peaks showed us another polymeric species initiated by hydrogen and ended by OH group. The peaks calculated theoretical was matched exactly with the isotopic mass distribution of the experimentally obtained. Finally, it could be concluded that the polymeric structure having cobalt complexes core phthalocyanine was synthesized in the desired form. The synthesized form of the polymeric and cobalt complexed phthalocyanine compound was showed a polymeric distribution which have almost between n=3–25 styrene monomer repeating units.

DSC curves of SCP-ball type CoPc2 and pure polystyrene (PSt) prepared by free radical polymerization method were recorded at heating rate of 20 ^{o}C/min, and are shown in Figure 3.8. For comparison, DSC curve of pure polystyrene (PSt) is also shown in Figure 3.8. While the glass transition temperature (Tg) of pure PSt was estimated as 102 ^{o}C from DSC curve. Whereas, that of SCP-ball type CoPc2 was 116 ^{o}C, and thereby increased the endothermic peak. The shift in endothermic peak, that is the Tg increase of the later sample can be ascribed to Pc tetramerization in the single chain polymer structure meaning that has restricted chain mobility. Also, the Tg of SCP-ball type CoPc1 was measured between polystyrene and SCP-ball type CoPc2

Thermal decomposition temperatures of pure PSt, P(PNDEAMSt6%-co-St)2, SCP-ball-type CoPc1 and SCP-ball type CoPc2 were estimated by thermogravimetric analysis (TG). They were indicated compared to each other as indicated in Figure 3.9. The weight loss (TG) curves of pure PSt, SCP-ball type CoPc1 and SCP-ball type CoPc2 at a heating rate of 10^{o}C/min under an argon flow are displayed in Figure 3.8. All the TG curves of SCP- ball type CoPcs have a similar trend, but the starting (T_i) and residue amounts (%) in completion (T_f) temperatures, and the temperature at the maximum decomposition rate (T_p) for all the curves showed difference from each other. From the TG curves, the initial decomposition temperature, the temperature at 50% weight loss ($T_{\%50}$), final degradation temperature and residue% were estimated. Compared to pure polystyrene, thermal stability of the SCP-ball type CoPc1 and SCP-ball type CoPc2 are always higher and residual% and maximum decomposition temperature appears to increase as the content of CoPc in the single chain polymer structure increases. So, while pure PSt exhibits degradation occurring in a single stage, which is in the temperature range from 305 °C to 600 °C, with weight losses 98%, and those of SCP-ball type CoPc1 and SCP- ball type CoPc2 showed a degradation with weight loss 96% and 84%, respectively. For instance, the temperature at 50% weight loss of SCP- ball type CoPc1 and SCP-ball type CoPc2 is 31^{o}C and 34^{o}C, respectively higher than that of pure polystyrene. This behavior can be atributed to more energy absorbtion of CoPc units in the

single chain polymer molecules. The thermal degradation pathway of pure polystyrene has been in detail investigated. The possibility that the presence of the inorganic filled causes some chemical changes in the degradation pathway of polystyrene composites was emphasized. Those research results have implied that thermal stability of polystyrene considerably increased [72, 73]. The results of TG measurement were summarized in Table 3.10.

FT-IR spectrum recorded in presence of KBr for residue of SCP-ball type CoPc1 heated to 600 ^{o}C has been showed in Figure 3.10. It showed important bands at 1625 cm^{-1}, 1424 cm^{-1}, 1134 cm^{-1} (C-O), 667 cm^{-1} and 579 cm^{-1}. The weak band at 1625 cm^{-1} is due to the bending mode of water molecules. Two distinctive bands at 667 cm^{-1} and 579 cm^{-1} are the characteristics of the Co-O stretching vibrations being characteristic for formation of Co_3O_4 [74]. Also, the weak adsorptions at 3430 cm^{-1} and 1630 cm^{-1} correspond to the bending and stretching vibration modes of absorbed water molecules on the surface. The strong peak at about 3500 cm^{-1} is attributed to the stretching vibration of the O-H group of molecular water and hydrogen-bond O-H groups [75-77]. The weak band at 1625 cm^{-1} (O-H) is due to the bending mode of water molecules. While the band at 962 cm^{-1} is ascribed to ν (Co-OH) bending modes and the band at 512 cm^{-1} is ascribed to (Co-OH) vibration [78]. Whereas, for residue in the 600 ^{o}C of SCP-ball type CoPc2, the new distinctive bands at 667 and 579 cm^{-1} revealed. They are the characteristics of the Co-O stretching vibrations being characteristic for formation of Co_3O_4. This case implies that residue converts from $Co(OH)_2$ to Co_3O_4.

The kinetic parameters of thermal degradation are possible to estimate from the TGA curves using various methods. One of them is multiple heating rate kinetics (MHRK) method. Ea (activation energy) of a system is associated with the energy barrier, A with the frequency of vibrations of the activated complex [29]. In this context, the E_a for the thermal decomposition of SCP-ball type CoPc1 was determined by Flynn–Wall–Ozawa method, which is widely used.

The kinetic analysis of the degradation of samples was performed by utilizing the thermograms obtained from the TGA curves. For this purpose, the dynamic thermal degradation measurements on SCP-ball type CoPc1 were performed at temperature range from room temperature to 600 ^{o}C under a nitrogen flow (10 ml/min), at different heating rates (5.0, 10.0, 15.0, 20.0, 25.0 and 35.0 ^{o}C/min). Increase in the heating rate results in a shift toward higher temperatures in the thermograms as indicated in the Figure 3.11 The reason for this behavior is that the sample needs shorter time to catch a given temperature for a faster heating rate. If a series of experiments are carried out at different heating rates, E_a can be estimated from the slope of the linear plot of log(heating rate) (logβ) versus 1/T. For a study of the kinetic in the thermal degradation of polymers, TG (thermogravimetry) or ITG (isothermal thermogravimetry) at different heating rates can be selected. It is shown in Figure 3.13 that the fitted lines are nearly parallel, which indicates approximate activation energies at different conversions and

consequently implies the possibility of the unification of multiple reaction mechanisms. According to the Flynn–Wall–Ozawa (FWO) method [30], E_a of the apparent thermal decomposition can be defined from the TGA thermogram measurements. The TGA curves were recorded at the end of each measurement and the weight losses were then transferred to a computer at diverse temperatures. Also, Figure 3.12 shows kinetic analysis using the specific results of application of Ozawa's method for ball type CoPc1 degradation in argon gas flow. The curves obtained at different conversion rates are observed to be roughly parallel to each other and the correlation coefficient of the linearity for the calculation of each activation energy are larger than 0.97. Also, there is no systematic divergence from linearity. Therefore, it is suggested that the method fitted well for the nonisothermal degradation of SCP-ball type CoPc1 and rate order of degradation is 1 in the SCP-ball type CoPc1. The plot logβ vs. 1/T obtained from a series of experiments performed at several heating rates, should be a straight line whose slope allows evaluation of E_a:

$$\ln(\beta) = \text{Constant} - 1.052\frac{E_a}{R.T} \tag{4.1}$$

where R is a constant and β is the heating rate (^{o}C/min). According to Equation (4.1) above monitored, the E_a of decomposition can be obtained from the slope of the linear relationship between log(heating rate) and the reciprocal of the temperature, as indicated in Figure 3.12; it was found that the activation energy for weight loss from 7% to 90% was increased 33.1 and, 56.7%, respectively. Average apparent activation energies of the thermal degradation of SCP-ball type CoPc1 calculated by three model-free methods in a period of $\alpha = 0.07–0.90$ have been summarized in Table 3.12. Figure 3.13 shows the plots of activation energy as a function of conversion for, extent of conversion, $\alpha = 0.07–0.90$ for SCP-ball type CoPc1 based on iso-conversional method. The estimated activation energy range is clearly observed in Figure 3.13 with a "band" shape between 33 and 57 kJ/mol. The sharply increase of activation energies after $\alpha = 0.5$ implied the possible occurrence of accelerated decomposition process of main composition which is approaching balance in the initial stage. It is noted that this accelerated process might be different from the one at the very beginning period ($\alpha = 0–0.07$), which is mainly caused by the decomposition of low molecular composition. The reaction mechanism, however, also might change in comparatively higher conversion periods according to unsatisfied parallel line of $\alpha = 0.6$.

Figure 3.14 shows refractive index, n, for the SCP-ball type CoPc1 as a function of wavelength. It is seen that the values of n are decreased with increasing wavelength. It is well known that they possess two kinds of energy bands. One of them is called the Q band, and other one is called the B band. It was observed from Figure 14 that the refractive index is very low in

the Q band region and in the B band region the refractive index is high. The large decrease in the reflectance about from 480 to 600 nm is due to a decrease in the refractive index. The refractive index has not almost changed between 600 and 700 nm. This range is related to the visible region (600–700 nm, Q-band) and this behavior implies that refractive index not changes as a result that a strong intermolecular interaction between the Pc rings in ball type CoPc complexes is expected to result in a splitting of the molecular orbitals. The large increase in the reflectance about from 700 to 900 nm is due to a increasing in the refractive index.

Dielectric behavior of a normal material can be characterized by dielectric constant (ε'), dielectric loss factor (ε”), loss tangent (tanδ) and conductivity (σ_{ac}). Relative permittivity (compared to free space) is a frequency dependent complex quantity:

$$\varepsilon* = \varepsilon' - i\varepsilon'' \qquad (4.2)$$

The real (ε′) and imaginary (ε″) relative permittivity values are related to the stored energy and dissipated energy, respectively, within the material [31]. In this context, it has a great importance to investigate with an impedance analyzer as a well-known technique for measuring the dielectric properties of precursor copolymer and SCP-balltype CoPc2. We have performed dielectric measurements such as the dielectric constant, dielectric loss factor, tanδ and alternative conductivity (σ_{ac}) results of precursor copolymer2 and SCP-ball type CoPc2 for frequencies varying in the frequency range of 100 Hz to 2000 Hz. In this context, graphs of precursor copolymer and SCP-ball type CoPc2 have been indicated in Figure 3.15 (a-d) and Figure 3.16 (a-d), respectively. The frequency dependence on the dielectric constant, (ε') for precursor copolymer2 and SCP-ball type CoPc2 is showed in Figure 3.15a and Figure 3.16a. Below 1 kHz, ε', rapidly decreases with increasing frequency for both precursor copolymer2 and SCP-ball type CoPc2. Dielectric constants of precursor copolymer and SCP-ball-type CoPc2 at room temperature are 9.85 and 5.39, respectively. The precursor copolymer shows high dielectric values from than SCP-ball type CoPc2 due to the increasing number of dipoles at low frequencies. Cause of this increase in ε’ results from polarity of two nitrile (CN) groups in the precursor copolymer indicating its strong influence on the interfacial polarization. But, those values in the increasing frequency range not importantly changed. The change in real part values of the dielectric constant of the samples in the frequency range that were measured was due to the effectiveness of the applied field frequency on the polarization mechanism of the two samples. Figure 3.15 (b) and Figure 3.16 (b) show the variations of ε" with frequency for the precursor copolymer2 and SCP-ball type CoPc2, respectively. Those Figures present same variations for both samples. Dielectric loss factor, ε", of precursor copolymer2 and SCP-ball type CoPc2 at room temperature are 1.06 and 0.02, respectively. Also, this behavior implies that precursor copolymer2 is tend to dissipate a fraction of the more stored energy from than SCP-ball type

CoPc2. Figure 3.15 (c) and Figure 3.16 (c) indicate loss tangent (tanδ=ε″/ε′) versus frequency for precursor copolymer2 and SCP-ball type CoPc2 at room temperature. The loss tangent (tanδ=ε″/ε′) value is also an evidence of the dissipative behavior in a material. Real and imaginary relative permittivity values were almost independent of frequencies in the X-band [30, 79, 80].

Loss tangent, tanδ, of precursor copolymer2 and SCP-ball type CoPc2 at room temperature are 0.1 and 0.00378, respectively. The high tanδ of precursor copolymer2 means generally that will tend to dissipate a fraction of the more stored energy and more energy storing in the form of heat. The alternative conductivity (σ_{ac}) versus frequency for precursor copolymer-2 and SCP-ball-type CoPc2 were measured. The graphs of precursor copolymer-2 and SCP-ball type CoPc2 have been indicated in the Figure 3.15 (d) and Figure 3.16 (d), respectively. The results revealing indicated that σ_{ac} not changed with increasing frequency at fixed temperature. The σ_{ac} value decreased from $6.9x10^{-09}$ S/cm to $2.78x10^{-09}$ S/cm at 1 kHz and 298K. Both precursor copolymer2 and SCP-ball type CoPc2 indicated that are an insulator material from above mentioned results.

4.2. Linear copolymer precursor, SCP-CoPc 3 and their composites

Linear copolymer precursor, poly(DEAMSt12%-co-St), was prepared by free radical copolymerization of PNDEAMSt and styrene monomers at 60 °C in the presence of 1,4-dioxane using AIBN as initiator. Then, P(PNDEAMSt12%-co-St) was reacted from reaction of P(DEAMSt12-co-St) with 4-nitrophthalonitrile in presence of Na_2CO_3 via 2. pathway like that reaction scheme was seen in Figure 2.2.

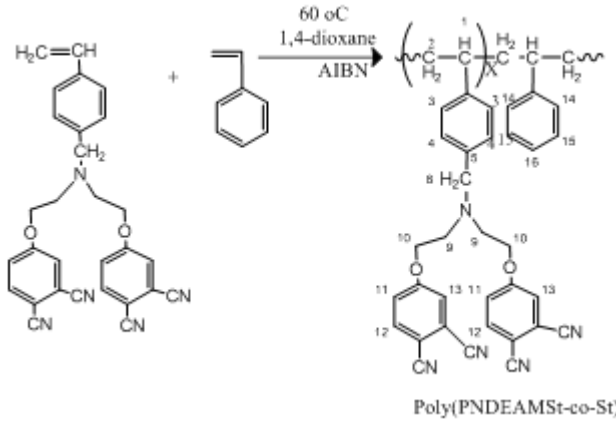

Figure 2.4. shows structure of linear copolymer precursor, in this regard, FT-IR spectrum indicated in the Figure 3.18 for poly(DEAMSt12%-co-St) indicated at the most characteristic O-H stretching bands at 3400 cm^{-1}, C=C stretching at 1601 cm^{-1}, C-O stretching at 1265 cm^{-1}. Figure 3.18 shows ^{1}H-NMR spectrum of poly(DEAMSt12%-co-St). In this regard, ^{1}H-NMR spectrum

of poly(DEAMSt12%-co-St) indicated the most important signals such as -CH_2- in the main chain at 1.25-1.9 ppm, -CH_2N- at 2.75 ppm, -OH at 4.12 ppm.

Figure 2.4. shows structure of linear copolymer precursor, poly(PNDEAMSt12%-co-St). FT-IR spectrum indicated in the Figure 3.19 for PNDEAMSt indicated the most characteristic bands at 2230 cm^{-1} atributed to -C≡N group, C=C stretching at 1596, 1605 cm^{-1} and Aryl-C-O-C-Aryl vibrational band at 1258 cm^{-1}. Figure 3.20 indicates ^{1}H-NMR spectrum P(PNDEAMSt12%-*co*-St). The ^{1}H NMR spectrum of linear copolymer precursor, P(PNDEAMSt12%-*co*-St), confirmed a distinctive sharp singlet that is allocated to the peripherally located proton on the CNArAH moiety at 7.79 ppm. The copolymer composition of linear copolymer precursor was estimated by measuring the integrated peak areas of aromatic orto protons on styrene units and aliphatic protons in the PNDEAMSt moities. The ^{1}H NMR spectrum of linear copolymer precursor integrates to 0.6 unit the total number of 10 protons belonging to aliphatic protons between two aryl groups of PNDEAMSt unit. The integration value per one hydrogen in PNDEAMSt unit is 0.06, two hydrogen contains 0.12 units together other orto protons of PNDEAMSt moiety. So this value is estimated as 0.88 and substracted from 1.0 unit integrated for two orto protons at 6.7 ppm. The integration value per a hydrogen of styrene in the linear copolymer precursor is 0.44. The total number of mol is calculated as 0.5. Thus, it was estimated that the PNDEAMSt and St ratios of linear copolymer precursor at this our study were 12% and 88% (by mole), respectively as shown in Figure 3.4. The preparation of new binuclear SCPM-ball type CoPc was carried out from reaction of P(PNDEAMSt12%-co-St) and $Co(CH_3COO)_2.4H_2O$ in the presence of high concentration pthalonitrile under diluted cyclohexanol conditions at 140-150 ^oC under argon gas. The structure and purity of the SCPM-ball type CoPc were confirmed by FT-IR, UV–Vis and MALDI-TOF-MS instruments. The controllable cobalt centered phthalocyanine containing polymer molecules were entirely soluble in many other routine organic solvents such as dichloromethane, $CHCl_3$, DMSO, acetone and THF. This behavior indicates that the SCPM-ball type CoPc complex does not ocur crosslink structure among the polymer chains during the reaction in the presence of excess cyclohexanol. FT-IR spectrum of the SCPM-ball type CoPc3 was indicated in the Figure 3.21. On the other hand, FT-IR spectra of P(PNDEAMSt12%-co-St) and SCPM-ball type CoPc3 were compared with each other in Figure 3.23 a and b, respectively. As seen in the Figure 3.5b indicates the successful formation of SCPM-ball type CoPc3 whose structure showed as scheme in Figure 2.7 was confirmed by comparing with that of linear copolymer precursor. In this regards, while the Figure 3.5a shows C≡N stretching band at 2233 cm^{-1}, b almost no showed C≡N stretching band at 2233 cm^{-1}. The disappearance of the nitrile bands in the linear copolymer precursor due to the completion of the reaction confirms that SCPM-ball type CoPc exists. The cause of addition of excess phthalonitrile to the reaction medium was intended to prevent the formation of cross links. The IR spectrum of

SCPM-ball type showed Ar-C-O-C-Ar stretching band at 1258 cm^{-1}. The SCPM-ball type CoPc structure having two double core or more double core phthalocyanine was confirmed by MALDI-TOF-MS in positive ion and reflectron mode and the spectrum is indicated in Figure 3.7. The MALDI-TOF-MS spectrum showed a polymeric distribution of styrene repeating units following the 104 Da mass differences in SCPM-ball type CoPc. In order to get intense MALDI-TOF-MS spectrum silver trifluoroacetic acid was added in MALDI matrix. The mass of the one double core phthalocyanine cobalt complex without styrene monomer units in the CoPc -ball type CoPc was 2010 Da nominal mass as seen in the Figure 3.22. On the other hand, the mass of the two double core phthalocyanine cobalt complex without styrene monomer units was 4020 Da nominal mass. When each peak mass was analyzed, it was noted that hydrogen initiated the polymer with a cobalt-complexed phthalocyanine core and ended with hydrogen again. Each polymer species has also been ionized by silver adducts. In addition, the signals started around 6550 Da represent the three double cobalt core polymeric structure. But the intensities of these signals are low compared to the other signals. The reason of this event is due to low concentration of these species and also signal intensity comes down at high molecular weight region due to the suppression effect of the low molecular weight species signals. All peak masses, which were evaluated checking the isotopic mass distribution corresponded these phenomena. Every peak, however, on the other side, followed another repeating peak with a mass of 16 Da greater than the strong peaks. Another polymeric species initiated by hydrogen and terminated by OH groups showed us these peaks. The isotopic mass distribution of the predicted theoretical peaks was accurately matched to the experimentally obtained isotopic mass distribution. The synthesized form of the two double core in the polymeric ball type cobalt phthalocyanine structure was shown to have a polymeric distribution in its structure that has repeating units between n= 6-22 styrene monomer. Figure 3.24 exhibited two broad peaks at 598 nm and 660 nm in the UV-vis spectrum of SCPM-ball type CoPc. Those spectra were plotted depending upon concentration. The phthalocyanines have electronic transitions in the two main absorption regions. One of them is in the UV region (320-350 nm) band (B-band) and another is in the visible region (600-700 nm) Q-band. The UV-vis spectrum of the SCPM-ball type CoPc complex prepared in the dichloromethane solution shows bands in the 598 nm region, which may be a mixture of vibronic bands due to the excitation coupling between the two rings. In typical ball type phthalocyanines, it is known that the intensities of the B bands are higher than the Q band for the complexes that could be due to intramolecular interactions between Pc rings. Literature studies have shown that the distance between two Pc units of ball-type molecules and the degree of interaction between rings is greatly affected by aromatic groups [81]. Figure 3.25 a plan view SEM micrograph in the various magnitidues of SCPM-ball type CoPc material. Also, SEM analysis show that SCPM-ball type CoPc material is comprising of the various particles. And the SCPM-ball type CoPc

molecules agglomerates with particle size greater than 2 μm. The confirmation of the involvement of cobalt in the formation of SCPM-ball type CoPc complex was done by energy dispersive X-ray (EDX) analysis. The amount of Co in structure was estimated as 5.14% (by mole) at 20.0 kV. Whereas, the Co content in SCPM-ball type CoPc was therotically 5.9% (by mole). So, this value indicated that the therotical and experimental results were virtually agreement with each others.

The glass transition phenomenon is known that is rather a kinetic effect instead of a phase transition as defined in terms of thermodynamics [82]. The most common equipments used for estimating the glass transition temperature of polymers with amorph structure are differential scanning calorimetry (DSC), differential thermal analysis (DTA) and dynamic mechanical thermal analysis (DMTA) instruments. In this regard, DSC curves of P(DEAMSt12%-co-St), P(PNDEAMSt12%-co-St), P(PNDEAMSt12%-co-St)/GO 3.6% (by wt), P(PNDEAMSt12%-co-St)/GO 4.5% (by wt) and SCPM-ball type CoPc were indicated in Figure 3.26. As seen in Figure 3.26, P(DEAMSt12%-co-St) indicated a Tg at 114 ^{o}C. The addition of two phthalonitrile groups instead of hydroxyl in the diethanolamine group of the para position of polystyrene decreased from 114 ^{o}C to 80 ^{o}C the value of Tg. Normally, one would have expected P(DEAMSt12%-co-St) to have had a higher Tg value than that of P(DEAMSt12%-co-St), because of the presence of the bulkier p-substituent in the P(PNDEAMSt12%-co-St). But, the more massive two phthalonitrile groups increase the free volume and the mobility of the molecules in the amorphous polymer matrix. Hence, the Tg value of P(PNDEAMSt12%-co-St) decreased significantly. The similar behavior has been recorded in the literature studies as well [83]. The glass transition temperatures of P(PNDEAMSt12%-co-St)/GO 3.6% and 4.5% (by wt) were observed at 89^{o}C and 86^{o}C, respectively. This behavior implies that the segmental motions of the P(PNDEAMSt12%-co-St) among the GO galleries partially increases as the amount of GO in the composite matrix increases. On the other hand, Tg value of SCPM-ball type CoPc was measured as 126 ^{o}C. This behavior confirms to that cobalt phthalocyanine core in the SCPM-ball type CoPc decreased free volume.

Thermal stabilities of P(DEAMSt12%-co-St) and linear copolymer precursor and SCPM-ball type CoPc were investigated, and their TG curves (red lines) measured with heating rate of 10 ^{o}C/min were showed in Figure 3.27 and Figure 3.28, respectively. The initial decomposition temperature, the maximum decomposition temperature (T_{max}) and residue % were estimated from the TG curves. The results revealed from TG measurements are also given in Table 3.20. As seen (red line) in Figure 3.26, while thermal decomposition of P(DEAMSt12%-co-St) and linear copolymer precursor occurs in one step, that of SCPM-ball type CoPc ((red line) as seen in Figure 3.26) occurs mainly in two stages. This was due to the fact that the metallo pthallocyanine core in the SCPM-ball type CoPc structure had increased the resistance to thermal degradation, especially

in the second stage of temperature range beyond 424°C. A mass loss 36% in the first step for SCPM-ball type CoPc was observed between room temperature and 420 °C. The second stage was beyond 420 °C, and total mass loss to 500 °C was 42%. The onset decomposition temperature for P(DEAMSt12%-co-St) as compared to those of P(DEAMSt12%-co-St) and linear copolymer precursor was less. This is propably due to decomposition of diethanol amine group bonded to styrene unit in the P(DEAMSt12%-co-St). As both the amount of CoPc in the single chain polymer structure and PNDEAMSt moiety in the lineer copolymer precursor increased was observed an increasing in residual (% by wt). In this regard, amounts of residual for P(DEAMSt12%-co-St) and SCPM-ball type CoPc were 25% and 22%, respectively. Whereas, amounts of residual for P(DEAMSt 6%-co-St) (precursor copolymer2) and SCP-ball type CoPc2 that we have synthesized at a previous study [84] were 18% and 16%, respectively

The more information on the kinetic analysis of the thermal decomposition of polymer or polymer composites can be obtained from studies related to TGA. In order to provide guidance for designing an efficient and realistic decomposition process, a complete understanding of thermal decomposition kinetics is of great importance [85]. On the basis of a recommendation from the Kinetics Committee of the International Confederation for Thermal Analysis and Calorimetry (ICTAC, Kinetics Comittee), one of the main objectives of this section is to carry out a kinetic analysis on the apparent activation of energy, Ea. The kinetic properties of decomposition of the linear copolymer precursor and SCPM-ball type CoPc were revealed by calculating the activation energy (E_a) by the FWO and KAS models, which are iso-conversional methods. For the kinetic study of two copolymer, and b indicate eight conversion rates (α = 0.1–0.8) obtained from the curves of TGA for the linear copolymer precursor and SCPM-ball type CoPc at the heating rates of 5, 10, 20 and 30°C/min, respectively. It is well known that the thermal decomposition is strongly dependent on the dynamic heating schedule because characteristic temperature points of TGA curves will move to a higher value as the heating rate increases from 5 to 30 °C/min. The all measurements conditions were almost applied for the amount of same samples due to conditions directly affecting kinetic parameters type of carrier gas, the solid or powder form of samples, heating rate and gas flow rate a, and b show the kinetic graphs calculated by the iso-conversional methods FWO (equation 4.3) and KAS (equation 4.4) given following as, for the linear copolymer precursor and SCPM-ball type CoPc, respectively. For the conversion range worked, the graphs indicate almost parallel linearizations calculated by both methods. So, those behaviors show that the methods used considerably describe the process of devolatilization of linear copolymer precursor and SCPM-ball type CoPc. The FWO method is one of the notable model-free techniques commonly used for the estimation of kinetic parameters for a most of materials. The plots of iso-conversional FWO method show a general trend of activation energy and b indicate that the fitted lines are nearly parallel, which indicate

approximate activation energies at different conversions of linear copolymer precursor and SCPM-ball type CoPc. In the FWO method, ln(β) is plotted against 1/T (from equation 4.3) for a series of experiments at different heating rates against 1/T giving rise to a straight line whose slope (slope ≅ 1.052 E/R) yields the activation energy, E_a.

$$\ln\beta = \ln AE/g(\alpha)R - 5.331 - 1.052.E/R.T \quad (4.3)$$

As shown in Table 3.21, while the apparent activation energy the according to FWO method was determined in the range of approximate 115-138 kJ/mol for linear copolymer precursor in the conversion range, that of SCPM-ball type CoPc was estimated at range of 99.7-369.0 kJ/mol. In addition, the Kissinger-Akahira-Sunose (KAS) method has been used to calculate the activation energies more extensively than any other multiple-heating rate technique because of its simple use. By means of the following equation 4.4, the KAS method proposes a relationship between the heating rates and the activation energy.

$$\ln(\beta/T^2)=\ln[(AR/E_a\, g(\alpha)] - (E_a/RT) \quad (4.4)$$

The E_a of a certain decomposition stage can be estimated from slope (= $-E_a/R$), which is obtained from the plot between $\ln(\beta/T^2)$ versus 1/T giving rise to a straight line whose slope yields the activation energy for a certain conversion point (α) and **Hata! Başvuru kaynağı ulunamadı.**a and b indicate that ploted lines are nearly parallel, which indicates approximate activation energies via F-W-O and KAS methods at different conversions of linear copolymer precursor and SCPM-ball type CoPc, respectively. The apparent activation energy values, which are estimated by KAS methods for linear copolymer precursor and SCPM-ball type CoPc is about 110.5-133.1 $kJmol^{-1}$ and 96.5-339.3 $kJmol^{-1}$, respectively. The parallel lines were indicated in the both the FWO method and the KAS method, considering the conversion range (α) studied. In this regard, the averages of activation energy of linear copolymer precursor by FWO and KAS methods were calculated as 128.7 kJ/mol and 124.0 kJ/mol, respectively. Whereas, those of SCPM-ball type CoPc were average 161.9 kJ/mol and 153.8 kJ/mol, respectively. As seen from those results, the similarity between these values indicates notable the validity and conformity of two the models used at our work to determine kinetics of thermal decomposition of linear copolymer precursor and SCPM-ball type CoPc. Figure 3.31 shows activation energy, E_a, variation with conversion, determined from FWO and KAS methods for a linear copolymer precursor and SCPM-ball type CoPc. The variation in activation energy with increasing conversion may be attributed to polymer heterogeneity in which residual in the polymer fraction possesses a private devolatilisation characteristic. That is, as the thermal decomposition process progresses, could influence variation in activation energy. Furthermore, the devolatilisation kinetics due to revealing different products from thermal decomposition of both polymers can be

accurately interpreted by a multi-step mechanism. On the other hand, from Table 3.21, we can say that apparent activation energy for FWO method was not same for all conversion. The apparent value of activation energy estimated by FWO method for linear copolymer precursor and SCPM-ball type CoPc is about 115-138 kJmol^{-1} and 99.7-369.6 kJ mol^{-1}, respectively. Those data indicate the minimum amount of energy needed to initiate a thermal decomposition reaction. Also, those results mean that the reaction mechanism is not the same in the full decomposition process and that activation energy dependent on conversion. As seen in aforementioned, Figure 3.31 (α−E_a), these conversional curves designed a slanted profile, and depending on increasing conversion the curves shifted toward the higher activation energy. Activation energies of linear copolymer precursor and SCPM-ball type CoPc overlap at conversion of 0.42. But, activation energy (E_a) of SCPM-ball type CoPc after conversion of 0.42 indicates a notable increasing with comparison in linear copolymer precursor. A similar behavior has been also observed for KAS method, which is seen in the Figure 10. It can observe a variation of activation energy versus α for the FWO model from 115.2 kJ/mol (α = 0.1) to 134.7 kJ/mol (α = 0.5), which mainly corresponds to the contribution of devolatization of linear copolymer precursor. Subsequently, there is an increase in E_a to 138.1 kJ/mol (α = 0.7) and a decrease to 128.7 kJ/mol (α = 0.8), mainly due to difference in the decomposition products. This trend of E_a was also observed in the KAS model. On the other hand, it is possible to observe a variation of activation energy versus α for the FWO model from 99.7 kJ/mol (α = 0.1) to 149.8 kJ/mol (α = 0.5), which mainly corresponds to the contribution of devolatization of SCPM-ball type CoPc. Subsequently, there is an immediate increase in E_a to 138.1 kJ/mol (α = 0.7) and a decrease to 127.7 kJ/mol (α = 0.7). But, it has been observed suddenly an increase to 369.6 kJ/mol (at α = 0.8). This increase implies that the stronger bonds for decomposition of CoPc core in SCPM-ball type CoPc are broken. Such a trend of E_a was also observed in the KAS model. The similar behaviors to our study were recorded for the same conversion range for guarana seed residues [86] and pyrolysis of acai seed biomass [87]. The values of E_a for each conversion for FWO method and the KAS method are summarized in Table 3.21.

In general, a material's dielectric constant is given relative to that of free space, and it is known as relative permittivity (ε'_r) or dielectric constant (ε'). In terms of complex permittivity (which is expressed by its real and imaginary parts), the dielectric response of the composites at different frequencies is defined. The real $\varepsilon'(\omega)$ and the imaginary $\varepsilon''(\omega)$ parts of the complex dielectric constant is described as $\varepsilon^*(\omega) = \varepsilon'(\omega) - i\varepsilon''(\omega)$. The real $\varepsilon'(\omega)$ part of the dielectric constant is described as [82]. The dielectric loss tangent ($\tan\delta$) is defined as equation 4.5.

$$\tan\delta = \varepsilon''/\varepsilon' \tag{4.5}$$

where, tanδ is the loss angle or dissipation factor. Figure 3.32, Figure 3.33 and Figure 3.34 show frequency dependence of dielectric constant, dielectric loss factor and tanδ at different temperatures (40, 90 and 130 ^{o}C), P(PNDEAMSt12%-co-St) 6.5% (by wt) loaded GO composite. The dielectric constant at all frequencies as indicated in Figure 3.36 was recorded to be increased depending increase in temperature. The dielectric constant of linear copolymer precursor/6.5 wt% GO composite at 1 kHz for 40, 90 and 130^{o}C were estimated as 53.3, 93.0 and 696.4, respectively. The dielectric constant at 130^{o}C is considerably bigger than other temperatures. The homogeneous dispersion of GO into linear copolymer precursors and the better compatibility between linear copolymer precursors and GO is due to one of the causes of improvement in the dielectric constant values of composite depending on temperature. Thus, on the dielectric properties of a such composite can be optimized by adjusting the dispersion phase of GO and the interfacial interaction between GO and the polymer matrix. The dielectric constant value of linear copolymer precursor/6.5 wt% GO composite at 130^{o}C was considerably bigger than others. The homogeneous dispersion of GO into linear copolymer precursors and the better compatibility between linear copolymer precursors and GO is one of the causes of improvement in the dielectric constant values of composite depending on temperature. The another cause of enhancement in the dielectric constant is propably related to being more well polarizable of GO in the amorphous and rubbery polymer at temperatures whose Tg is over 80 ^{o}C. Frequency dependence of dielectric loss factor (ε") at 40, 90 and 130 ^{o}C, for linear copolymer precursor/6.5 wt% GO composite was given in Figure 3.36. As temperature increases the dielectric loss factor notable increased. For example, dielectric loss factor at 1 kHz for 130 ^{o}C was found as 266614.4. Whereas, that of 40 ^{o}C was 64524.5. The behavior of variation of ε" with frequency is nearly the same as that of ε' with frequency. The behavior of dielectric loss factor, ε", decreased with increase in frequency. At the higher frequencies (about >1.5x10^{3} Hz), the decrease of ε" becomes nearly constant. One of the significant properties of dielectric materials is dielectric loss (tanδ), which results from the inability of the polarization mechanism to follow the rate of change of the electric field applied. In general, the dielectric loss in dielectric materials results from dipolar, distortional, interfacial, and conduction loss [83]. The variation in the dielectric loss (tanδ) of linear copolymer precursor/6.5 wt% GO composite is depicted in Figure 3.33. The dielectric loss values of linear copolymer precursor/6.5 wt% GO composite for 40, 90 and 130 ^{o}C at 1 kHz were 1210.1, 1037.2 and 382.8, respectively. They were high at low frequencies, and as the frequency increases, the dielectric loss decreased. The dielectric constants of SCPM-ball type CoPc/14 wt% GO composite at 1 kHz for 40, 90 and 130 ^{o}C were 10.99, 11.57 and 109.58, respectively. As indicated in Figure 3.35, the dielectric loss factors of SCPM-ball type CoPc/14 wt% GO composite from above mentioned temperatures were measured as 208, 100 and 5050, respectively. The variations in tanδ of the same composite indicated in the Figure 3.36 were

18.98, 8.64 and 30.0, respectively. When those results were compared with those of linear copolymer precursor composite, it was revealed that the ability of dipolar and interfacial polarization process to follow the rate of change of applied electric field was lower.

The *ac* conductivity (σ_{ac}) depends on frequency according to the empirical universal dynamic response given by equation 4.6 following as:

$$\sigma_{ac}(\omega) = \sigma_{dc} + A\,\omega^{s} \tag{4.6}$$

where A is a constant, ω is the angular frequency, and s is the frequency exponent parameter which determines ac conduction mechanism. The s parameter can be interpreted by different power laws. One of them is Correlated Barrier Hoping (CBH) Mechanism. According to this mechanism, value of s should be $0 < s < 1$ [84]. So, the behavior of the exponent factor s depending upon temperature can be used to estimate the origin of the conduction mechanism.

Figure 3.37 shows as comparison with each other for the variations of $\ln\sigma_{ac}$ versus $\ln\omega$ at different temperatures (for 90 and 130°C) of linear copolymer precursor/6.5 wt% GO and SCPM-ball type CoPc/14wt% GO composites (for 90°C). The angular frequency exponent value (s) was calculated from the slope of this figure. The value of exponent ‘‘s’’ for composites at 90 °C and 130°C was estimated between 0.143 and 0.062, respectively. In addition, that of SCPM-ball type CoPc/14wt% GO composite from the slope of Figure 3.37 was estimated as 0.310 at 90 °C. In general, those conductivity values implie that shows closer behavior to dc conductivity. Among them, when their conductivities of two composites were compared with each other for two temperatures, linear copolymer precursor/6.5wt% GO possess very close behavior to dc conductivity. So, from those results, it was observed that the estimated values of exponent s parameter were decreased with temperature. This event presents that the conduction mechanism is correlated with barrier hopping. It is known that graphite oxide is a good electricity conductor. But, linear copolymer precursor or SCPM-ball type CoPc prepared at our study is an insulators. So, the results indicated that GO increased electrical conductivity both the linear copolymer precursor/GO and SCPM-ball type CoPc/GO composites. Therefore, the electrical conductivity of linear copolymer precursor and SCPM-ball type CoPc composites were investigated. In this regard, by adding suitable fillers to polymers or copolymer materials with any insulating property, their electrical properties can be improved depending on the content and type of fillers [85]. For this purpose, the electrical transport mechanisms of liner copolymer precursor doped with GO 3.6 wt%, 4.5 wt% and 6.5 wt% and SCPM-ball type CoPc/14wt% GO composites were investigated in terms of dc conductivity as a function of temperature. The conductivity can be analyzed by Arhenius’s equation 4.7 [86] following as:

$$\sigma_{dc} = \sigma_o.\exp(-\Delta Ea/\kappa_B T) \quad (4.7)$$

where E_a is the activation energy, σ_o is the pre-exponential factor, k_B is the constant of Boltzmann constant, and T is the Kelvin temperature.

It is well known that electrical conductivity is performed thermally through electrons and holes [87]. Depending upon increasing temperature, the charge carriers participate in the electrical conduction because most of charge carriers surpass the activation energy barrier [88]. The graphs of electrical conductivity of linear copolymer precursor/GO and SCPM-ball type CoPc/GO composites were indicated in Figure 3.38, Figure 3.39, Figure 3.40 and Figure 3.41. The dc conductivity increased exponentially over the studied range of temperatures. The dc electrical conductivity of linear copolymer precursor/GO and SCPM-ball type CoPc/GO composites increases with increasing amount of GO. The activation energy values for composites were estimated from their slopes. As indicated in Figure 3.38, Figure 3.39 and Figure 3.40, the activation energies of linear copolymer precursor doped with GO 3.6 wt%, 4.5 wt% and 6.0 wt% were estimated as 0.236 eV, 0.227 eV and 0.084 eV, respectively. Those values are the activation energy of mobile charge carrier. So, as amount of GO in the composites increases, the activation energy value decreased. In this context, the composite doped with 6.5 wt% GO among linear copolymer precursor composites indicates that overcome easer the activation energy barrier due to more participitating the charge carriers in the electrical conduction. As seen in Figure 3.41, the activation energy from slope of SCPM-ball type CoPc/14 wt% GO composite was estimated as 0.790 eV. This behavior shows that it is a little more difficult for the charge carriers to overcome the activation energy barrier compared to the linear copolymer precursor/GO composites, because GO is not well dispersed in the SCPM-ball type CoPc/14 wt% GO. This event means fewer spaces between molecule that are less spaces among molecules in the SCPM-ball type CoPc containing bulky substituents. On the other hand, it shows that possess poorer semi conductivity behavior. So, it is estimated that there are more gaps between networks due to formation of more aggregation doping with GO particles of the amorphous SCPM-ball type CoPc. Hence, this behavior means that conductivity decreases. However, the results of dc conductiviy indicate that the linear copolymer precursor/GO and SCPM-ball type CoPc/GO composites possess a semi conductive behavior.

Figure 3.42 shows current–voltage (I–V) relationship of the linear copolymer precursor/GO composites with different graphite oxide content. For the neat linear copolymer precursor, there was no electric current over the applied voltage of 0.1–20V, because the linear copolymer precursor material is electrically insulating. On the other hand, the electrical current linearly increased with the applied voltage for composite materials with high graphite oxide content above 3.6 wt%, and the slopes of the I-V curves also became steeper with increasing graphite oxide

quantity in the composite materials. So, for all the samples, it was revealed that the current (A) increased linearly when the applied voltage (V) and the amount of percent of graphite oxide incorporated into the polymer matrices were increased. In addition, it is clear that voltage sensitivity versus to current of linear copolymer precursor/GO 6.5wt% among I–V curves indicates are observed from Figure 3.42. In addition, the analysis of linear copolymer precursor/6.5wt% GO among I–V curves indicate that considerably possess a good leakage current mechanism. In this context, the literature data have recorded that the positive deviation from the linear I–V curves at applied high voltages is believed to be caused by the increased electric charge flows in the composite materials due to the electric heating effect [89].

5. CONCLUSIONS

In this research, we have reported the first examples of SCP-ball type CoPc and their composites with GO. By controlling the number of PNDEAMSt units in the copolymer using free radical polymerization, and the number of cobalt phthalocyanines integrated into single chain polymers increased. One of the important evidences for the formation of SCP-ball type CoPc complex is almost disappearance of –C≡N vibration band at 2230 cm^{-1}. However, the very weak band at 2230 cm^{-1} shows –C≡N band in the PNDEAMSt unit in the precursor copolymers not forming complex with cobalt. And a new peak corresponding to an imine (–C=N:–) group appeared at 1720 cm^{-1}. So, almost disappearing of –C≡N band at 2230 cm^{-1} and formation of imine band at 1720 cm^{-1} are important evidence confirming formation of SCP-ball type CoPc complex. The SCP-ball type CoPc1 and SCP-ball type CoPc2 showed characteristic absorptions around 601 and 673 nm in the Q band region at Uv-vis spectroscopy. MALDI-TOF-MS spectrum showed a polymeric distribution following 104 Da mass difference that have styrene repeating unit used in synthesis of phthalocyanine containing polymer. Mass of cobalt complex of double core phthalocyanine without monomer units was 2010 Da nominal mass. it could be concluded that the polymeric structure having cobalt complexes core phthalocyanine was synthesized in the desired form. The single chain polymeric structures containing cobalt phthalocyanine were soluble in organic solvents, such as dichloromethane, chloroform, THF, DMS and acetone. Average apparent activation energies of the thermal degradation of SCP-ball type CoPc1 calculated by three model-free methods in a period of α = 0.07–0.90 have been estimated, and the activation energy for weight loss from 7 % to 90% was increased 33.16 and, 56.73%, respectively. Both precursor copolymer2 and SCP-ball type CoPc2 indicated that are insulator materials from dielectrical measurements.

In this work, it was reported as virtually the first example of preparing ball type CoPc result of formation of phthalocyanine by macrocyclization of the pendant groups over single chain polymer molecule using a linear copolymer precursor in different copolymer composition (synthesized by free radical polymerization). The structure of SCPM-ball type CoPc was confirmed by FT-IR, MALDI-TOF-MS and UV spectroscopy techniques. The C≡N stretching band at 2233 cm^{-1}, which was observed in FT-IR spectrum of the linear precursor copolymer were fully consumed due to completion of the reaction of SCPM-ball type CoPc complex. So, disappear of this band was one of important evidences confirming structure of the SCPM-ball type CoPc. The mass of the two double core phthalocyanine cobalt complex without styrene monomer unit was 4020 Da nominal mass. When each peak mass was analyzed, it was noted that hydrogen initiated the polymer with a cobalt-complexed phthalocyanine core and ended with hydrogen again. Each polymer species has also been ionized by silver adducts.

Furthermore, the signals started around 6550 Da represent the three double cobalt core polymeric structure. This event could be concluded that the polymeric structure having cobalt complexes core phthalocyanine was synthesized in the desired structure. UV-vis spectrum confirmed structure of SCPM-ball type CoPc with two broad peaks at 598 nm and 660 nm in the UV-vis spectrum of SCPM-ball type CoPc. FWO and KAS models were employed to determine the kinetic data of linear copolymer precursor and SCPM-ball tpe CoPc and the results were comparable. The results of FWO and KAS showed that the linear copolymer precursor's activation energies were as average 128.7 kJ/mol and 124.0 kJ/mol and those of SCPM-ball type CoPc were average 161.9 kJ/mol and 153.8 kJ/mol, respectively. It was estimated that the conduction mechanism from the frequency dependence of ac conductivity (σ_{ac}) of linear copolymer precursor/6.5wt% GO and SCPM-ball type CoPc/GO 14 wt% posssess Correlated Barrier Hoping (CBH) Mechanism. The dielectric and electrical measurements indicated that dispersion of GO in SCPM-ball type CoPc with compared in linear copolymer precursor was less. The activation energies of linear copolymer precursor doped with 3.6 wt%, 4.5 wt% and 6.5 wt% GO were estimated as 0.236 eV, 0.227 eV and 0.084 eV, respectively. Whereas, that of SCPM-ball type CoPc/14 wt% GO composite was estimated as 0.790 eV.

REFERENCES

[1] Pious, C. and Thomas, S. (2016). *Polymeric materials—structure, properties, and applications, Printing on Polymers*: William Andrew Publishing, Vol. 21-39.

[2] Pritchard, G., (2012). Plastics additives: an AZ reference, *Springer Science & Business Media.*

[3] Conejo-Dávila, A.S., Hernández-Escobar, C.A., Vega-Rios, A., Rodríguez-Sánchez, I., Estrada-Monje, A., de León-Gómez, R.E.D., and Zaragoza-Contreras, E.A. (2020). Selective polymerization of a new bifunctional monomer via free radical polymerization and oxidative route, *Synthetic Metals*, Vol. 259 116258.

[4] Isse, A.A., Lorandi, F., and Gennaro, A. (2019). Electrochemical approaches for better understanding of atom transfer radical polymerization, Current Opinion in Electrochemistry, Vol. 15 50-57.

[5] Praveen, K.M., Pious, C.V., Thomas, S., and Grohens, Y., Chapter 1 - Relevance of Plasma Processing on Polymeric Materials and Interfaces, in Non-Thermal Plasma Technology for Polymeric Materials, S. Thomas, M. Mozetič, U. Cvelbar, P. Špatenka, and P. K.M, Editors. (2019). *Elsevier.* p. 1-21.

[6] Resconi, L., Piemontesi, F., and Jones, R.L., High-Molecular-Weight Atactic Polypropylene from Metallocene Catalysts. Influence of Ligand Structure and Polymerization Conditions on Molecular Weight, in Metallocene Catalyzed Polymers, G.M. Benedikt and B.L. Goodall, Editors. (1998). *William Andrew Publishing:* Norwich, NY. p. 43-55.

[7] Jiang, Q., Xia, D., Liu, C., Jiang, Q., Li, J., Han, B., Jiang, B., Huang, W., Xue, X., and Yang, H. (2020). Does bimolecular termination dominate in benzoyl peroxide initiated styrene free-radical polymerization, *Polymer*, Vol. 189 122184.

[8] O'Driscoll, K. (1981). Free radical polymerization kinetics-revisited, *Pure and Applied Chemistry*, Vol. 53 (3), pp: 617-626.

[9] Moad, G., Chiefari, J., Mayadunne, R.T., Moad, C.L., Postma, A., Rizzardo, E., and Thang, S.H. (2002). *Initiating free radical polymerization in Macromolecular Symposia*. Wiley Online Library.

[10] Darling, T.R., Davis, T.P., Fryd, M., Gridnev, A.A., Haddleton, D.M., Ittel, S.D., Matheson Jr, R.R., Moad, G., and Rizzardo, E. (2000). Living polymerization: Rationale for uniform terminology, *Journal of Polymer Science Part A: Polymer Chemistry*, Vol. 38 (10), pp: 1706-1708.

[11] Matyjaszewski, K. and Xia, J. (2001). Atom transfer radical polymerization, *Chemical reviews*, Vol. 101 (9), pp: 2921-2990.

[12] Tsarevsky, N.V., Braunecker, W.A., Tang, W., Brooks, S.J., Matyjaszewski, K., Weisman, G.R., and Wong, E.H. (2006). Copper-based ATRP catalysts of very high activity derived from dimethyl cross-bridged cyclam, *Journal of Molecular Catalysis A: Chemical*, Vol. 257 (1-2), pp: 132-140.

[13] Jawad, S.A., Al-Jundi, J., and El-Ghanem, H. (2003). DC electrical properties of graphytized carbon-black filled rubbers, *International Journal of Polymeric Materials*, Vol. 52 (9), pp: 809-820.

[14] Sumita, M., Sakata, K., Asai, S., Miyasaka, K., and Nakagawa, H. (1991). Dispersion of fillers and the electrical conductivity of polymer blends filled with carbon black, *Polymer Bulletin*, Vol. 25 (2), pp: 265-271.

[15] Nagata, K., Iwabuki, H., and Nigo, H. (1998). Effect of particle size of graphites on electrical conductivity of graphite/polymer composite, *Composite interfaces*, Vol. 6 (5), pp: 483-495.

[16] Chung, D. (2002). Review graphite, *Journal of materials science*, Vol. 37 (8), pp: 1475-1489.

[17] Botas, C., Álvarez, P., Blanco, P., Granda, M., Blanco, C., Santamaría, R., Romasanta, L.J., Verdejo, R., López-Manchado, M.A., and Menéndez, R. (2013). Graphene materials with different structures prepared from the same graphite by the Hummers and Brodie methods, *Carbon*, Vol. 65 156-164.

[18] Talyzin, A.V., Mercier, G., Klechikov, A., Hedenström, M., Johnels, D., Wei, D., Cotton, D., Opitz, A., and Moons, E. (2017). Brodie vs Hummers graphite oxides for preparation of multi-layered materials, *Carbon*, Vol. 115 430-440.

[19] Hontoria-Lucas, C., López-Peinado, A., López-González, J.d.D., Rojas-Cervantes, M., and Martin-Aranda, R. (1995). Study of oxygen-containing groups in a series of graphite oxides: physical and chemical characterization, *Carbon*, Vol. 33 (11), pp: 1585-1592.

[20] Lavin-Lopez, M.d.P., Romero, A., Garrido, J., Sanchez-Silva, L., and Valverde, J.L. (2016). Influence of different improved hummers method modifications on the characteristics of graphite oxide in order to make a more easily scalable method, *Industrial & Engineering Chemistry Research*, Vol. 55 (50), pp: 12836-12847.

[21] Sengupta, R., Bhattacharya, M., Bandyopadhyay, S., and Bhowmick, A.K. (2011). A review on the mechanical and electrical properties of graphite and modified graphite reinforced polymer composites, *Progress in polymer science*, Vol. 36 (5), pp: 638-670.

[22] Kumar, H.V., Woltornist, S.J., and Adamson, D.H. (2016). Fractionation and characterization of graphene oxide by oxidation extent through emulsion stabilization, *Carbon*, Vol. 98 491-495.

[23] Keller, T.M. (1994). Synthesis and polymerization of multiple aromatic ether phthalonitriles, *Chemistry of materials*, Vol. 6 (3), pp: 302-305.

[24] Wu, Z., Han, J., Li, N., Weng, Z., Wang, J., and Jian, X. (2017). Improving the curing process and thermal stability of phthalonitrile resin via novel mixed curing agents, *Polymer international*, Vol. 66 (6), pp: 876-881.

[25] Augustine, D., Mathew, D., and Nair, C.R. (2013). Phenol-containing phthalonitrile polymers–synthesis, cure characteristics and laminate properties, *Polymer international*, Vol. 62 (7), pp: 1068-1076.

[26] McKeown, N.B. (2000). Phthalocyanine-containing polymers, *Journal of Materials Chemistry*, Vol. 10 (9), pp: 1979-1995

[27] Günsel, A., Bilgiçli, A.T., Tüzün, B., Pişkin, H., Atmaca, G.Y., Erdoğmuş, A., and Yarasir, M.N. (2019). Synthesis of tetra-substituted phthalocyanines bearing 2-(ethyl (m-tolyl) amino) ethanol: computational and photophysicochemical studies, *Journal of Photochemistry and Photobiology A: Chemistry*, Vol. 373 77-86.

[28] Sorokin, A.B. (2013). Phthalocyanine metal complexes in catalysis, *Chemical reviews*, Vol. 113 (10), pp: 8152-8191.

[29] Atkins, P. and de Paula, J. (2006). *Atkins, Physical chemistry*, Vol. 8 798..

[30] Flynn, J.H. and Wall, L.A. (1966). A quick, direct method for the determination of activation energy from thermogravimetric data, *Journal of Polymer Science Part B: Polymer Letters*, Vol. 4 (5), pp: 323-328.

[31] Grill, A. and Patel, V. (2001). Ultralow-k dielectrics prepared by plasma-enhanced chemical vapor deposition*, Applied Physics Letters*, Vol. 79 (6), pp: 803-805.

[32] Chiu, M.H. and Prenner, E.J. (2011). Differential scanning calorimetry: An invaluable tool for a detailed thermodynamic characterization of macromolecules and their interactions, *Journal of Pharmacy and Bioallied Sciences*, Vol. 3 (1), pp: 39.

[33] Wendlandt, W.W., (1974). *Thermal methods of analysis*,

[34] O'neill, M. (1964). *The Analysis of a Temperature-Controlled Scanning Calorimeter, Analytical Chemistry*, Vol. 36 (7), pp: 1238-1245.

[35] Jurinke, C., Oeth, P., and van den Boom, D. (2004). MALDI-TOF mass spectrometry, *Molecular biotechnology,* Vol. 26 (2), pp: 147-163.

[36] Pasch, H. and Schrepp, W., (2013). *MALDI-TOF mass spectrometry of synthetic polymers*, Springer Science & Business Media.

[37] Fedulova, E., Nazarov, M.M., Angeluts, A., Kitai, M., Sokolov, V., and Shkurinov, A. (2012). Studying of dielectric properties of polymers in the terahertz frequency range. in Saratov Fall Meeting 2011: *Optical Technologies in Biophysics and Medicine XIII*. International Society for Optics and Photonics.

[38] Karasz, F., (2012). Dielectric Properties of Polymers: *Proceedings of a Symposium held on March 29–30, 1971, in connection with the 161st National Meeting of the American Chemical Society in Los Angeles, California*, March 28–April 2, 1971, Springer Science & Business Media,

[39] Pozzo, M., Davies, C., Gubbins, D., and Alfè, D. (2014). *Thermal and electrical conductivity of solid iron and iron–silicon mixtures at Earth's core conditions, Earth and Planetary Science Letters*, Vol. 393 159-164.

[40] Epstein, A.J., *Electrical conductivity in conjugated polymers, in Conductive Polymers and Plastics* (1999). Elsevier. p. 1-9.

[41] Mamunya, Y.P., Davydenko, V., Pissis, P., and Lebedev, E. (2002). Electrical and thermal conductivity of polymers filled with metal powders, *European polymer journal*, Vol. 38 (9), pp: 1887-1897.

[42] Aguilar, J., Bautista-Quijano, J., and Avilés, F. (2010). Influence of carbon nanotube clustering on the electrical conductivity of polymer composite films, *Express Polym Lett*, Vol. 4 (5), pp: 292-299.

[43] Neugebauer, C. and Webb, M. (1962). Electrical conduction mechanism in ultrathin, evaporated metal films, *Journal of Applied Physics*, Vol. 33 (1), pp: 74-82.

[44] Praveen, K., Pious, C., Thomas, S., and Grohens, Y., (2019). Relevance of Plasma Processing on Polymeric Materials and Interfaces, in Non-Thermal Plasma Technology for Polymeric Materials, Elsevier. p. 1-21.

[45] Jin, Y.-S., Kim, G.-J., and Jeon, S.-G. (2006). Terahertz dielectric properties of polymers, *Journal of the Korean Physical Society*, Vol. 49 (2), pp: 513-517.

[46] Campo, E.A., (2008). *Selection of polymeric materials: how to select design properties from different standards*, William Andrew,

[47] Malmberg, C. and Maryott, A. (1956). Dielectric Constant of Water from 00 to 1000 C, Journal of research of the National Bureau of Standards, Vol. 56 (1), pp: 1.

[48] Heaney, M.B. (2000). Electrical conductivity and resistivity, *The measurement, instrumentation and sensors handbook*, Vol. 1332-1345.

[49] Nyfors, E. and P. Vainikainen. (1989). *Industrial Microwave Sensors*, *chapter 2. Boston, MA: Artech House*, Norwood.

[50] Chen, L. F.; Ong, C. K.; Neo, C. P.; Varadan, V. V.; Varadan, Vijay K. (2004). Microwave Electronics: Measurement and Materials Characterization. ISBN 9780470020456.

[51] Wöhrle, D. (2001). Phthalocyanines in macromolecular phases–methods of synthesis and properties of the materials, *Macromolecular rapid communications*, Vol. 22 (2), pp: 68-97.

[52] Kadish, K.M., Smith, K.M., and Guilard, R. (2010). *The porphyrin handbook, World scientific*, Vol. 2011 1-20.

[53] Huang, C. and Zhang, Q.M. (2005). Fully Functionalized High-Dielectric-Constant Nanophase Polymers with High Electromechanical Response, *Advanced Materials*, Vol. 17 (9), pp: 1153-1158.

[54] Choi, S., Hong, S.H., Cho, S.H., Park, S., Park, S.M., Kim, O., and Ree, M. (2008). High-Performance Programmable Memory Devices Based on Hyperbranched Copper Phthalocyanine Polymer Thin Films, *Advanced Materials*, Vol. 20 (9), pp: 1766-1771.

[55] Yang, X., Wang, Q., Zhang, Y., and Jiang, Z. (2012). The microstructure and dielectric properties of modified poly (aryl ether ketone)/metallophthalocyanine composites, *Polymer journal*, Vol. 44 (10), pp: 1042-1047.

[56] Jeong, J., Lee, Y.-J., Kim, B., Kim, B., Jung, K.-S., and Paik, H.-j. (2015). Colored single-chain polymeric nanoparticles via intramolecular copper phthalocyanine formation, *Polymer Chemistry*, Vol. 6 (18), pp: 3392-3397. doi: 10.1039/C4PY01559B.

[57] Kimura, M., Ueki, H., Ohta, K., Hanabusa, K., Shirai, H., and Kobayashi, N. (2004). Nanoscopic fibrous assemblies made of metallophthalocyanine-terminated amphiphilic polymers, *Chemistry*, Vol. 10 (20), pp: 4954-9. doi: 10.1002/chem.200400341.

[58] Clarkson, G.J., Cook, A., McKeown, N.B., Treacher, K.E., and Ali-Adib, Z. (1996). Synthesis and characterization of mesogenic phthalocyanines containing a single poly (oxyethylene) side chain: an example of steric disturbance of the hexagonal columnar mesophase, *Macromolecules*, Vol. 29 (3), pp: 913-917.

[59] Ceyhan, T., Altindal, A., Özkaya, A.R., Erbil, M.K., Salih, B., and Bekaroğlu, Ö. (2006). Synthesis, characterization, and electrical, electrochemical and gas sensing properties of a novel ball-type four t-butylcalix[4]arene bridged binuclear zinc(ii) phthalocyanine, *Chemical Communications*, Vol. (3), pp: 320-322. doi: 10.1039/B510225A.

[60] De la Torre, G., Claessens, C.G., and Torres, T. (2007). Phthalocyanines: old dyes, new materials. Putting color in nanotechnology, *Chemical Communications*, Vol. (20), pp: 2000-2015.

[61] Ceyhan, T., Altindal, A., Özkaya, A.R., Erbil, M.K., Salih, B., and Bekaroğlu, Ö. (2006). Synthesis, characterization, and electrical, electrochemical and gas sensing properties of a novel ball-type four t-butylcalix [4] arene bridged binuclear zinc (II) phthalocyanine, *Chemical Communications*, Vol. (3), pp: 320-322.

[62] Acikses, A., Taskan, G., and Barim, G. (2018). A study on copolymer systems of styrene with diethanolamine side group and methyl methacrylate, *Journal of Chemistry*, Vol. 2018.

[63] Zheng, W., Wan, C.-Z., Zhang, J.-X., Li, C.-H., and You, X.-Z. (2015). Facile synthesis of phthalocyanine at low temperature with diisopropylamide anion as nucleophile, *Tetrahedron letters*, Vol. 56 (30), pp: 4459-4462.

[64] Schmiedova, V., Pospisil, J., Kovalenko, A., Ashcheulov, P., Fekete, L., Cubon, T., Kotrusz, P., Zmeskal, O., and Weiter, M. (2017). Physical properties investigation of reduced graphene oxide thin films prepared by material inkjet printing, *Journal of Nanomaterials*, Vol. 2017.

[65] Bekaroğlu, Ö., (2010). *Functional phthalocyanine molecular materials*, Springer Science & Business Media,

[66] Odabaş, Z., Dumludağ, F., Özkaya, A.R., Yamauchi, S., Kobayashi, N., and Bekaroğlu, Ö. (2010). Novel homo-and heterobinuclear ball-type phthalocyanines: synthesis and electrochemical, electrical, EPR and MCD spectral properties, *Dalton Transactions*, Vol. 39 (35), pp: 8143-8152.

[67] Odabaş, Z., Koç, İ., Altındal, A., Özkaya, A.R., Salih, B., and Bekaroğlu, Ö. (2010). Synthesis and electrochemical, in situ spectroelectrochemical, electrical and gas sensing properties of ball-type homo-and hetero-dinuclear phthalocyanines with four [1a, 8b-dihydronaphtho [b] naphthofuro [3, 2-d] furan-7, 10-diyl] bridges, *Synthetic Metals*, Vol. 160 (9-10), pp: 967-977.

[68] Hassan, B.M., Li, H., and McKeown, N.B. (2000). The control of molecular self-association in spin-coated films of substituted phthalocyanines, *Journal of Materials Chemistry*, Vol. 10 (1), pp: 39-45.

[69] De la Torre, G., Bottari, G., Hahn, U., and Torres, T., Functional Phthalocyanines: *Synthesis, Nanostructuration, and Electro-Optical Applications, in Functional Phthalocyanine Molecular Materials,* J. Jiang, Editor 2010, Springer Berlin Heidelberg: Berlin, Heidelberg. p. 1-44.

[70] Açıkbaş, Y., Evyapan, M., Ceyhan, T., Çapan, R., and Bekaroğlu, Ö. (2009). Characterization and organic vapor sensing properties of Langmuir–Blodgett film using a new three oxygen-linked phthalocyanine incorporating lutetium, *Sensors and Actuators B: Chemical*, Vol. 135 (2), pp: 426-429.

[71] Guan, H., Shao, C., Wen, S., Chen, B., Gong, J., and Yang, X. (2003). A novel method for preparing Co3O4 nanofibers by using electrospun PVA/cobalt acetate composite fibers as precursor, *Materials Chemistry and Physics*, Vol. 82 (3), pp: 1002-1006. doi: https://doi.org/10.1016/j.matchemphys. 2003.09.003.

[72] Ceyhan, T., Altındal, A., Özkaya, A., Çelikbıçak, Ö., Salih, B., Erbil, M.K., and Bekaroğlu, Ö. (2007). Synthesis, characterization and electrochemical properties of novel metal free and zinc (II) phthalocyanines of ball and clamshell types, *Polyhedron*, Vol. 26 (15), pp: 4239-4249.

[73] Jang, B.N. and Wilkie, C.A. (2005). The thermal degradation of polystyrene nanocomposite, *Polymer*, Vol. 46 (9), pp: 2933-2942.

[74] Guan, H., Shao, C., Wen, S., Chen, B., Gong, J., and Yang, X. (2003). A novel method for preparing Co3O4 nanofibers by using electrospun PVA/cobalt acetate composite fibers as precursor, *Materials Chemistry and Physics*, Vol. 82 (3), pp: 1002-1006.

[75] Su, L.-H., Zhang, X.-G., Mi, C.-H., Gao, B., and Liu, Y. (2009). Improvement of the capacitive performances for Co–Al layered double hydroxide by adding hexacyanoferrate into the electrolyte, *Physical Chemistry Chemical Physics*, Vol. 11 (13), pp: 2195-2202.

[76] Villegas, J.C., Giraldo, O.H., Laubernds, K., and Suib, S.L. (2003). New layered double hydroxides containing intercalated manganese oxide species: synthesis and characterization, *Inorganic chemistry*, Vol. 42 (18), pp: 5621-5631.

[77] Xu, R. and Zeng, H.C. (2003). Dimensional control of cobalt-hydroxide-carbonate nanorods and their thermal conversion to one-dimensional arrays of Co3O4 nanoparticles, *The Journal of Physical Chemistry B*, Vol. 107 (46), pp: 12643-12649.

[78] Xie, X., Shang, P., Liu, Z., Lv, Y., Li, Y., and Shen, W. (2010). Synthesis of nanorod-shaped cobalt hydroxycarbonate and oxide with the mediation of ethylene glycol, *The Journal of Physical Chemistry C*, Vol. 114 (5), pp: 2116-2123.

[79] Shi, S., Zhang, L., and Li, J. (2009). Complex permittivity and electromagnetic interference shielding properties of Ti3SiC2/polyaniline composites, *Journal of materials science*, Vol. 44 (4), pp: 945-948..

[80] Açikses, A., Çömez, N., and Biryan, F. (2019). Metal complexes of a homopolymer system containing diethanolamine side group: synthesis and dielectrical behaviors, *Journal of Macromolecular Science, Part A,* Vol. 56 (3), pp: 253-266.

[81] Canlıca, M., Booysen, I.N., and Nyokong, T. (2011). Synthesis and electrochemical behavior of novel peripherally and non-peripherally substituted ball-type cobalt phthalocyanine complexes, *Polyhedron*, Vol. 30 (3), pp: 522-528.

[82] Rieger, J. (2001). The glass transition temperature Tg of polymers—comparison of the values from differential thermal analysis (DTA, DSC) and dynamic mechanical measurements (torsion pendulum), *Polymer Testing*, Vol. 20 (2), pp: 199-204.

[83] Coşkun, M., Barim, G., and Demirelli, K. (2007). A grafting study on partially dehydrochlorinated poly (vinyl chloride) by atom transfer radical polymerization, *Journal of Macromolecular Science, Part A*, Vol. 44 (5), pp: 475-481.

[84] Abubakar, A.M., Demirelli, K., Tuncer, H., and Salih, B. (2021). Characterization and preparation of green colored intramolecular novel ball type cobalt phthalocyanine complexes with single-chain polymer structure, *Journal of Molecular Structure*, Vol. 1227 129389. doi: https://doi.org/10.1016/j.molstruc.2020.129389.

[85] Navarro, J., Roig, A., Noguera, P., Vicente, F., Vilaplana, J., and López, J. (1994). Electrochemical behaviour and electrical percolation in graphite-epoxy electrodes, *Journal of materials science*, Vol. 29 (17), pp: 4604-4610. doi: 10.1007/BF00376284..

[86] Tauc, J., (2012). *Amorphous and liquid semiconductors*, Springer Science & Business Media.

[87] Yakuphanoglu, F., Şenkal, B.F., and Saraç, A. (2008). Electrical conductivity, thermoelectric power, and optical properties of organo-soluble polyaniline organic semiconductor, *Journal of Electronic Materials*, Vol. 37 (6), pp: 930-934..

[88] Aydın, C., Abd El-sadek, M.S., Zheng, K., Yahia, I.S., and Yakuphanoglu, F. (2013). Synthesis, diffused reflectance and electrical properties of nanocrystalline Fe-doped ZnO via sol–gel calcination technique, *Optics & Laser Technology,* Vol. 48 447-452. doi: https://doi.org/10.1016/j.optlastec.2012.11.004..

[89] An, J.-E. and Jeong, Y.G. (2013). Structure and electric heating performance of graphene/epoxy composite films, *European Polymer Journal*, Vol. 49 (6), pp: 1322-1330. doi: https://doi.org/10.1016/j.eurpolymj.2013.02.005.

CURRICULUM VITAE

Abdullahi Musa ABUBAKAR

[redacted]

[redacted]

[redacted]

[redacted]

[redacted]

[redacted]

ACADEMIC ACTIVITIES

Paper:

[1] Demirelli, K., Abubakar, A.M., Tuncer, H., and Salih, B., 2021. Preparation, characterization and electrical behaviors of greenish single-chain polymeric molecule-via intramolecular ball type cobalt phthalocyanines/ graphite oxide composites, Journal of Molecular Structure, 1235, 130132.

[2] Abubakar, A.M., Demirelli, K., Tuncer, H., and Salih, B., 2021. Characterization and preparation of green colored intramolecular novel ball type cobalt phthalocyanine complexes with single-chain polymer structure, Journal of Molecular Structure, 1227, 129389.

[3] Abubakar, A.M., Biryan, F., and Demirelli, K., 2021. Electrical properties, characterization, and preparation of composite materials containing a polymethacrylate with α-naphthyl side group and nanographene fillers, Journal of Thermoplastic Composite Materials, 34(1), 102-125.

[4] Biryan, F., Abubakar, A.M., and Demirelli, K., 2018. Product analysis, electrical and dielectric properties depending on thermal influence of poly(N-isopropyl acrylamide)/graphite-filled composite, Thermochimica Acta, 669, 66-79.

[5] Demirelli, K., Abubakar, AM., Ahmad, AA., Bagci, E., 2021.The effect of end group and graphene on dielectric properties and thermal degradation of poly(benzyl methacrylate) prepared by ATRP method, Polymer Bulletin, DOI10.1007/s00289-021-04003-2

[6] Demirelli, K., Barım, E., Tuncer, H., Barım, G., and Abubakar, A.M., 2021. Synthesis and characterization of N-(2-acetyl benzofuran-3-yl) methacryl amide and ethyl methacrylate copolymer/graphite oxide composites and study of their kinetic and electrical properties, Polymer bulletin, DOI: 10.1007/s00289-021-03730-w.